Thiol-ene Cross-linked Poly(glycidol) / Hyaluronic Acid Based Hydrogels for 3D Bioprinting

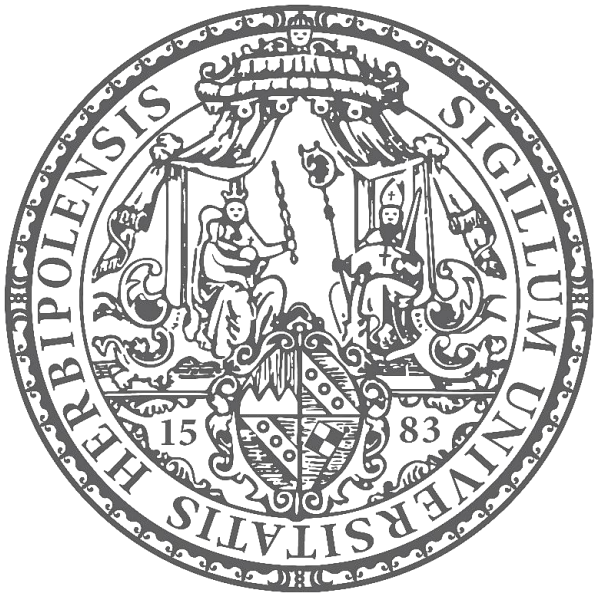

Dissertation zur Erlangung des
naturwissenschaftlichen Doktorgrades
der Julius-Maximilians-Universität Würzburg

vorgelegt von
Diplom Chemikerin
Simone Schäfer, geb. Stichler
aus Würzburg

Würzburg 2018

Für meine Familie

Eingereicht bei der Fakultät für Chemie und Pharmazie am

_____

Gutachter der schriftlichen Arbeit

1. Gutachter: _____
2. Gutachter: _____

Prüfer des öffentlichen Promotionskolloquiums

1. Prüfer: _____
2. Prüfer: _____
3. Prüfer: _____

Datum des öffentlichen Promotionskolloquiums

_____

Doktorurkunde ausgehändigt am

_____

Die vorliegende Arbeit wurde in der Abteilung für Funktionswerkstoffe der Medizin und Zahnheilkunde, Universität zu Würzburg, Würzburg, Deutschland in der Zeit von Januar 2013 bis August 2017 unter der Leitung von Herrn Prof. Dr. Jürgen Groll angefertigt.

COPYRIGHT REMARKS

Parts of this thesis have previously been published and are adapted with permission from:

S. Stichler, T. Böck, N. Paxton, S. Bertlein, R. Levato, V. Schill, W. Smolan, J. Malda, J. Teßmar, T Blunk, J. Groll, Double printing of hyaluronic acid/poly(glycidol) hybrid hydrogels with poly(ε-caprolactone) for MSC chondrogenesis, *Biofabrication* **2017**, doi: 10.1088/1758-5090/aa8cb7.

S. Stichler, S. Bertlein, J. Teßmar, T. Jüngst, J. Groll, Thiol-ene Cross-Linkable Hydrogels as Bioinks for Biofabrication, *Macromol. Symp*. **2017**, *372*, 102-107.

S. Stichler, T. Jüngst, M. Schamel, I. Zilkowski, M. Kuhlmann, T. Böck, T. Blunk, J. Teßmar, J. Groll, Thiol-ene clickable poly(glycidol) hydrogels for biofabrication, *Ann. Biomed. Eng*. **2017**, *45*, 273-285.

LIST OF PUBLICATIONS

1. S. Stichler, T. Böck, N. Paxton, S. Bertlein, R. Levato, V. Schill, W. Smolan, J. Malda, J. Teßmar, T Blunk, J. Groll, Double printing of hyaluronic acid/poly(glycidol) hybrid hydrogels with poly(ε-caprolactone) for MSC chondrogenesis, *Biofabrication* **2017**, doi: 10.1088/1758-5090/aa8cb7.

2. S. Stichler*,* S. Bertlein, J. Teßmar, T. Jüngst, J. Groll, Thiol-ene Cross-Linkable Hydrogels as Bioinks for Biofabrication, *Macromol. Symp*. **2017**, *372*, 102-107.

3. S. Stichler, T. Jüngst, M. Schamel, I. Zilkowski, M. Kuhlmann, T. Böck, T. Blunk, J. Teßmar, J. Groll, Thiol-ene clickable poly(glycidol) hydrogels for biofabrication, *Ann. Biomed. Eng*. **2017**, *45*, 273-285.

4. B. Baumann, T. Jungst, S. Stichler, S. Feineis, O. Wiltschka, M. Kuhlmann, M. Lindén, J. Groll, Control of Nanoparticle Release Kinetics from 3D Printed Hydrogel Scaffolds, *Angew. Chem. Int. Ed.* **2017**, *56*, 4623-4628.

5. M. Glogger, S. Stichler, I. Subota, S. Bertlein, M.-C. Spindler, J. Teßmar, J. Groll, M. Engstler, S. F. Fenz, Live-cell super resolution imaging of intrinsically fast moving flagellates, *J. Phys. D: Appl. Phys.* **2017**, *50*, 074004/1-074004/7.

Table of contents

Abbreviations

AGE	allyl glycidyl ether
a.u.	arbitrary unit
Col	collagen
d	day
3D	three-dimensional
DCC	N,N'-dicyclohexylcarbodiimide
DMAP	4-(dimethylamino)pyridine
DMF	dimethylformamide
DMPA	2,2-dimethoxy-2-phenylacetophenon
DN	double network
DTPA	3,3'-dithiodipropionic acid
DTPH	3,3'-dithiobis(propanoic dihydrazide)
DTT	1,4-dithiothreitol
ECM	extracellular matrix
EDC	N-(3-dimethylaminopropyl)-N´-ethylcarbodiimide)
EEGE	ethoxy ethyl glycidyl ether
eq.	equivalent
et al.	et alii / et aliae (and others)
EtOH	ethanol
F-HA	fluorescein hyaluronic acid
FITC-dextran	fluorescein isothiocyanate-dextran
G	glycidyl
gelMA	gelatin-methacrylamide
HA	hyaluronic acid
HA-SH	thiol-functionalized hyaluronic acid
HEA	2-hydroxyethyl acrylate
hMSC	human mesenchymal stromal cell
HMW	high molecular weight
I2959	Irgacure 2959: 2-hydroxy-1-[4-(hydroxyethoxy)-phenyl]-2-methyl-1-propanone
IPN	interpenetrating polymer network
IR	infrared

LIFT	laser-induced forward transfer
LMW	low molecular weight
M_n	number-averaged molar mass
M_w	weight-averaged molar mass
MA-HA	methacrylated HA
MWCO	molecular weight cut-off
NMR	nuclear magnetic resonance
PBS	phosphatem buffered saline
PCL	poly(ε-caprolactone)
PEG	poly(ethylene glycol)
PEG-DA	diacrylated PEG
PEG-DMA	dimethacrylated PEG
PG	poly(glycidol)
$PG\text{-}SH_{ec}$	ester-containing thiol-functionalized poly(glycidol)
$PG\text{-}SH_{ef}$	ester-free thiol-functionalized poly(glycidol)
rt	room temperature
SEC	size exclusion chromatography
SR	swelling ratio
TCEP	tris(2-carboxyethyl)phosphine hydrochloride
THF	tetrahydrofuran
*p*TsOH	*p*-toluenesulfonic acid monohydrate
UV	ultraviolet

Chapter 1

Introduction and aim of the thesis

Tissue Engineering and Regenerative Medicine already aim to regenerate living tissues since the last century and thereby try offer treatment options for organ failures or congenital defects.[1, 2] In recent years the newly emerging field of Biofabrication holds great promise to improve the outcome by creating better hierarchical constructs to engineer tissue analogues.[2] Three-dimensional (3D) bioprinting, one of the main approaches within this emerging field, enables the computer-controlled deposition of cells and biomaterials, termed as bioinks, to create biologically functional 3D constructs of cells and materials. The deposition of these bioinks occurs in a layer-by-layer fashion, which allows the generation of more exact hierarchical tissue-like structures.[1, 3]

The printable formulation of cells and biomaterial is also termed bioink. Deposition of these bioinks occurs in a layer-by-layer fashion, which allows the generation of hierarchical tissue-like structures.[4-6] This simultaneous deposition of cells and biomaterials through automated processes makes 3D bioprinting a promising technology for the research field of tissue engineering and regenerative medicine. However, progress in the field is hampered due to the lack of suitable bioinks. Since bioinks need to meet a number of partially contradictive demands, the development of these inks is extremely challenging. They have to be printable at cell friendly conditions with high shape fidelity and at the same time be cytocompatible and support cell survival and activity.[1, 3, 7, 8]

Hydrogels, 3D cross-linked hydrophilic polymer networks, are broadly used as bioinks, as they allow encapsulation of cells in an environment similar to the natural extracellular matrix (ECM).[1, 3, 7, 9-12] Hydrogels can be based on natural polymers such as alginate[13, 14], gelatin[15-17] and hyaluronic acid (HA)[18-21] or on synthetic polymers such as poly(ethylene glycol) (PEG)[22].[23] Linear poly(glycidol) (PG), a functional structural analog of PEG, represents an attractive alternative to PEG as it allows for multiple side-chain functionalization.[24-26] In general, polymers of both origins feature different benefits as well as drawbacks. The main advantage of natural polymers over synthetic ones is their inherent biocompatibility, whereas synthetic polymers benefit from their molecular tailorability, which enables the reproducible fabrication of hydrogels with pre-determined properties. To combine the advantages provided by natural and synthetic polymers, hybrid hydrogels can be prepared, which include both polymer types. Furthermore, synthetic polymers can be endowed with biological active moieties to overcome their bio-inert nature.[11, 27, 28]

In addition to the polymer origin, the cross-linking mechanism has a strong influence on hydrogel properties, especially on the stability and shape fidelity of the printed constructs. Physical cross-linking results in hydrogels with weak, noncovalent bonds, which are ideal for the printing process, but are usually insufficient for the production of stable constructs. Therefore, most printed hydrogels are additionally stabilized by chemical post-processing cross-linking.[1, 3] Photo-induced reactions are widely used for chemical cross-linking as they provide fast network formation directly after printing and facile control over the spatiotemporal formation of the gel.[29, 30] The most prominent approach for photo-fabrication is the free-radical polymerization of (meth-)acrylate functionalized polymers.[16, 21, 31-33] However, the random chain-growth mechanism of this reaction involves several drawbacks, such as fabrication of heterogeneous hydrogel networks with undefined degradation products and oxygen inhibition.[34] In contrast, the photo induced thiol-ene reaction, a dimerization reaction between thiol-groups and double bounds, occurs through a step-growth mechanism. Even though thiol-ene chemistry provides advantages over free-radical polymerization such as no oxygen inhibition and more homogenous networks due to dimerization, it is yet rarely applied in the field of biofabrication.[34]

Therefore, **the major aim of this thesis** was to develop thiol-ene cross-linked hydrogels based on functionalized PG and HA as bioinks for extrusion-based 3D bioprinting. The established hydrogels should provide adequate mechanical properties and support chondogenesis of embedded cells as a potential application for cartilage regenerative purpose, which was further evaluated in detail by cooperation partners within the EU-project HydroZONES[I]. Two different thiol-ene cross-linked hydrogel systems (synthetic and hybrid) were established and compared concerning physical properties, printability and biological applicability.

Thiol-ene reaction was also used for the selective functionalization of PG with peptides. Subsequently, the formation of physical cross-linked hydrogels with these polymers was investigated in a proof of principle study. This approach presents a photo-independent alternative cross-linking method and demonstrates the direct incorporation of biomolecules into synthetic polymers.

[I] Seventh Framework Programme FP7/2007-2013 under grant agreement n°309962.

The present work is structured as follows:

Chapter 2 is devoted to a literature review of hydrogels for 3D bioprinting. First, there is an insight into the different bioprinting technologies as well as into the desired requirements bioinks have to meet (**chapter 2.1**). Subsequently, in **chapter 2.2**, the characterizations and classifications of hydrogels are described, including the different cross-linking mechanisms. Lastly, **chapter 2.2.3** focuses on polymers of different origin used for hydrogel formation in the field of biofabrication. Especially the polymers HA and PG, which were used throughout this thesis as precursor polymers for hydrogel preparation, are presented and compared to widely applied polymers.

In **Chapter 3** the results of this thesis are presented and discussed. It is divided into polymer synthesis (**chapter 3.1**), thiol-ene cross-linked hydrogels (**chapter 3.2**) and hydrogels cross-linked via ionic interactions (**chapter 3.3**).

Chapter 3.1 deals with the synthesis and analysis of polymers for hydrogel formation, including allyl- and thiol-functionalized PGs and thiol-modified HAs for thiol-ene cross-linked hydrogels, as well as peptide-functionalized PGs for hydrogel cross-linking via ionic interactions. For thiol-ene cross-linked hydrogels, three different thiol-modified precursor polymers were synthesized, including synthetic ester-containing PG-SH ($PG\text{-}SH_{ec}$), ester-free PG-SH ($PG\text{-}SH_{ef}$) and the natural polymer based HA-SH. All three were thoroughly analyzed and compared. Especially, the topic of batch-to-batch variations of functionalized HA (HA-SH) was explored. The chapter closes with the peptide functionalization of allyl-functionalized PGs via thiol-ene reaction and their analysis.

Chemically cross-linked hydrogels via UV-induced thiol-ene reaction, are the subject of **Chapter 3.2**. The chapter comprises the formation, characterization and printing of these hydrogels. To investigate the physical properties of the gels, swelling profiles, mechanical compression tests and diffusion experiments were conducted. Moreover, extrusion based 3D bioprinting of the developed hydrogels is evaluated, including hydrogel only and double printing with reinforcing poly(ε-caprolactone) PCL.

In **Chapter 3.3** the suitability of peptide-functionalized PG for physically cross-linked hydrogels was investigated. For this purpose, the physical interaction between peptide-functionalized PG and high molecular weight (HMW) HA were examined by rheological measurements.

In **Chapter 4**, the results of this thesis are summarized in German and in English.

Lastly, the experimental section, **Chapter 5**, provides detailed information about each experiment carried out throughout this thesis. This includes precise descriptions of all applied methods as well as synthesis instructions and characterization of the polymers.

In the **Appendix** the biological examination, more specifically, the cell survival and chondrogenic differentiation of embedded human mesenchymal stromal cells (hMSCs), is discussed to determine the suitability of these hydrogels for cartilage regeneration.

Chapter 2

Theoretical background

Parts of this chapter have previously been published and are adapted with permission from:

S. Stichler, T. Böck, N. Paxton, S. Bertlein, R. Levato, V. Schill, W. Smolan, J. Malda, J. Teßmar, T Blunk, J. Groll, Double printing of hyaluronic acid/poly(glycidol) hybrid hydrogels with poly(ε-caprolactone) for MSC chondrogenesis, *Biofabrication* **2017**, doi: 10.1088/1758-5090/aa8cb7.

S. Stichler, S. Bertlein, J. Teßmar, T. Jüngst, J. Groll, Thiol-ene Cross-Linkable Hydrogels as Bioinks for Biofabrication, *Macromol. Symp*. **2017**, *372*, 102-107.

S. Stichler, T. Jüngst, M. Schamel, I. Zilkowski, M. Kuhlmann, T. Böck, T. Blunk, J. Teßmar, J. Groll, Thiol-ene clickable poly(glycidol) hydrogels for biofabrication, *Ann. Biomed. Eng*. **2017**, *45*, 273-285.

2.1 3D bioprinting

2.1.1 Bioprinting techniques

The most widespread bioprinting technologies can be subdivided into three groups including laser-based, inkjet-based and extrusion-based bioprinting (Figure 1).[1, 3, 8, 35] Each of these techniques has limitations and benefits and the choice of the method depends on the desired scaffold size, architecture and resolution as well as on the applied bioink.

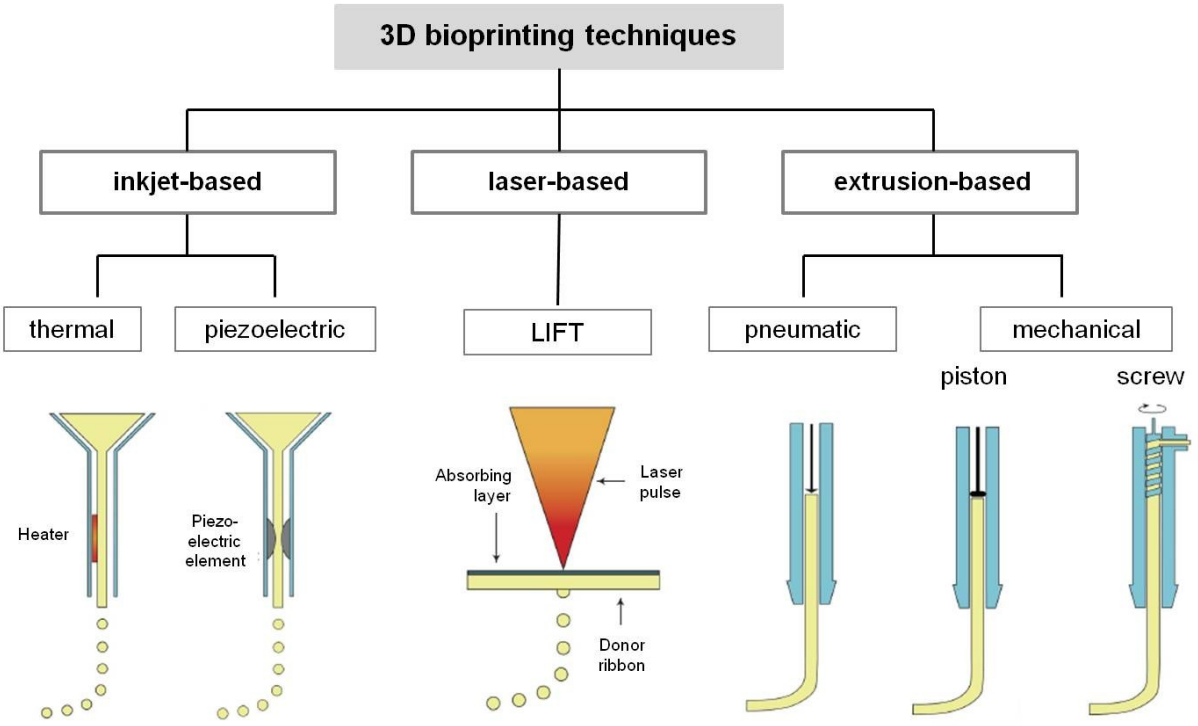

Figure 1: Overview of the three most common bioprinting techniques: inkjet- (left), laser- (middle) and extrusion-based (right) bioprinting. Adapted from literature[8], Copyright © 2016 IOP Publishing Ltd.[II]

Inkjet-based bioprinters dispense droplets of the bioink through a small orifice onto a collector substrate (Figure 1, left).[8] Thereby, the droplets can be either generated by thermal or piezoelectric stimulation. The thermal inkjet system comprises a micro-heater, which locally vaporizes the bioink and thus triggers a pulse that expels droplets from the nozzle tip, whereas in piezoelectric systems a piezoelectric element

[II] This work is licensed under the Creative Commons Attribution 3.0 Unported License. To view a copy of this license, visit http://creativecommons.org/licenses/by/3.0/ or send a letter to Creative Commons, PO Box 1866, Mountain View, CA 94042, USA.

is included which causes an acoustic wave that pushes small droplets through the nozzle.[1, 8, 36] Due to the small orifice diameters this technology is limited to the use of bioinks with low viscosities (3.5-12 mPa s).[3] Bioinks with higher viscosities will led to clogging of the nozzle. Furthermore, the deposition of small droplets is the main bottleneck for the fabrication of larger constructs.

For laser-induced forward transfer (LIFT) three major components are needed: a pulsed laser, a donor slide (ribbon) covered with a laser energy absorbing layer and a layer of bioink and a receiving substrate (Figure 1, middle).[8] The pulsed laser beam is focused onto the donor substrate and causes local evaporation of the absorbing layer and thereby creating a high gas pressure propelling the bioink to the collection plate. Thus, LIFT enables the fabrication of 3D structures with high accuracy by nozzle-free deposition of bioinks via droplets. The nozzle-free nature of this technique has the advantage that it is not affected by clogging issues and shear stress. Nevertheless, the low overall flow rate and thus the long fabrication time hamper the fabrication of constructs in mm range.[1, 3, 8]

Extrusion-based bioprinting, also referred to as robotic dispensing, is the most wide spread method to fabricate cell-laden scaffolds. For this technique, the bioink is loaded into plastic syringes or reservoirs and dispensed through a nozzle onto a collector plate via pneumetic or mechanical-driven dispensing (Figure 1, right).[8] In contrast to other techniques, extrusion-based printing is based on the dispensing of continuous bioink filaments instead of droplets. The resolution, in the sence of fibre diameter, is thus directly related to the diameter of the nozzle. With a nozzle size from 20 µm to mm range, the resolution achieved by this technique is the lowest among all the presented methods. The printing of bioink strands is possible with high fabrication speed which enables the production of constructs of clinically relevant sizes within short time frames.[1, 3, 8]

The different driving mechanisms of dispensing have particular benefits as well as disadvantages. An advantage of piston-driven over pneumatic-driven systems is the direct control over the flow of the bioink. In pneumatic-based systems this control is lowered by the delay of the compressed gas volume. The mechanically-based screw-driven system can generate higher pressures and is thus used for materials

exhibiting higher viscosities. However, these high pressures simultaneously generate high shear stress which can be harmful for embedded cells. Pneumatic-driven deposition is known to be the most versatile extrusion-based printing technique, since it enables the printing of various bioinks with a wide range of viscosities, due to the adjustable air pressure.[1, 3, 8, 35]

Table 1 summarizes the key characteristics of the three different printing techniques.[3] Depending on the viscosity of the bioink and the desired resolution as well as construct size, a particular technique is preferred to be applied.

Table 1: Comparison of the three different bioprinting techniques. Adapted with permission from literature[3], Copyright © 2015 American Chemical Society.

	laser-based	**inkjet-based**	**extrusion-based**
viscosity bioink[6, 37-40]	1 - 300 mPa s	3.5 - 12 mPa s	30 - 6 x 10^7 mPa s
resolution[41-44]	10 – 100 µm	~ 75 µm	100 µm to mm range
nozzle size[44-46]	nozzle free	20 – 150 µm	20 µm to mm range
fabrication time	long	long – medium	short
commercially available[35]	no	yes	yes

2.1.2 Bioink requirements for extrusion-based bioprinting

Developing bioinks is known to be the most challenging aspect in the field of bioprinting, as bioinks need to fulfill a number of often contrary requirements: on the one hand they have to support cell survival and differentiation and on the other hand they have to meet the physical and mechanical demands of the printing process.[1, 7]

The key properties of bioinks and their effect on printability, construct stability and cell performance are summarized in Figure 2.[1, 7] It shows the individual impacts of each property as well as reveals the interlinking between the different characteristics.

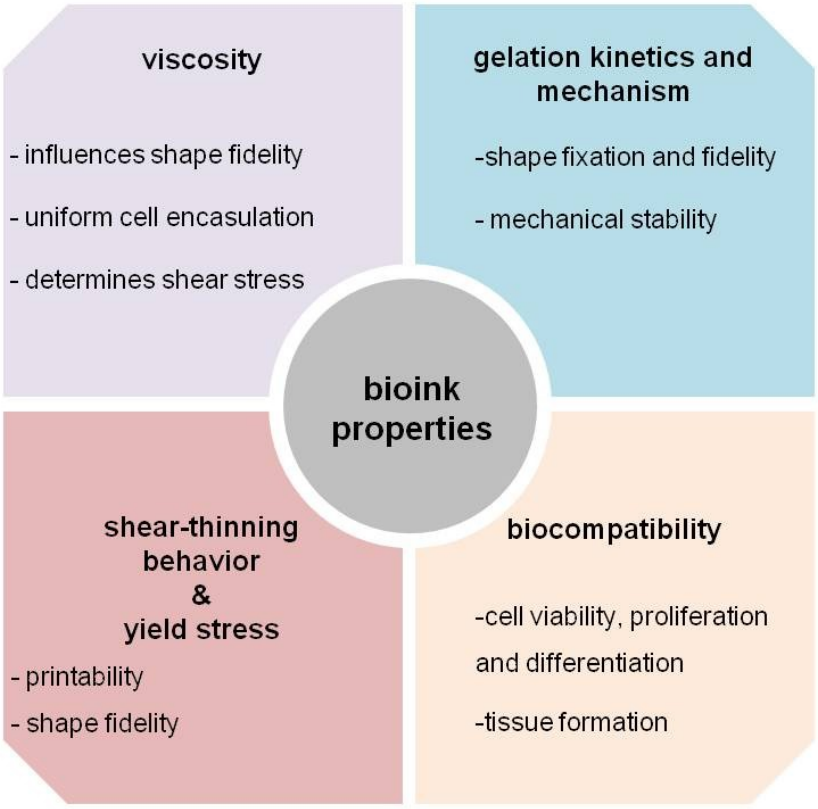

Figure 2: Bioink key properties and their effects. Figure idea adapted from literature[7], Copyright © 2016 Biomedical Engineering Society.

Since hydrophilic polymer networks, so-called hydrogels, are most commonly used as bioinks (**chapter 2.2**), the following property descriptions focus on these materials.

2.1.2.1 Rheological requirements

Viscosity, shear-thinning behavior and yield stress of the bioink are determing factors for printability. In extrusion-based printing, the viscosity of the ink must be high enough to enable formation of continous strands instead of droplets at the nozzle. Viscosity of polymeric solution depends mainly on the polymer concentration and molecular weight.[1]

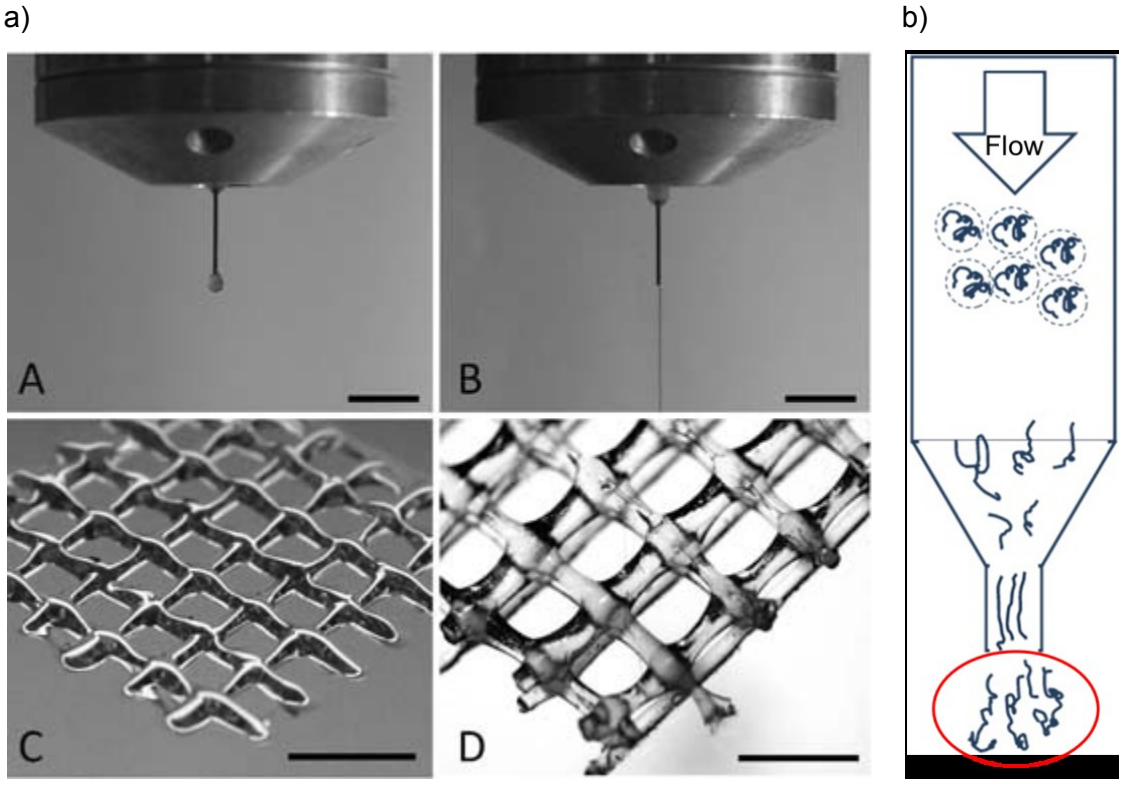

Figure 3: a) 3D Printing of gelMA with (B) and without (A) additional HMW HA demonstrating the influence on strand formation (A + B) and shape fidelity of printed constructs (B + C),[16] Copyright © 2013 John Wiley & Sons, Inc. b) Shear profile of polymeric chains during extrusion-based printing,[47] Copyright © 2017 John Wiley & Sons, Inc.

The influence of viscosity on strand deposition and printing fidelity was demonstrated for gelatin-methacrylamide (gelMA) hydrogels (Figure 3a).[16] By increasing the viscosity of the gelMA (20 %) bioink with addition of 2.4 % high molecular weight (HMW) hyaluronic acid (HA), filaments could be printed, resulting in scaffolds with high shape-fidelity. In contrast, the low-viscosity gelMA solution could only be deposited in droplets. The direct relation between increasing viscosity and increasing printability as well as printing fidelity was also shown for dextran based hydrogels.[31]

However, when adjusting the viscosity to achieve printability, the influence of the viscosity on cells has also to be considered. A certain viscosity is desired to ensure an even distribution of cells, nevertheless, too high viscosities increase the shear stress during printing and hamper the survival and matrix formation of included cells.[1, 48-50]

In addition to viscosity, the shear-thinning behavior of the bioink material is of importance for printability. Shear-thinning is described as the decrease in viscosity by increasing shear rate.[51] In polymeric solution, the increase in shear rate usally leads to a reduced entanglement and an alignment of the polymer chains in the direction of the flow and hence a reduced viscosity (Figure 3b).[47] After the polymer solution leaves the nozzle tip, the shear stress decreases and the polymer chains start to relaxate. Thereby, the re-gelation process has to be fast enough to ensure shape fidelity of the printed construct.[15, 47] Like in the case of viscosity, the shear-thinning behavior of polymeric solutions also depends on the concentration and molecular weight of the polymers. It was shown for alginate solutions and dextran based hydrogels that solutions with higher polymer concentrations or molecular weights feature a stronger shear-thinning behavior, demonstrated by an increased relative reduction in viscosity.[31, 52]
Additional to the shear-thinning behavior the yield stress is an important parameter for bioink development, as it describes the minimum stress which has to be applied to initiate material flow. Below the yield stress the material is form stable, so that after the applied stress the material is able to recover again.[1, 53] In summary, these rheological properties provide information about printability and shape fidelity of the bioink.

Paxton *et al.* recently published a proposal to assess printability of bioinks including the use of these rheological measurements.[54] They introduce a two-step method which helps to develop printable inks without the need of a bioprinter (Figure 4). The two steps are divided into a first initial screening (Figure 4, 1.) followed by a rheological evaluation of the bioink (Figure 4, 2.). The initial screening, a manual dispensing of the solutions through a syringe, provides information about the ability of the material to form strands and can be related to the viscosity of the polymer solution. In addition to the aforementioned flow initiation (yield stress) and shear

thinning behavior a rheological recovery test is examined. The alternation between high and low shear rates mimic the applied shear conditions during and after printing and hence gives information about the post printing recover abilities of the solution.[54]

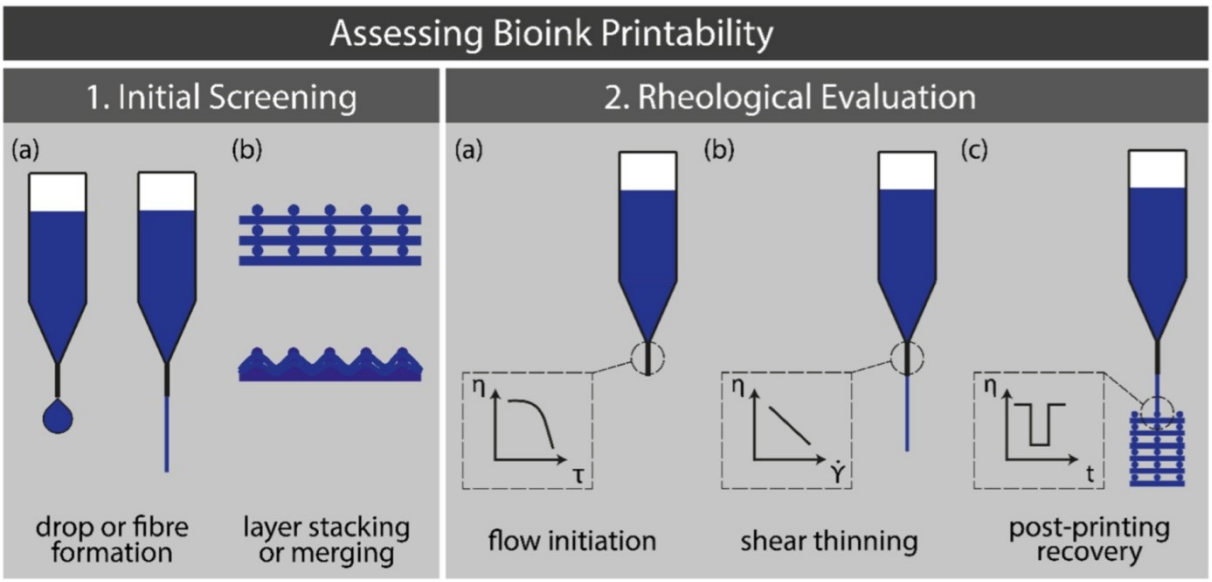

Figure 4: Two-step approach to assess printability of a bioink.[54] initial screening (1.) and rheological evaluation (2.), including a shear stress ramp (2a), a shear viscosity (2b) test and a recovery test (2c), Copyright © 2017 IOP Publishing Ltd.[III]

2.1.2.2 Mechanical requirements

In addition to rheological properties which mainly influence the printability of the ink, the bioink needs to fulfill mechanical requirements to ensure post-printing stability of the construct. After printing of the bioink, the shape fidelity as well as sufficient mechanical stability of the construct should be ensured. To achieve shape fidelity with high resolution, the bioink has to feature rapid re-gelation. However, fast re-gelation and high viscosity of the polymeric solution are not enough for obtaining stable constructs, since without further stabilisation all solutions will eventually collapse. Therefore, the structure of the printed construct has to be further stabilized.[1, 3]

[III] This work is licensed under the Creative Commons Attribution 3.0 Unported License. To view a copy of this license, visit http://creativecommons.org/licenses/by/3.0/ or send a letter to Creative Commons, PO Box 1866, Mountain View, CA 94042, USA.

One possibility is the stabilization through post-fabrication cross-linking of the gels. As the mechanical strength of the resulting gels is mainly dependent on the type of cross-linking and the cross-linking density, the stiffness of the gels can be tailored by selection of these parameters.[11] In general, chemical cross-linking introduces irreversible covalent bonds into the network and thus provides stiffer gels compared to physical cross-linking (more detailed information about the different cross-linking methods are given in **chapter 2.2.2**). Additional, by increasing the cross-linking density, the stability of the construct can be further improved.[1, 3]

Although the type of cross-linking and the network density can control the stability of the printed gel, their influence on the biological properties must also be considered. A highly cross-linked gel indeed provides high shape fidelity, but, simultaneously limits the activity of embedded cells. This discrepancy between desirable mechanical and biological properties is expressed by Figure 5, which depicts the direct influence of network density/polymer concentration on cell performance and shape fidelity. The biofabrication window contained therein indicates the cross-linking density, which presents a compromise between mechanical and biological properties.[1]

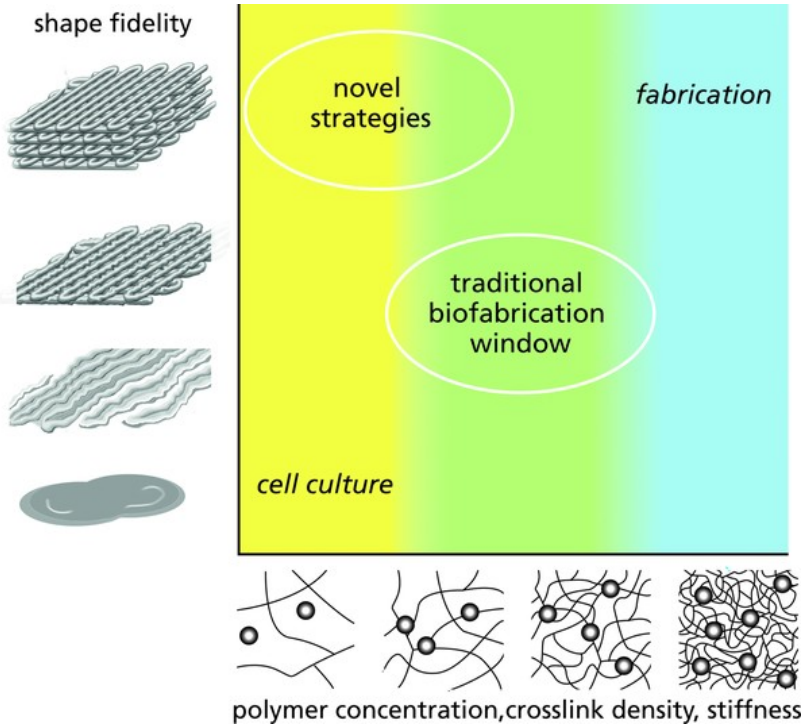

Figure 5: Influence of network density and polymer concentration on shape fidelity and cell activity,[1] Copyright © 2013 John Wiley & Sons, Inc.

In order to overcome this compromise and to allow fabrication of constructs with high shape fidelity combined with high cell activity, reinforcement strategies have been developed.

There are several reinforcement approaches, including interpenetrating polymer networks (IPNs)[55-57], and a special subgroup of IPN, the double networks (DNs)[58-60], as well as reinforced gels which are double-printed, meaning alternating printing of hydrogel solution and thermoplastic polymers[61-63]. It has been demonstrated that IPN and DM networks have enhanced mechanical strength compared to the single component networks and furthermore allow the fabrication of robust hydrogels.[7, 57] The IPN hydrogel developed by Hong *et al* which comprises a covalently cross-linked PEG and an ionically cross-linked alginate gel is a nice example of a tough, printable hydrogel.[57] Besides printability, they proved the cytocompatibility of their IPN gel, however, the direct printing of cells in these robust gels was not demonstrated.
Reinforcing methods with thermoplastics offers an alternative to the printing of dense networks or solutions with high polymer concentrations. The thermoplastic polymer poly(ε-caprolactone) (PCL) is mainly used for this approach. Alternating double printing of PCL and hydrogel results in two-component constructs. Thereby, the thermoplastic PCL offers the mechanical stability and the hydrogel fulfils the biological demands.[16, 61] In contrast to hydrogel only printing, this technique enables the printing of hydrogels with lower polymer concentration while simultaneously resulting in robust scaffolds. It is extremely useful for applications which require scaffolds with high mechanical strength. Nevertheless, this strategie is also challenging as the hydrogel solutions are printed between the PCL strands and thus are wetting the attached thermoplastic fibres. High wetting of PCL fibres hamper the attachement of the subsequent PCL layer.

2.1.2.3 Biological requirements

In addition to rheological and mechanical requirements, the bioink has to fulfill biological demands. It has to provide an interactive environment for the encapsulated cells, supporting cell viability and cell function. The extent of cell adherence, migration and viability is dependent on, amongst other things, the aforementioned viscosity and cross-linking density of the hydrogels. Thereby, a compromise between

homogeneous cell distribution without cell sedimentation and ideal matrix stiffness regarding cell viability and permissivity allowing matrix remodeling has to be found.[1, 7] Furthermore, especially the origin of the used polymers has a great effect on the biological properties of the hydrogels.[64, 65] The benefits and disadvantages concerning biological and chemical aspects of natural and synthetic derived polymer building blocks are further discussed in **chapter 2.2.3**. In general, synthetic polymers lack intrinsic bio-functionality compared to natural polymers. In order to increase the intrinsic bioactivity of hydrogels, different bio-functionalization strategies have been applied[64-67], for example the the incorporation of biological cues such as growth factors[68-70] and peptides[68, 71]. The effects of these incorporated molecules were demonstrated for different gel systems, for instance for poly(ethylene glycol) (PEG) hydrogels. Functionalization of these bioinert gels with the most frequently implemented peptide arginine-glycine-aspartic acid (RGD), a cell-adhesion sequence, derived from fibronectin, allowed for cell adherence and thus demonstrated the influence of such peptides on the biological properties of synthetic hydrogels.[64, 68, 71]

When the incorporated cells start to remodel the hydrogel matrix and to produce ECM the hydrogel properties are changed. An increased hydrogel stiffness after cell encapsulation is an indication for high ECM production of the cells.[8] Several studies as well as theoretical models investigated the relation between cell density and mechanical stiffness of hydrogels to allow a prediction of hydrogel properties with active cells.[8, 72-76] However, the different studies use various protocols and cell types which makes it difficult to give a general statement about the influence of cells on mechanical properties.

Besides the already mentioned parameters the biological suitability of the printing process and of the cross-linking mechanism must be ensured as well. Regarding the printing process, the temperature should be within a cell friendly range and shear stress should be limited to a minimum.[77] Furthermore, it must be ensured that the cells are not harmed by toxic by-products or UV irradiation of the cross-linking mechanism. This aspect will be highlighted again in the discussion of the different gelation mechanisms in the following chapter.

2.2 Hydrogels

Hydrogels are 3D networks of cross-linked hydrophilic polymers that can trap high amounts of water without dissolution of the polymer network.[27, 78] The polymeric origin and the cross-linking mechanism have a pronounced influence on the hydrogel characteristics. In this chapter first the major properties of gels are summarized (**chapter 2.2.1**) and subsequently the different cross-linking mechanisms (**chapter 2.2.2**) and hydrogel sources (**chapter 2.2.3**) are reviewed.

2.2.1 Major hydrogel properties

There are a lot of different approaches to characterize hydrogels and depending on the application of the specific hydrogel different properties are of major interest. In this chapter the important hydrogel characteristics are discussed, namely mechanical properties and swelling behavior.

2.2.1.1 Mechanical properties

The mechanical stiffness of hydrogels, the so-called Young's modulus, provides information about the network density, meaning the cross-linking degree, of a hydrogel and can be determined by mechanical testing, such as compression tests (unconfined or confined). In general, a higher cross-linking degree results in stiffer gels. Through compression testing, load-displacement data is obtained which can be converted to stress-strain data. The Young's modulus is then given by the slope of the stress-strain curve in the linear elastic range of hydrogel. For hydrogels the Young's modulus is in the range of kPa.[79-81] In these compression measurements, hydrogels are placed between to plates and compressed.[79-81] Thereby the most challenging part is the fixation of the gels, as it has to be ensured that the hydrogels cannot slip out of the testing plates. To overcome this issue, different fixation methods have been applied, such as enhancing the sample grip with double-sided tape and glue.[79, 82] Furthermore, care must be taken that the gels do not dry out during measurement, as the water content of gels has a significant influence on their mechanical stiffness.[80]

Oyen reported on the difficulty to compare mechanical stiffness data of hydrogels of the same composition in literature.[79] He showed a data comparison for a 2 % agar

gel that ranged from values of 1 to 300 kPa and thereby emphasized the challenge in the field of mechanical measurements of hydrogels. The challenge is on the one hand the measurement itself (fixation and hydration state of the gel) and on the other hand the interpretation of the data (slope of the linear range is variable). In literature, most mechanical tests are conducted without almost any calibration or verification of the testing method with standards and no standard protocols are used for hydrogel measurements.[79] Therefore, when comparing hydrogel Young's moduli it has to be ensured that the values were determined by using the same measurement setting and conditions.

2.2.1.2 Swelling behavior

In swelling studies information about the hydrogel structure can be obtained. In Figure 6 the hydrogel network is depicted, showing the hydrogel characteristics, mesh size ξ and average molecular weight between two cross-linking points $\overline{M}_c$. The mesh size is defined as the distance between two cross-linking points and also referred to as pore size.[27, 78, 79] Throughout this thesis only the term mesh size is used and describes the free diffusional space for molecules through the hydrogel network.[78]

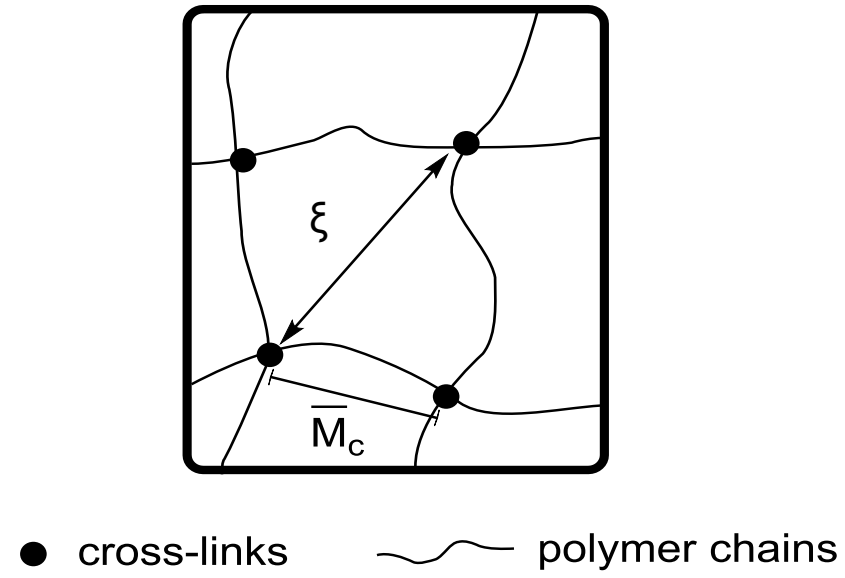

Figure 6: Hydrogel structure ξ with mesh size and average molecular weight between cross-links $\overline{M}_c$. Figure according to literature.[27]

Additional to the mesh size and the average molecular weight between cross-links, the polymer volume fraction in the swollen state (v_{s2}) is an important factor to characterize a hydrogel network. It is defined as the ratio of the polymer volume to the volume of the swollen gel and is the reciprocal of the swelling ratio (SR).[27] In swelling measurements, the hydrogel is incubated into a solution and the equilibrium swelling, meaning the stable mass of the gel over time, and the maximum water uptake are determined.[27, 78] When drying the gels, the SR is accessible by the following equation: $SR = W_s / W_d$ (equation 1), with W_s: swollen weight of the gel and W_d: dry weight of the hydrogel.[20, 21] Whereby, an increased SR indicates a higher swollen network and thus a less dense network.

The average molecular weight between cross-links $\overline{M}_c$ can be calculated by the Flory-Rehner theory as a function of v_{s2}.[83, 84] This theoretical method is not further discussed, since it includes several average values and material constants, such as average molecular weight and a polymer-water interaction parameter, which are difficult to match for not-uniform hydrogel networks, which are used throughout this thesis.[64] In order to compare the different hydrogels prepared the swelling ration SR is used instead to compare and describe the hydrogel networks.

The hydrogel mesh size stands in correlation with $\overline{M}_c$ and can be experimentally determined by diffusion measurements.[64, 85] In diffusion measurements, fluorescence-labeled molecules of known average molecular weight and thereby average size diffuse through the sample and thereby help to estimate the mesh size.[85] The determined mesh size allows to approximate the transport of small molecular weight substances, like nutrients, oxygen and waste products, but also high molecular weight substances, like growth factors or antibodies, in hydrogels during cultivation.

2.2.2 Cross-linking mechanism

Hydrogels are classically classified by their cross-linking mechanism or polymeric origin (Figure 7).[1, 27] In this chapter the different cross-linking methods, physical or chemical, are discussed, whereas the following chapter focuses on the polymer origin of the hydrogels.

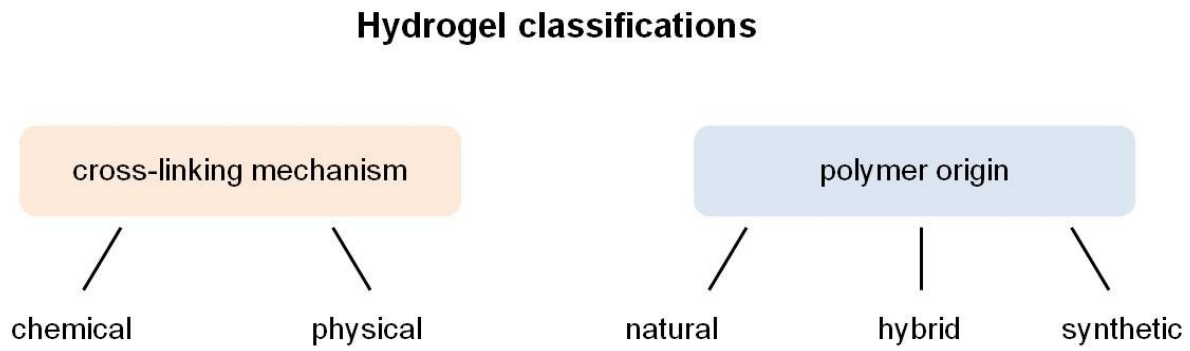

Figure 7: The two major classifications: classified by cross-linking mechanism and polymer origin (**chapter 2.2.3**).

2.2.2.1 Physical cross-linking

Physically cross-linked networks are formed by noncovalent bonds between polymer chains. These bonds can rely on different physical interactions such as hydrogen bridges, ionic interactions, hydrophobic interactions and entanglements of high molecular chains. Physical cross-links are dynamic and reversible which is of great benefit for 3D printing processes. Furthermore, physical gels are characterized by their mild gelation conditions and thus are known to feature excellent compatibility with biological cues and cells. Besides the positive effects of physical cross-linking on printing and bio-compatibility, the resulting gels lack mechanical stability, due to the weak physical interactions. For enhancing the stability of physical cross-linked gels the used precursor polymers can additionally be endowed with functional groups which enable chemical post-processing-cross-linking.[1, 3, 8, 27]

Ionic interactions

In the field of 3D bioprinting alginates, linear unbranched block copolymer of *β*-D-mannuronate (M) and *α*-L-gluronate (G), are frequently used as polymers for physical cross-linked hydrogels. Network formation of alginate hydrogels occur via ionic interactions between the anionic polysaccharide and divalent cations, usually Ca^{2+} (Figure 8a). Alginate hydrogels have already been applied as bioinks in a wide variety of extrusion-based printing studies.[14, 43, 61, 86-93] In the different studies, the polymer concentration was varied in the range between 1-10% (w/v). Bioinks with higher alginate concentrations result in better defined structures, nevertheless, the mechanical stability of these printed constructs decreased rapidly during culture.[3] The ionic interactions are sensitive to ionic changes in the culture medium and Ca^{2+}-ions can be washed out, which leads to this stability loss.

Besides the most prominent example of ionic cross-linked hydrogels, alginates, hydrogel formation via ionic interaction is also applied for other anionic polysaccharide, such as hyaluronic acid (HA).[94, 95] For example, Cross *et al.* established a hydrogel system based on HA and a synthetic cationic block co-polymer (Figure 8b).[95] In their study they investigated the influence of the cationic polymer structure (four-arm star or linear), the charge ratio (from 1:8 to 4:1, positive:negative charge) and the solvent (deionized water, isotonic glucose or phosphate buffer) on hydrogel formation. The mixtures of HA with linear poly(2-aminoethyl methacrylate) (PAEM) and PEG resulted in precipitation instead of hydrogels. Whereas, the hydrogel solutions of star shaped PEG and linear HA (1:1 charge ratio) in water or isotonic glucose resulted in robust gels. Due to the ionic interactions the selection of the solvent is critical for the hydrogel formation. Ionic interactions are shielded in ionic solutions by the ions of the solvent and thus the hydrogel can not be formed. On the one hand, the example of Cross *et al.* demonstrates the possibility of using HA in ionic gels and, on the other hand, shows that aspects as solvent, charge ratio and molecular shape of the polymers can have an important influence on hydrogel formation of such gels.

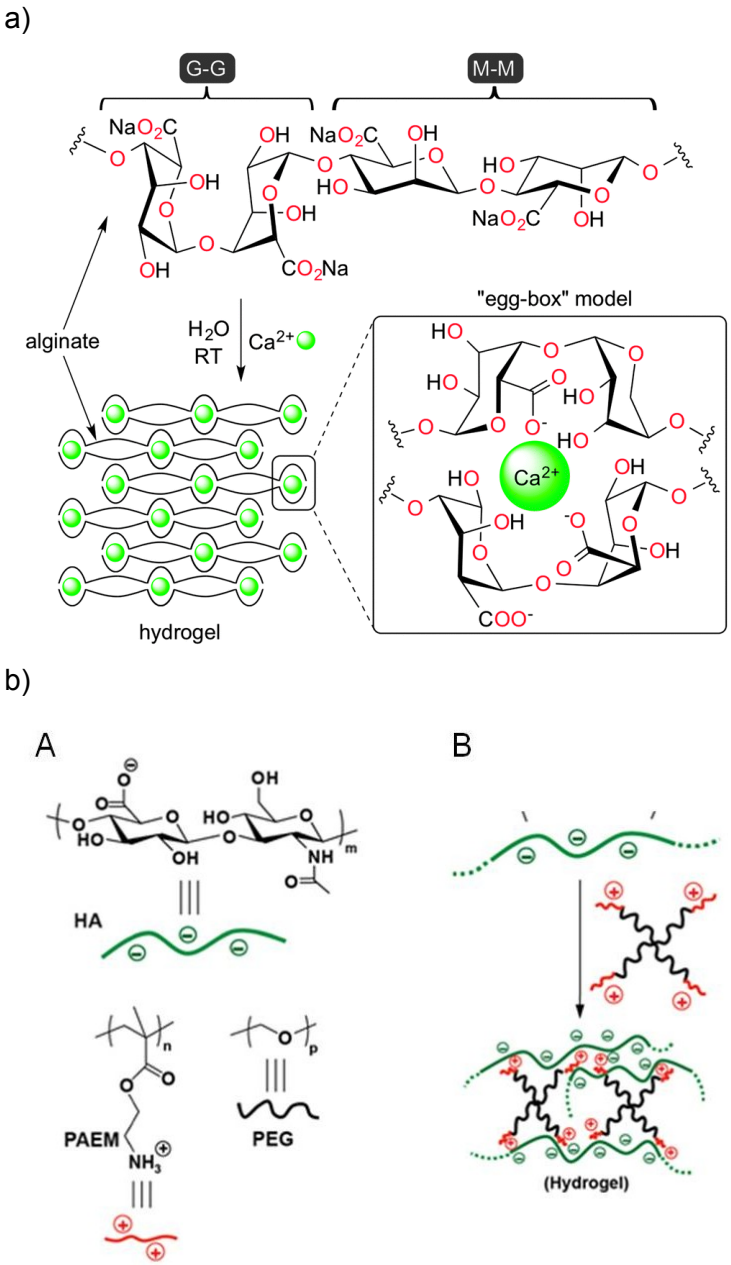

Figure 8: a) Network formation of alginate hydrogels by addition of Ca^{2+} cross-linker to alginate (Na-salt); the so-called “egg-box” model depicts the coordination of one Ca^{2+} to carboxylate and hydroxyl groups of four G monomers,[96] Copyright © 2015 The Royal Society of Chemistry and the Centre National de la Recherche Scientifique.[IV] and b) HA hydrogels cross-linked by cationic block co-polymers,[95] Copyright © 2015 John Wiley & Sons, Inc.

In summary, it can be said, that the physically cross-linked hydrogels feature beneficial characteristics for the printing process, however, as a consequence of their

[IV] This work is licensed under the Creative Commons Attribution 3.0 Unported License. To view a copy of this license, visit http://creativecommons.org/licenses/by/3.0/ or send a letter to Creative Commons, PO Box 1866, Mountain View, CA 94042, USA.

poor mechanical properties, they are often additionally stabilized by chemically cross-linking after printing.

2.2.2.2 Chemical cross-linking

Hydrogel network formation can also occure through covalent chemical cross-linking. Compared to physically cross-linked hydrogels, the hydrogel network formed by chemical cross-links is rather immobile, which might cause clogging issues during printing. Therefore, the chemical cross-linking is mainly applied after ink extrusion to enhance the mechanical strength of the printed constructs. To ensure shape fidelity, the post-processing cross-linking has to occur rapidly.[1, 8]

In principle, a wide variety of chemical reactions can be used for chemical cross-linking, but care must be taken that no toxic by-products are formed and no cytotoxic precursor polymers remain unreacted. In addition, it must be ensured that cells are not harmed by the reaction conditions. Commonly used chemical cross-linking reactions are, for example, Michael addition,[97, 98] native chemical ligation,[99, 100] click chemistry[101, 102] and photo reactions.[16, 30] Photo reactions proved to be extremely suitable for post-processing cross-linking either directly during or after printing, since they provide fast curing rates, often in the range of seconds. Another advantage of photo-induced reactions is, that they allow spatial control over cross-linking. These two features of photo-cross-linkable hydrogels make them attractive for their use in bioprinting.[29, 30, 34]

Photo reactions

The most widely applied photo reaction for hydrogel formation is the free radical photo-polymerization of (meth)acrlyated polymers.[17, 20, 30, 33, 53] The precursor solution includes a photoinitiator which creates free radicals upon ultraviolet (UV) (or visable) light exposure. These radicals initiate the polymerization by reaction with vinyl bonds of the precursor polymer. By reaction of the active species with additional precursor polymers, the network structure is formed through a random chain growth mechanism. This reaction implies several disadvantages, such as heterogeneous network formation, weak control over cross-linking kinetics, the formation of long undefined polymer chains and oxygen inhibition, meaning the reaction of free

radicals with airborne oxygen and thus termination of the reaction (Figure 9, left).[29, 30, 34, 103]

Radical-mediated thiol-ene reaction is an attractive alternative to the free photo-polymerization.[104, 105] Thiol-ene reactions rely on the addition of thiols to double bounds ('enes') which is triggered by photoinitiator radicals. Due to the step-growth mechanism of thiol-ene reactions more homogeneous hydrogel networks are obtained compared to the random chain growth mechanism (Figure 9, right). Another benefit of thiol-ene reaction is their lower oxygen sensitivity.[29, 34, 103, 106]

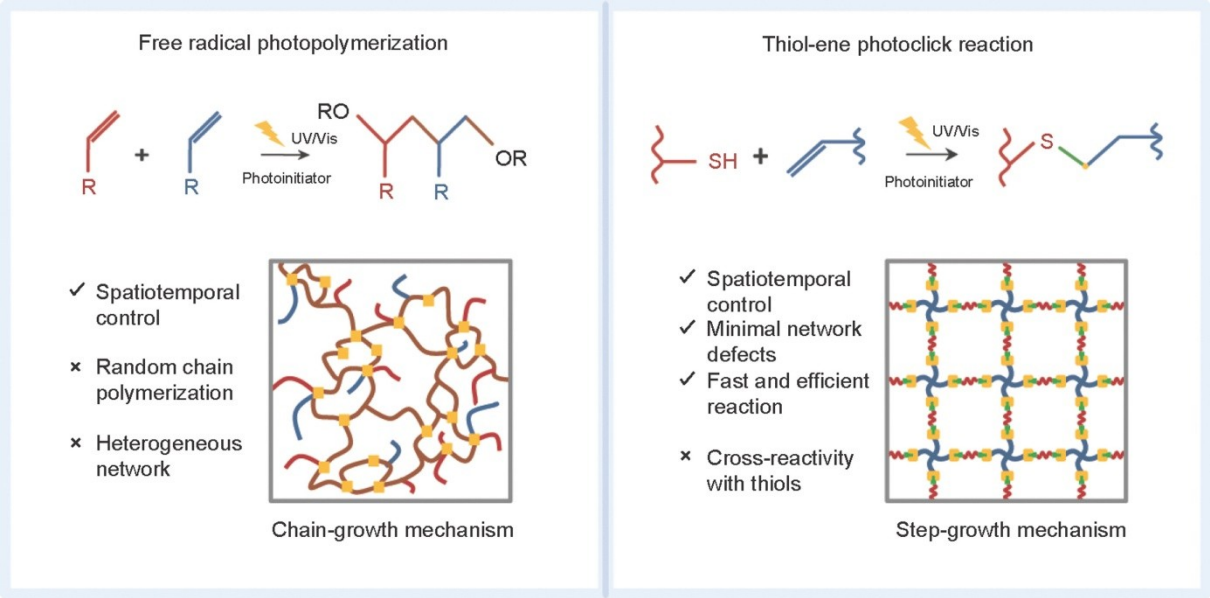

Figure 9: Comparison of two types of light-mediated cross-linking reactions: free radical photo-polymerization (left) and thiol-ene photo-click reaction (right),[34] Copyright © 2015 Higher Education Press & Engineering Sciences Press.

In studies comparing the two photo reactions, the different effects of the mechanism on the hydrogel properties could be demonstrated.[103, 107] Roberts *et al.* investigated the influence of the reaction mechanism on chondrogensis in PEG hydrogels. Their findings showed that chondrocytes embedded in thiol-ene hydrogels produced neo-tissue contain higher amounts of aggrecan and collagen II, indicating a more hyaline-like neo-tissue, compared to the tissue produced in free photo-polymerized hydrogels.[107] Furthermore, the formation of more homogeneous networks via step-growth thiol-ene reaction was substantiated by the studies of Tibbitt *et al.*.[103]

When using photo reactions for hydrogel formation including living cells, several aspects have to be considered. The exposure of cells to UV irradiation and free

radicals can potentially cause deleterious effects. Therefore, the reaction conditions must be carefully selected. Figure 10 depicts the key parameters of photo reactions, including wavelength, type of photoinitiator and photoinitiator concentration, irradiation intensity and time as well as cross-linking mechanism. Several studies investigated the influence of these parameters on cell viability and differentiation.[108-111] Even though the parameters have to be adjusted depending on the used system and cell type, some general statements can be concluded from literature.

The photoinitiator Irgacure 2959 (I2959) proofed to be well tolerated by a wide range of cell types and concentration (up to approximately 0.05 wt.%).[108-110] Furthermore, it was demonstrated that cells embedded in hydrogels are less harmed by free radicals and UV irradiation compared to cells in 2D culture.[110]

Both reactions were shown to be suitable for cell applications when selecting appreciate conditions and are therefore frequently used in tissue engineering approaches.[17, 105, 112-118] Yet, the free photo-polymerization is used significantly more often than the thiol-ene reaction.

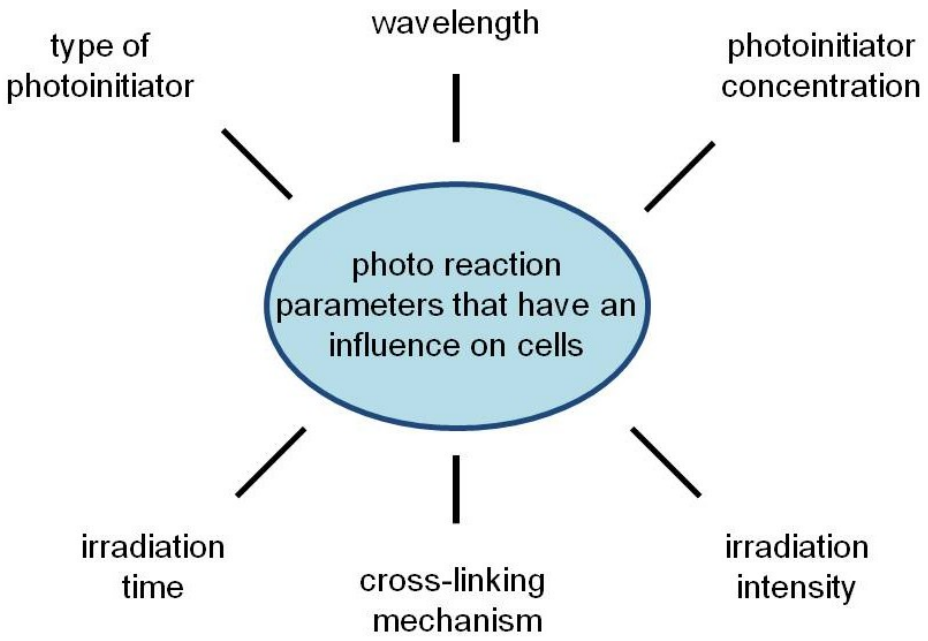

Figure 10: Overview of photo reaction parameters which have an influence on cells.

2.2.3 Polymer origin

For the formation of hydrogels, both synthetic and natural polymers as well as a combination of both are used. Hydrogels are therefore often classified based on their polymer origin as synthetic, natural or hybrid hydrogels. The gel properties, such as cytocompatibility, are decisively influenced by the selected polymers and can be adjusted with the polymer selection, among others.

2.2.3.1 Natural polymers

Due to the fact that naturally derived polymers provide inherent cytocompatibility and are readily available, they are widely used as hydrogel materials in biological applications. However, their origin also involves some disadvantages such as high batch-to-batch variations and potential risk of immunogenic reactions. Their batch variations can hamper the production of hydrogels with reproducible properties.[11, 65]
In the field of 3D bioprinting, alginate, gelatin[15] and HA[31] are the most frequently applied natural polymers.
Currently, a variety of research groups focus on the development of gelatin-based bioinks.[16, 17, 119, 120] For example in the study of Melchels *et al*., they combine physical cross-linking (ionic) of gellan gum with post-processing chemical photo cross-linking of the methacrylic groups of gelMA.[15] Through the photo cross-linking of the printed gelMA, constructs with high shape fidelity were obtained.[16] It was also demonstrated that embedded cells survive the printing as well as the cross-linking process.[15, 17]

Hyaluronic acid (HA)

HA, also referred to as hyaluronan, is a non-sulfated, anionic linear polysaccharide which is already clinically used for more than thirty years. Under physiological conditions, almost all HA molecules are present as salts, so-called hyaluronates, meaning the carboxylic groups of the HA monomers are present as ions and conjugated with Na^+ (Scheme 1). In general, the term HA is used for the salts as well as for the free acid HA, including different counterions as well as all degrees of dissociation. HA is an essential component of the ECM and is biodegradable in mammals by hyaluronidase. Moreover, it is available in a wide range of molecular weights up to several MDa.[18, 121]

In general, the functional groups of HA, including the hydroxyl groups, the carboxylic acid and the *N*-acetyl group, allow the chemical modification of HA. However, the introduction of a variety of different functional groups, such as thiols[122] and aldehydes[123] occurs mainly via chemical modification of the carboxylic acid and the primary hydroxlýl group. These functionalized HAs can be used for a wide range of different cross-linked hydrogels (Table 2).

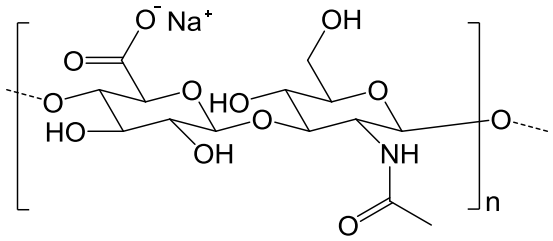

Scheme 1: Molecular structure of the HA Na-salt.

Table 2: Different HA modifications and their application as cross-linkers in hydrogels.

introduced functional group in HA	**cross-linking reaction**	**reference**
thiol	Michael addition	124
	oxidation	122
aldehyde	Schiff-base reaction	123
azide/alkyne	click chemistry	102
methacrylate	free radical photo reaction	20, 21
norborene	thiol-ene photo reaction	105
furan	Diels-Alder reaction	19

Furthermore, HA has already proven to be suitable for the use in 3D bioprinting: on the one hand as thickening agent[16] to adjust the viscoelastic properties of bioinks (**chapter 2.1.2.1**) and on the other hand as a cross-linkable bioink[31, 32]. As bioink, photo-cross-linkable methacrylated HA (MA-HA) is predominantly used. Different studies investigated MA-HA bioinks combined with gelMA.[32, 125] For example, Skardal *et al.* demonstrated cyto- and biocompatibility as well as the 3D bioprinting suitability of their MA-HA/gelMA hydrogel system.[32]

Taken together, HA is one of the most applicable polymers for bioink development as it combine excellent biological properties with an extensive chemical tunability.

2.2.3.2 Synthetic polymers

Besides natural polymers, synthetic polymers are also used as hydrogel precursors. The use of synthetic polymers for hydrogel formation is an attractive alternative to natural polymers, as they are better characterized and thus enable the production of hydrogels with highly adjustable properties in a reproducible manner. The possibility to produce hydrogels with controlled properties relies on the fact that synthetic polymers can be molecularly tailored. Molecular changes, such as functionality and chain length, have a direct influence on the gel properties.[27, 28]
The bio-inert nature of synthetic polymers can be changed by modification of these polymers with biological moieties, such as growth factors and peptides.[126, 127] Furthermore, synthetic polymers are often combined with natural polymers for hydrogel formation to make use of the benefits of both polymer sources.[98, 128]

Poly(ethylene glycol) (PEG)

Poly(ethylene glycol) (PEG) is the most commonly used synthetic polymer for hydrogel preparation in biomedical applications, due to its biocompatibility and high hydrophilicity.[27, 129, 130] The chemical properties of PEG are tunable either through the functionalization of the two hydroxyl end groups or the *co*-polymerization with other monomers. The introduction of a wide range of chemical groups, such as thiols[131], acrylates[132] and azides[133] allows the use of PEG derivates in a variety of cross-linking reactions. In addition to chemical functions, PEG can be functionalized with bioacitve agents, such as proteins and cell-adhesion ligands.[126] Without the biological modification, PEG is used as blank biological template and can serve as negative control to investigate the influence of functional domains.[65]

Photo-cross-linkable diacrylated PEG (PEG-DA) and dimethacrylated PEG (PEG-DMA) were already used as bioinks (Scheme 2). For example, Maher *et al.*[134] and Hockaday *et al.*[135] printed PEG-DA or a combination of PEG-DA with alginate via extrusion-based printing techniques. In their studies they could demonstrate the possibility of producing complex 3D constructs, such as aortic valve conduits with fast cross-linking PEG derivates.
PEG-DMA was used by the group of Cui *et al*[136, 137] as a bioink for inkjet printing. In one of their works they co-printed acrylated peptides and PEG-DMA, resulting in a

peptide conjugated PEG scaffold with high biocompatibility (hMSC viability of 87.9 ± 5.3 %).

PEG-DA **PEG-DMA**

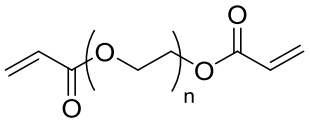

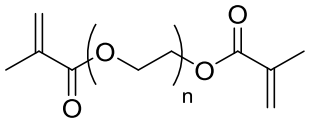

Hockaday *et al.*[135]
Maher *et al.*[134]

Cui *et al.*[136, 137]

extrusion-based printing inkjet-based printing

Scheme 2: Structural formula of diacrylated PEG (PEG-DA) and dimethacrylated PEG (PEG-DMA) and their use in 3D bioprinting.

Poly(glycidol) (PG)

Linear Poly(glycidol) (PG), a multifunctional analog of PEG, is an attractive alternative, since it allows for higher functionalization due to hydroxymethylene groups pending at each repeating unit (Scheme 3).[25] Like PEG, PG is hydrophilic and biocompatible and thus well suited for biomedical applications.[138, 139] Furthermore, PG was proven to be suitable as precursor polymer for hydrogels with embedded cells in studies of Singh *et al*..[140] Although PG provides excellent properties to be used as a bioink, it is yet not applied in the field of 3D bioprinting.

PEG **PG**

Scheme 3: Comparison of the structural formula of PEG and linear PG.

Linear PG is obtained by anionic polymerization of protected glycidol derivates with alkali metal based initiators (Scheme 4).[24, 25] A number of different protected glycidol monomers are used, whereby the most common ones are trimethylsilyl glycidyl ether, *tert*-butyl gylcidyl ether, allyl glycidyl ether (AGE) and ethoxy ethyl glycidyl ether (EEGE). EEGE is mainly used, due to the easy removal of the acetal protection group under acidic conditions. In contrast to *tert*-butyl glycidyl ether and AGE, EEGE

is not commercial available and has to be synthesized by reaction of ethyl vinyl ether and glycidol.[141]

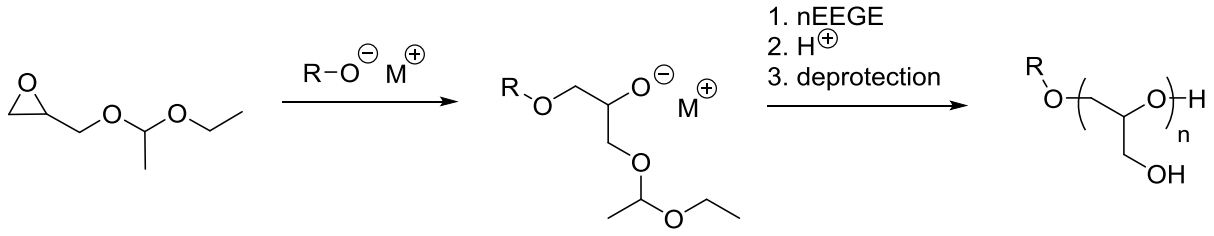

Scheme 4: Anionic polymerization of EEGE with alkali metal based initiator (RO^-M^+) and subsequent deprotection of the acetal protection group.

The molecular weight of linear PG achieved by anionic polymerization is limited to a maximum of approximately 30 000 g/mol, due to chain transfer reactions to the monomer (Scheme 5).[25, 142] In these reaction the active polymer chain end abstracts a proton form the EEGE monomer, resulting in a terminated P(EEGE) and an allyl alkoxide, which still is able to initiate a new polymerization. The formation of low molecular weight fractions can be detected in size exclusion chromatography (SEC) measurements (tailoring towards longer retention times) and the allylic end groups can be proven by ^{1}H-NMR sepectroscopy.

The influence of temperature and initiator on the chain transfer reaction was investigated by Hans *et al.*.[142] They could show that when using potassium as counter ion, the side reaction can be significantly decreased by a temperature reduction from 120 to 60 °C. However, for PG synthesized with lithium as counter ion, the side-reaction could not be prevented even when lowering the temperature to 20 °C, which is most likely due to the high basicity of the used *sec*-BuLi.

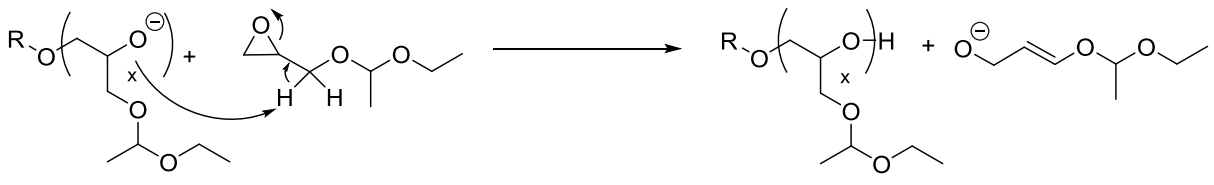

Scheme 5: Chain transfer reaction: Proton abstraction at EEGE by the active P(EEGE) chain.

A second side-reaction which can occure during anionic polymerization of EEGE is the abstraction of a proton at the epoxy ring by the living polymer chain or the

initiator.[142, 143] The abstraction yields in an enolate which is able to initiate a new polymerization resulting in a P(EEGE) with a ketone group at the chain end (Scheme 6). A polymer with ketone end group can couple with an alkoxide of an active chain end which leads to polymers with doubled molecular weight. These high molecular weight fractions can be detected in SEC measurements as a shoulder towards lower retention times.[142, 143] Kuhlmann *et al.* showed in a study, that this side-reaction can be reduced by slow monomer addition, meaning by keeping the monomer concentration low and thus decreasing monomer deprotonation.[143] The effect of this technique was even more pronounced for anionic polymerization of AGE.

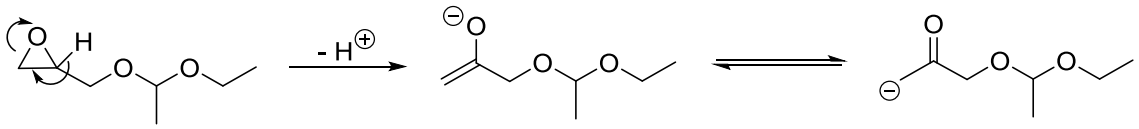

Scheme 6: Proton abstraction by the living chain or the initiator resulting in an enolate.

Through *co*-polymerization of differently substituted glycidol monomers different side chains can be introduced into the polymer backbone. AGE monomers (Scheme 7) provide double bonds and EEGE monomers serve as precursors for hydroxyl moieties. Both side groups allow subsequent functionalization of the polymer.[25, 130] For example, hydroxyl groups can be functionalized via Steglich esterification[144] and double bonds via thiol-ene photo reaction[145]. The thiol-ene reaction was already presented in **chapter 2.2.2.2** as an attractive cross-linking reaction for hydrogels. Concerning polymer functionalization the reaction enables the functionalization of double bonds with a huge variety of thiol-containing molecules, which underlines the versatility of thiol-ene reactions.

AGE

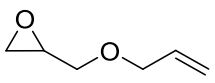

Scheme 7: Protected glycidol monomers allyl glycidyl ether (AGE).

Chapter 3

Results and discussion

Parts of this chapter have previously been published and are adapted with permission from:

S. Stichler, T. Böck, N. Paxton, S. Bertlein, R. Levato, V. Schill, W. Smolan, J. Malda, J. Teßmar, T Blunk, J. Groll, Double printing of hyaluronic acid/poly(glycidol) hybrid hydrogels with poly(ε-caprolactone) for MSC chondrogenesis, *Biofabrication* **2017**, doi: 10.1088/1758-5090/aa8cb7.

S. Stichler, S. Bertlein, J. Teßmar, T. Jüngst, J. Groll, Thiol-ene Cross-Linkable Hydrogels as Bioinks for Biofabrication, *Macromol. Symp*. **2017**, *372*, 102-107.

S. Stichler, T. Jüngst, M. Schamel, I. Zilkowski, M. Kuhlmann, T. Böck, T. Blunk, J. Teßmar, J. Groll, Thiol-ene clickable poly(glycidol) hydrogels for biofabrication, *Ann. Biomed. Eng*. **2017**, *45*, 273-285.

3.1 Synthesis and analysis of functional poly(glycidol)s (PG) and hyaluronic acid (HA)

In order to obtain hydrogel formation by cross-linking of functional groups such as allyl and thiol, precursor polymers were synthesized and characterized. The homopolymer poly(glycidol) (PG **3**) and the *co*-polymer poly(allyl glycidyl ether-*co*-glycidyl) (P(AGE-*co*-G) **5**) functioned as precursor polymers for further functionalized PGs.

Thiol- and allyl-functional poly(glycidol)s (P(SH-*co*-G) **6**, **7** and P(AGE-*co*-G) **5**) as well as thiol-functionalized hyaluronic acid (HA-SH) were used for hydrogels cross-linked by thiol-ene click reaction (**chapter 3.2**). In addition, P(AGE-*co*-G) (**5**) was endowed with peptides (P(peptide-*co*-G) **8**) via thiol-ene reaction and the resulting polymers were used for the development of a physical hydrogels based on ionic interactions (**chapter 3.3**).

In the subsequent sections, the synthesis as well as the analysis of those polymers is discussed.

3.1.1 Synthesis of linear PG (3)

In order to synthesize linear instead of branched and hyperbranched PG, the protected glycidol monomer, ethoxy ethyl glycidyl ether (EEGE, **1**) was synthesized by protection of the hydroxyl group of glycidyl with ethyl vinyl ether according to literature[141] (Scheme 8). The monomer **1** was purified by drying over CaH_2 and fractionated distillation under Ar atmosphere.

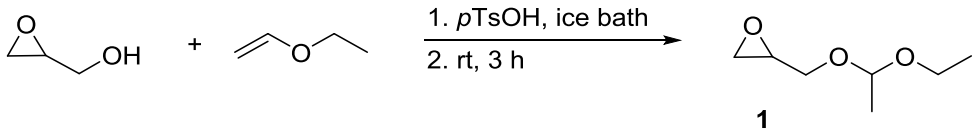

Scheme 8: Synthesis of the protected glycidol EEGE **1**.

Anionic polymerization of EEGE (**1**) with subsequent deprotection was conducted adapted from literature.[26] (Scheme 9). The polymerization was implemented under inert atmosphere at 60 °C for 24 h with KO^{t}Bu as initiator and terminated by addition of EtOH. The deprotection of the acetal group of the intermediate stage polymer P(EEGE) (**2**) with HCl yielded in linear PG (**3**). The successful synthesis of **3** was verified by ^{1}H-NMR and SEC.

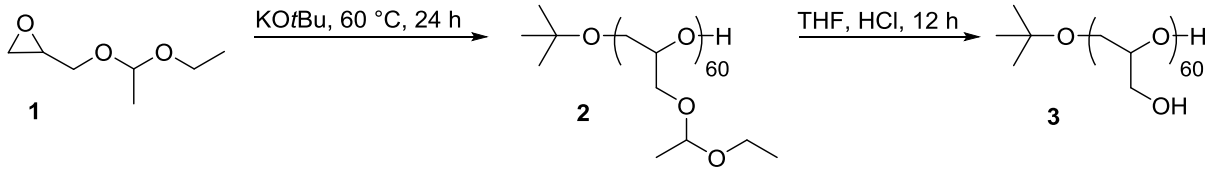

Scheme 9: Synthesis of linear PG **3**.

The molar ratio of initiator to monomer **1** was adjusted to 1:60 (Chapter 5.3.2.1) resulting in a theoretical length of 60 repetition units of the PG (**3**) backbone. Due to a partial cleavage of the initiator related *tert*-butyl ether during deprotection of the polymer backbone, the determined experimental number average molecular weight by ^{1}H-NMR was significantly higher than the theoretical value (Table 3). The relation between backbone deprotection and cleavage of the initiator group was examined by *Johanna Lutz* during her master thesis.[146] Briefly, she could show that the initiator

group is already partially cleaved under acid conditions after a few minutes. The percentage of initiator loss increased over time and with amount of HCl. She could further demonstrate that a deprotection time of 30 min and a reduced HCl amount (8 mL /15 g PG) is sufficient to fully deprotect the hydroxyl groups. Under these conditions the initiator cleavage could be minimized but still not completely prevented. The polymers shown throughout this thesis were synthesized before these investigations and hence deprotected for 12 h according to a lab protocol of the group of Prof. Groll.

The molecular weight of PG (**3**) was determined relative to PEG standards by aqueous SEC measurement (Figure 11). A shoulder toward lower retention time was detected, indicating high molecular weight fractions. These fractions are the result of coupling reactions between a ketone group and an alkoxide of a propagating chain end (see Scheme 6 , **chapter 2.2.3.2**).[142, 143] Another side-reaction, the chain transfer reaction which is initiated by a proton abstraction from an EEGE monomer (see Scheme 5, **chapter 2.2.3.2**) resulted in a tailoring and hence in fractions with low molecular weight PGs.[142] Since the hydrodynamic radius and the coiling behavior of PG differ from PEG, the elution time of both polymers cannot directly be compared. The obtained molecular weights of **3** are therefore related to a longer retention time of PG polymers on the column and consequently lower molecular weights once compared to PEG.

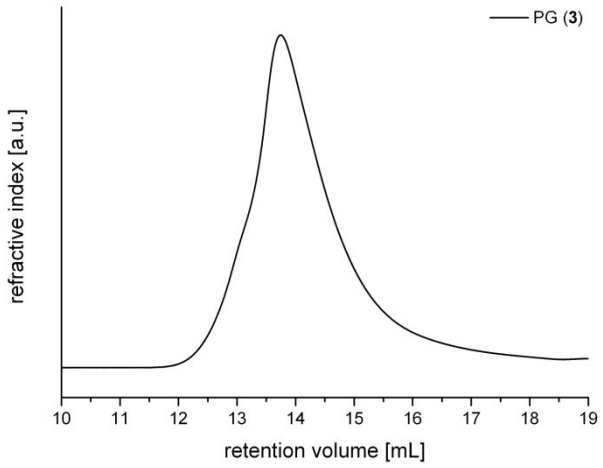

Figure 11: SEC elugram of linear PG (**3**).

Side-reactions yielding in high molecular weight (shoulder towards shorter retention time) and low molecular weight fractions (tailoring) as well as longer retention times were detected for all homo and *co*-polymers synthesized throughout this thesis and were always attributed to different coiling behavior, potential interaction with the column and side-reactions.

The theoretical, experimental (determined by ^{1}H-NMR) and relative (detected by water SEC measurements) molecular weights of PG (**3**) are listed in Table 3. The experimental molecular weight was calculated by integrating the initiator peak in the ^{1}H-NMR spectra of **3**. Due to partial cleavage of the initiator during deprotection of the acetal group, the experimental molecular weight was higher than the theoretical value. In contrast, the relative molecular weights determined against PEG standards by water SEC were significantly lower, since PG polymers have a different hydrodynamic radius and coiling behavior in water than PEG.
A higher experimental molecular weight compared to the theoretical value, was determined as well for *co*-polymers (**5a-c**) as these polymers are also synthesized with KO*t*Bu and with subsequent acidic deprotection.

Table 3: Comparison of theoretical, experimental and relative molecular weight of PG (**3**).

	$M_{n,\,theo.}$ [Da]	$M_{n,\,exp.}$ [Da]*	M_n [Da]**	M_w [Da]**	Đ**
3	4520	8080	1870	3220	1.73

*determined by ^{1}H-NMR

**determined by water SEC

Linear PG (**3**) served as a polymeric precursor for ester-containing thiol-functionalized PG (PG-SH_{ec}, **6**) (**chapter 3.1.3.1**).

3.1.2 Synthesis of the *co*-polymer P(AGE-*co*-G) (5)

Allyl-functionalized PG **5** was synthesized according to a method adapted from literature[26] by anionic co-polymerization of allyl glycidyl ether (AGE) with EEGE (**1**), followed by deprotection of the acetal group (Scheme 10). AGE was commercially purchased, dried over CaH_2 and distilled under inert atmosphere.

The polymerization was conducted at 60 °C under Ar atmosphere and terminated by addition of EtOH after 24 h. Subsequent to deprotection with HCl, the *co*-polymer P(AGE-*co*-G) (**5**) was received as a colorless oil. ^{1}H-NMR and SEC confirmed the successful synthesis of allyl-modified PG **5**.

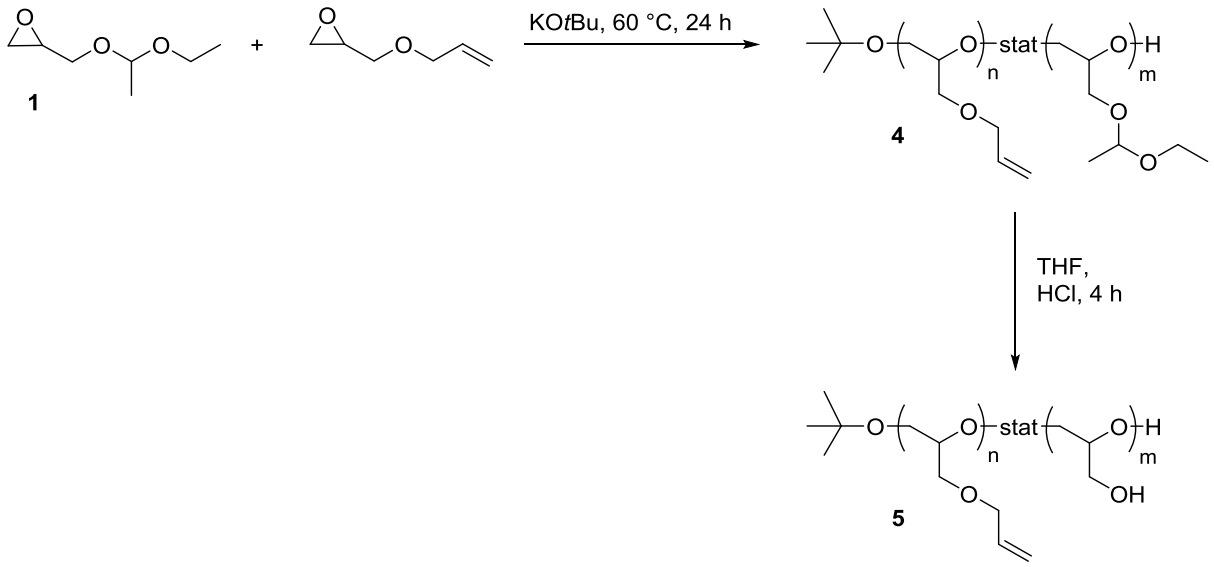

Scheme 10: Anionic *co*-polymerization of AGE with EEGE (**1**) followed by acidic deprotection.

By varying the molar ratio of AGE to EEGE, the AGE content of the allyl-functionalized PG **5** could be predetermined. P(AGE-*co*-G) (**5**) was synthesized using three different AGE to EEGE ratios (1/18, 1/9 and1/4, Chapter 5.3.2.3), resulting in *co*-polymers with 7 % (**5a**), 11 % (**5b**) and 20 % (**5c**) AGE-functionality. The AGE content was confirmed via ^{1}H-NMR, by correlating the proton signals of the allyl-group to the backbone signals (Figure 12).

The signals at 6.00-5.80, 5.30-5.20 and 4.05-4.03 ppm can be assigned to the protons *H*-7-9 of the allyl-group. The backbone protons *H*-4-6 and *H*-10-12 generate

a broad multiplet signal at 3.80-3.60 ppm and the signal at 1.20 ppm can be attributed to the remaining initiator protons *H*-1-3.

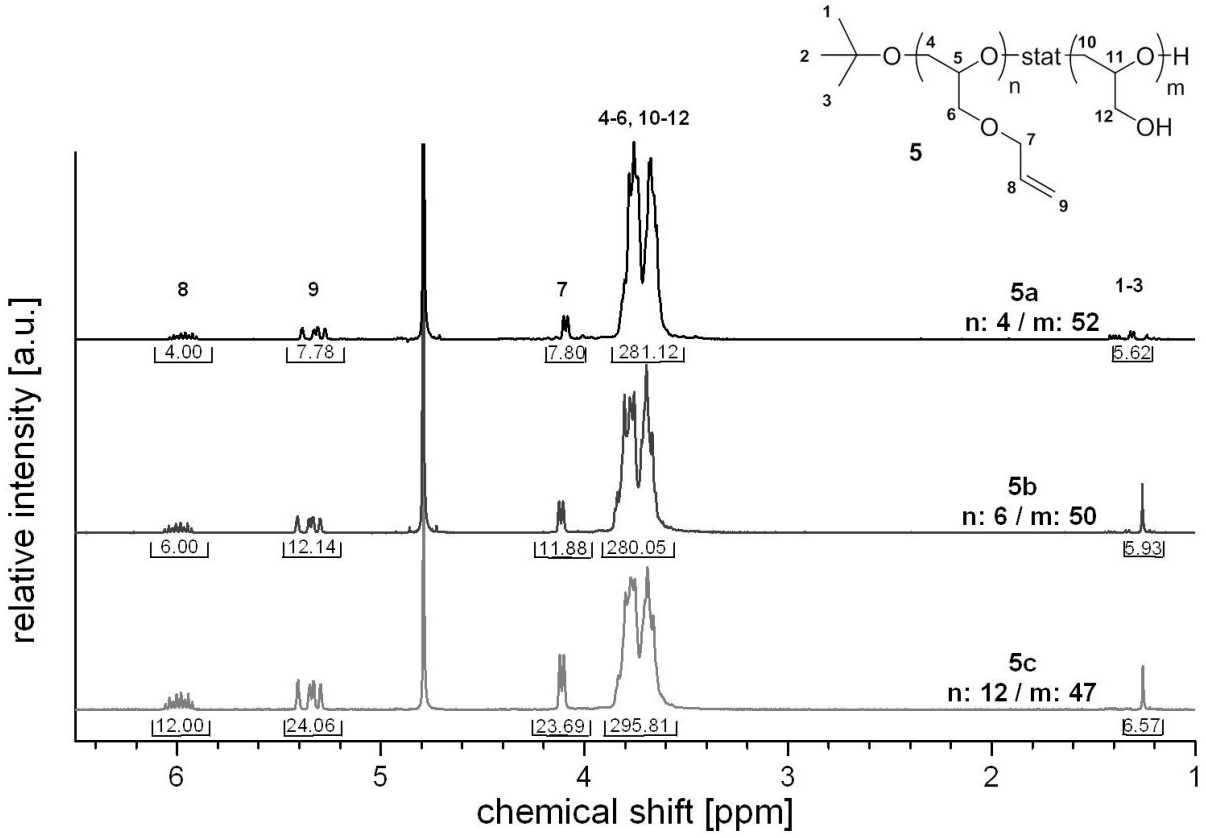

Figure 12: ^{1}H-NMR spectra of allyl-functionalized PGs **5a-c** with different allyl content.

The allyl-proton (*H*-8) was integrated and used as reference (4 H: **5a**, 6 H: **5b** and 12 H: **5c**), assuming that all AGE monomers reacted (Figure 12). This resulted in *co*-polymers with a backbone length of around 60 repetition units: **5a**: P(AGE_4-*co*-G_{52}), **5b**: P(AGE_6-*co*-G_{50}) and **5c**; P(AGE_{12}-*co*-G_{47}). By integration of the *tert*-butyl signal (*H*-1-3) the partial cleavage of the initiator group was confirmed (**chapter 3.1.1**).

Comparison of the three different allyl-functionalized *co*-polymers **5a-c** demonstrated a longer retention time for polymers with higher functionality, as a result of the fact that polymers with 20 wt.% allyl-functionality probably interacted most strongly with the column (Figure 13). As for the homo polymer PG (**3**), a shoulder towards shorter retention volume (high-molecular weight fractions) was detected for all three co-polymers in SEC measurements, which was attributed to side reactions during the polymerization.

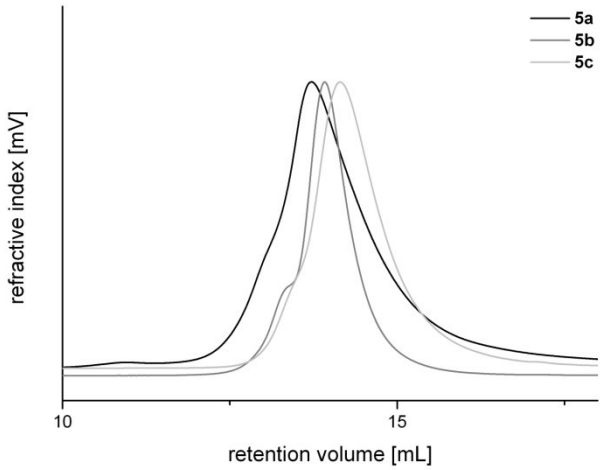

Figure 13: Comparison of SEC elugram of **5a-c**.

As previously discussed (**chapter 3.1.1**), the experimental molecular weights were higher for all P(AGE-*co*-G) polymers (**5a-c**) than the theoretical molecular weights. In contrast, the relative molecular weights determined against PEG standards by water SEC were significantly smaller, since the additional lipophilic side groups in the *co*-polymer **5** resulted in a different coiling behavior compared to PEG and an eventually interaction with the column.

Table 4: Theoretical, experimental and relative molecular weight of P(AGE-*co*-G) (**5**).

	AGE-functionality [%]*	**$M_{n,\ theo.}$ [Da]**	**$M_{n,\ exp.}$ [Da]***	**M_n [Da]****	**M_w [Da]****	**Đ****
5a	7	6160	7280	2020	3450	1.71
5b	11	4760	6730	2810	3450	1.23
5c	20	5560	6710	1870	2580	1.38

*determined by ^{1}H-NMR

**determined by water SEC

Allyl-functionalized PGs **5** were used as precursor polymers for hydrogel cross-linking (**chapter 3.2**) as well as for polymeric analogous functionalization of the allyl group with thiols and peptides (**chapter 3.1.3** and **3.1.5**).

3.1.3 Synthesis of thiol-functionalized PGs (P(SH-*co*-G) (6 and 7)

In addition to allyl-functionalized PG **5**, thiol-functionalized polymers were needed for thiol-ene cross-linked hydrogel systems (**chapter 3.2**). Therefore, two different thiol-functionalized PGs (P(SH-*co*-G) **6** and **7**) as well as thiol-functionalized HA (HA-SH) (**chapter 3.1.4**) were synthesized.
This chapter focuses on the synthesis of ester-containing (**6**) and ester-free (**7**) P(SH-*co*-G). For a better distinction between those two thiol-functionlized PGs, the ester-containing polymer is abbreviated as PG-SH_{ec} and the ester-free one is abbreviated as PG-SH_{ef}. PG-SH_{ec} **6** was synthesized with PG **3** as the polymeric precursor and PG-SH_{ef} **7** was synthesized by modification of the allyl-groups of P(AGE-*co*-G) (**5**). The presence of ester groups has a huge effect on the degradability of the resulting hydrogels (**chapter 3.2.2.1**).

Throughout this thesis, the results of the ester-containing P(SH-*co*-G) (**6**) as well as all results of hydrogels containing PG-SH_{ec} (**6**) are depicted in purple, and the results of ester-free P(SH-*co*-G) **7** and the corresponding hydrogels in blue.

3.1.3.1 Synthesis of ester-containing PG-SH (PG-SH_{ec}) (6)

PG-SH_{ec} **6** was synthesized in a two step reaction according to literature.[147] (Scheme 11). First, PG (**3**) was modified with the disulfide cross-linker DTPA followed by a reduction of the disulfides to thiols with TCEP. The esterification of **3** was mediated by DCC-DMAP activation of the carboxyl groups. Introduction of ester groups into the polymer backbone led to hydrolytically cleavable PG-SH_{ec} **6**.

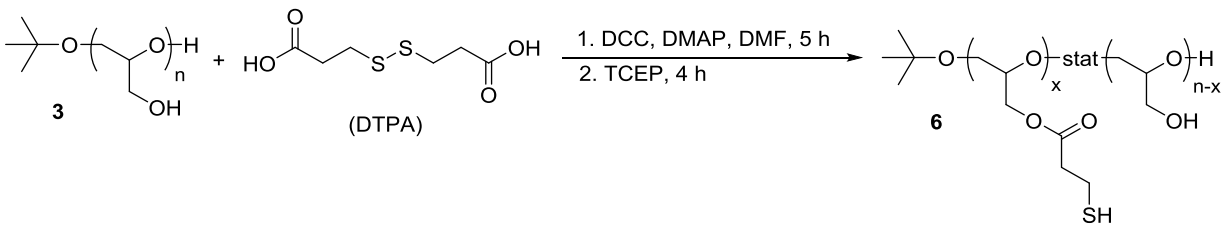

Scheme 11: Synthesis of ester-containing PG-SH **6**.

The comparison of the ^{1}H-NMR spectra of the polymeric precursor PG (**3**) and PG-SH_{ec} **6** is shown in Figure 14. The signals at 4.46-4.28 ppm and 2.28-2.81 ppm can be assigned to the methylene and ethyl protons (*H*-6-8) next to the ester group and verified the synthesis of **6**. Integration of proton *H*-6 indicated a conversion of 14 % hydroxyl groups to thiols.

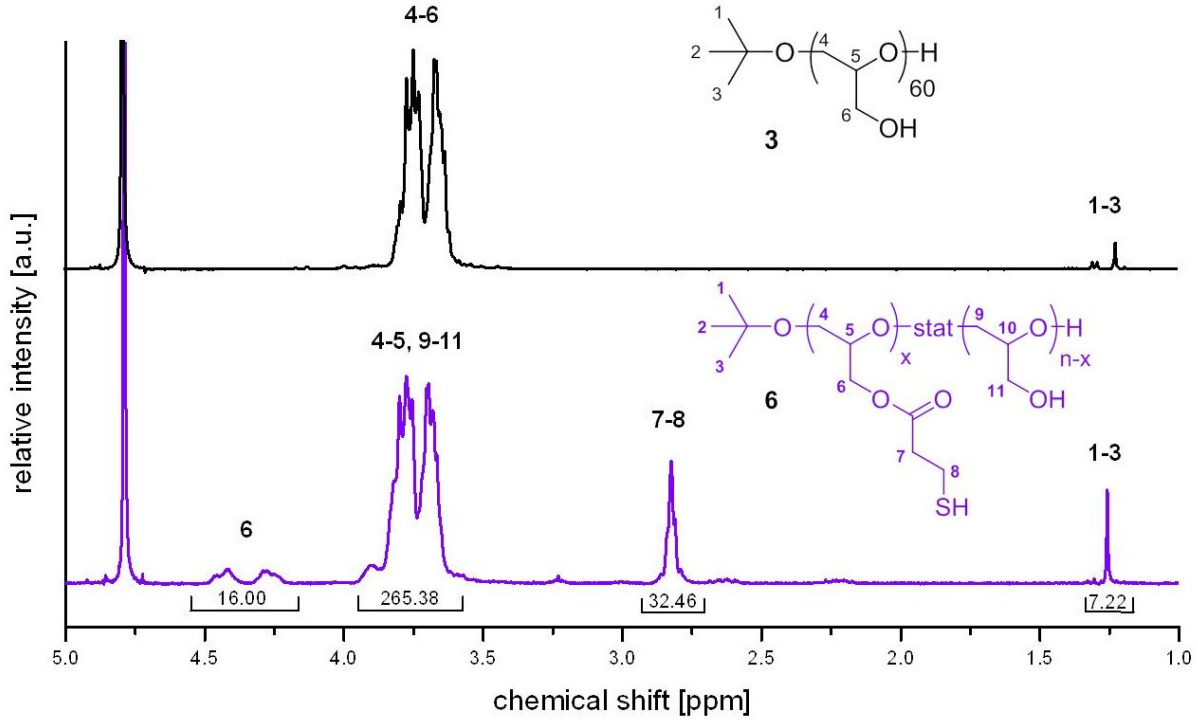

Figure 14: ^{1}H-NMR spectra of ester-containing PG-SH **6** (bottom, purple) compared to the polymeric precursor PG (**3**) (top, black).

Conversion of 14 % hydroxyl groups means that in average 8.4 out of 60 hydroxyl groups have been transferred to thiols. Therefore, the theoretical value was calculated for P(SH_8-*co*-G_{52}) (**6**) (Table 5). The trend for the experimental and relative molecular weights compared to the theoretical one was comparable to the trend discussed for **3** and **5** (Table 5).

Table 5: Molecular weight of **6**: theoretical, experimental and determined by SEC.

	SH-functionality [%]*	$M_{n,\ theo.}$ [Da]	$M_{n,\ exp.}$ [Da]*	M_n [Da]**	M_w [Da]**	Đ
6	14	5220	5920	1710	4220	2.47

*determined by ^{1}H-NMR

**determined by water SEC (with HEA quenching)

In order to determine the relative molecular weight of PG-SH_{ec} **6**, SEC measurements were conducted (Figure 15a). To avoid the oxidation of thiols and hence the blocking of the SEC column, thiol groups were quenched with HEA before the measurement.

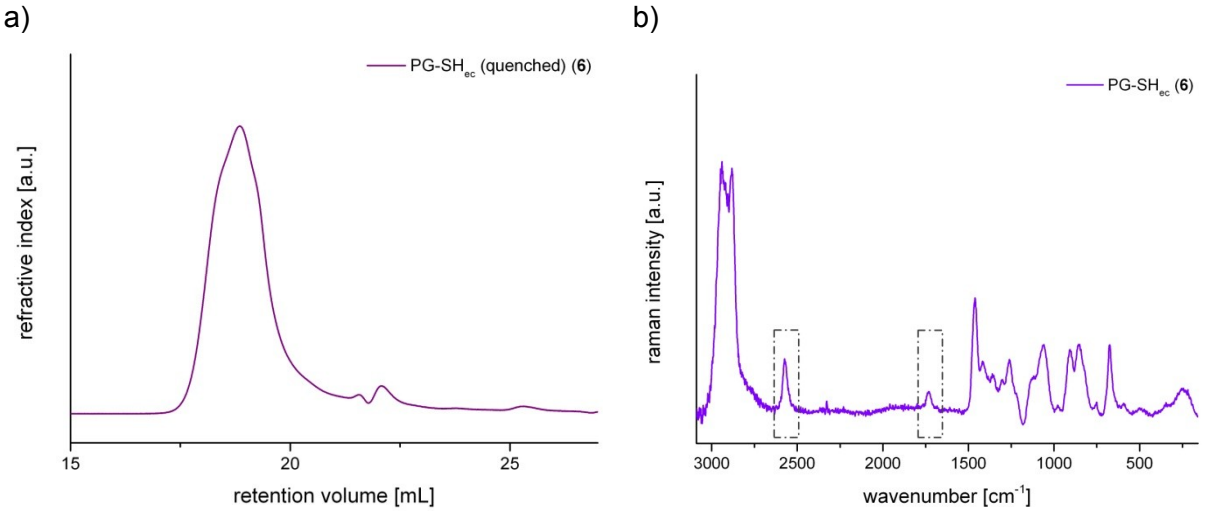

Figure 15: a) SEC elugram of PG-SH_{ec} **6**; b) Raman spectra of PG-SH_{ec} **6**.

For quenching two different approaches were conducted: reaction via Michael reaction and via thiol-ene reaction. After Michael reaction the Raman spectra still showed thiol peaks indicating an incomplete reaction, whereas the Raman spectra after quenching via thiol-ene reaction showed no thiol peaks. Therefore, PG-SH_{ec} (**6**) was implemented with HEA in a thiol-ene-reaction for SEC measurements. However, it has to be considered that by reaction with HEA the molecular structure and thus the hydrodynamic radius and the coiling behavior of the initial polymer **6** was changed. SEC measurement of the quenched polymer **6** showed a broad molecular weight

distribution attributed also to possible side products of the photo-reaction (e.g. polymerization of HEA).

Raman spectroscopy of PG-SH_{ec} **6** was conducted to verify the presence of thiols (Figure 15b). The expected vibrations of the thiol and ester group were detected at 2570 cm^{-1} (SH vibration) and 1730 cm^{-1} (C=O vibration). Due to the absence of disulfide vibrations at 550-450 cm^{-1}, the oxidation of PG-SH_{ec} **6** could be excluded.

PG-SH_{ec} **6** was used as precursor polymer for thiol-ene cross-linked hydrogels (**chapter 3.2**).

3.1.3.2 Synthesis of ester-free PG-SH (PG-SH_{ef}) (7)

PG-SH_{ef} **7** was synthesized by conversion of allyl-groups of P(AGE-*co*-G) (**5**) to thiol groups. Therefore, allyl-functionalized PG **5** was implemented with thioacetic acid in a thiol-ene click reaction for 2 h at 365 nm (Scheme 12). After alkaline hydrolysis of the thioester, the thiol-functionalized PG **7** was received. To avoid oxidation of the thiols, **7** was dialyzed against degassed water and stored under Ar atmosphere. The successful synthesis of PG-SH_{ef} **7** with different thiol amounts was achieved by using differently substituted *co*-polymers and was verified by SEC and ^{1}H-NMR measurements.

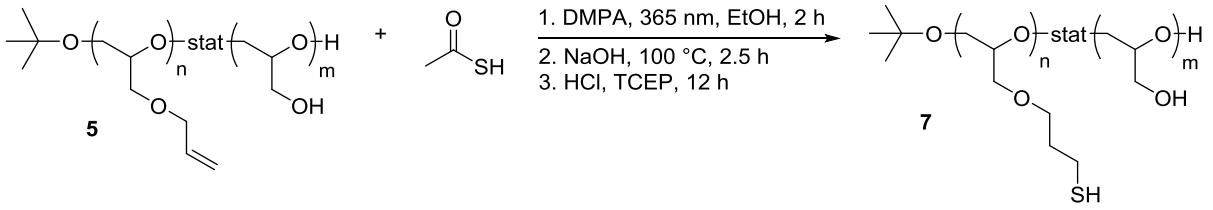

Scheme 12: Synthesis of ester-free PG-SH (**7**).

The absence of the allyl proton signals of the educt (6.00-5.89, 5.37-5.26 and 4.09-4.07 ppm) in the ^{1}H-NMR spectra of **7a-b** verified the total conversion of allyl- to thiol-groups (Figure 16). Depending on the used P(AGE-*co*-G) (**5**) the degree of thiol-functionalization could be predetermined. Two different PG-SH_{ef} **7** were synthesized: **7a** with 10 % and **7b** with 18 % thiol-functionality. The protons of the ethyl group next

to the thiol (*H*-8-9) generated signals at 2.62-2.58 and 1.89-1.84 ppm. Integration of those peaks verified the expected thiol-functionality.

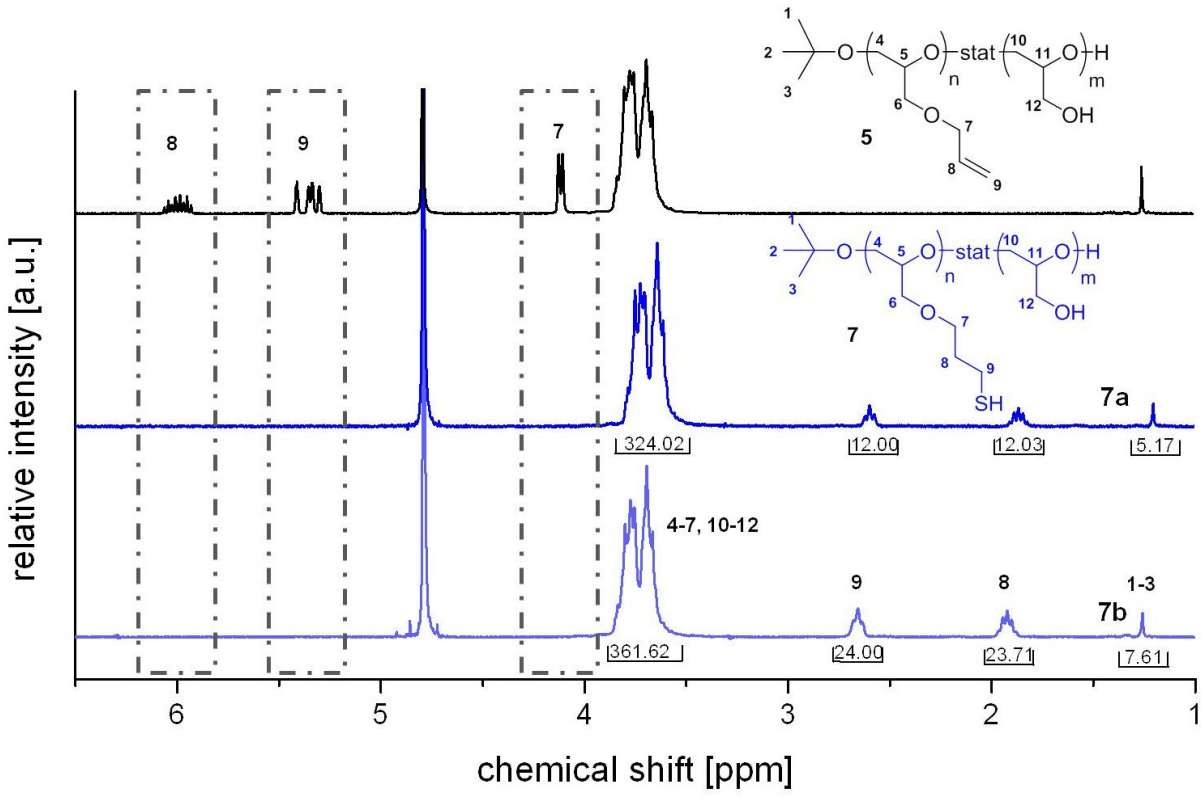

Figure 16: ^{1}H-NMR spectra of ester-free PG-SH **7a** (middle, blue) and **7b** (bottom, light blue) compared to the polymeric precursor P(AGE-*co*-G) (**5**) (black).

By integration of the initiator peak (*H*-1-3) to 9 H, the experimental molecular weight was determined (Table 6). The experimental molecular weight was higher than the theoretical value and contrarily, the relative molecular weight determined by water SEC measurement against PEG (Figure 18) was significantly lower than expected, as discussed before.

Table 6: Theoretical, experimental and relative molecular weights of **7a-b**.

	SH-functionality [%]*	$M_{n,\ theo.}$ [Da]	$M_{n,\ exp.}$ [Da]*	M_n [Da]**	M_w [Da]**	Đ**
7a	10	4960	8810	1330	2740	2.06
7b	18	5850	7180	549	1260	2.29

*determined by ^{1}H-NMR

**determined by water SEC (without quenching)

The presence of thiol groups as well as the absence of disulfide bonds was verified by Raman spectroscopy (Figure 17). While the vibrations at 2570 cm^{-1} could be assigned to the thiol stretch vibration, there was no vibration detected at 550-450 cm^{-1} (disulfide signal). The clear absence of the disulfide vibration in the Raman spectra excluded the oxidation of PG-SH_{ef} **7**. The comparison to the Raman spectra of the precursor polymer P(AGE-*co*-G) (**5**) shows the conversion of allyl- to thiol-groups, since the C=C vibration of the allyl-group at 1644 cm^{-1} was not detected in the spectra of the thiol-functionalized polymers **7**.

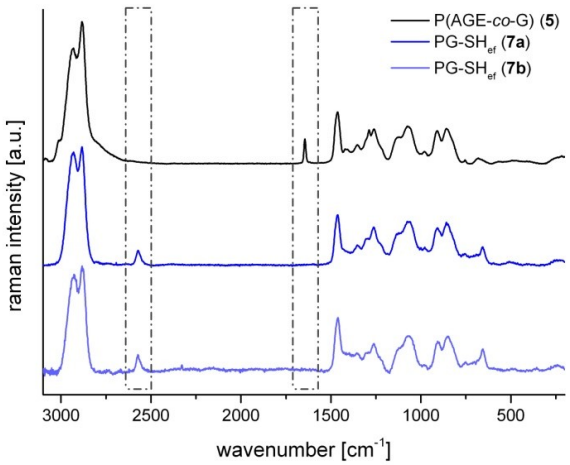

Figure 17: Raman spectra of PG-SH_{ef} **7a** (middle, blue) and **7b** (bottom, light blue) compared to P(AGE-*co*-G) (top, black) (**5**).

Thiol-functionalization of PG resulted in polymers, which probably interacted even stronger with the SEC column material than the precursor polymer **5** since oxidation of the thiol groups can occure during the measurement (Figure 18a). PG-SH_{ef} **7b** with the higher thiol-content showed the strongest interaction with the column and thus a very broad molecular weight distribution and high dispersity. Compared to the polymeric precursor **5**, only the side chain of the polymer backbone changed and hence the backbone length and dispersity remained the same. The change in dispersity and retention time measured by SEC could directly be attributed to the interaction of the thiol groups with the column and the different coiling behavior of **7** in the eluent. SEC measurements were conducted without quenching of **7** to avoid the additional measurement of several side products (**chapter 3.1.3.1**). This enabled the pure determination of the product polymer. Nevertheless, the broad distribution of **7b** can also indicate a partial oxidation, which was efficiently prevented by the quenching step.

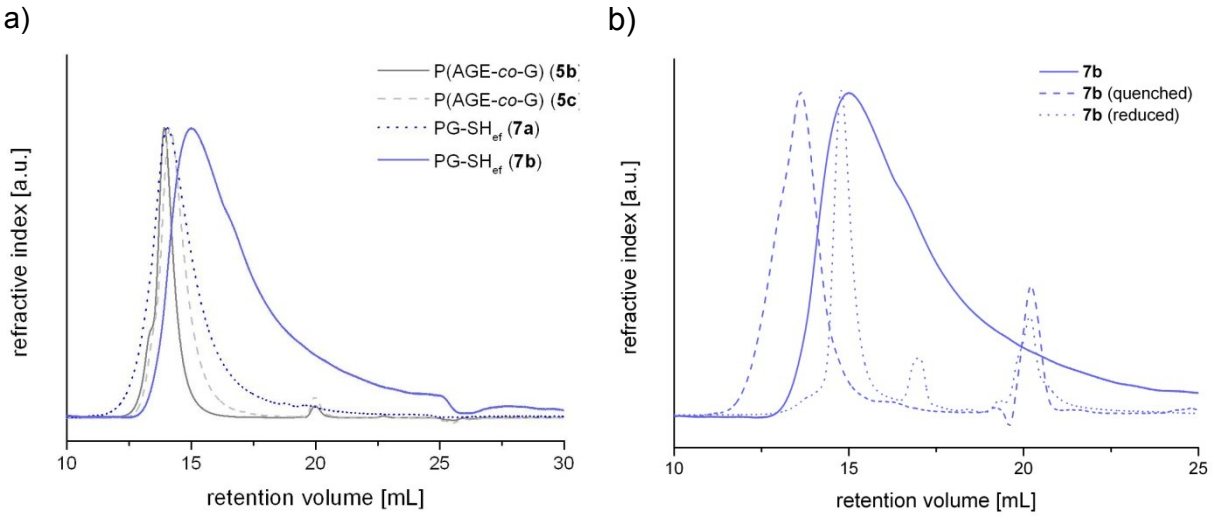

Figure 18: a) SEC elugrams of the precursor polymers P(AGE-*co*-G) (**5**, grey) and PG-SH_{ef} (**7**, blue); b) SEC elugrams of untreated (solid line), quenched (dashed line) and freshly reduced (dotted line) **7b**.

In order to investigate the influence of oxidation and quenching on the hydrodynamic radius and the interaction with the SEC column and hence on the relating molecular weights, **7b** was measured again firstly after reduction with TCEP and secondly after quenching with HEA by thiol-ene reaction (Figure 18b, Table 7). The strongest interaction with the column was measured for untreated **7b**, underlining the assumed

partial oxidation of **7b** during the measurement. The quenched polymer **7b** had the shortest retention time and the broadest molecular weight distribution, related to the synthesis of several polymeric side products and the addition of larger side groups during quenching with HEA. The narrowest molecular weight distribution was measured for the freshly reduced **7b**, accompanied with a small relative molecular weight compared to the theoretical value.

In summary, the study demonstrated a pronounced influence of side chain functionalization and side products on the coiling behavior, hydrodynamic radii and column interaction especially for thiolated polymers and hence the resulting measured molecular weights and dispersities of the polymers by SEC.

Table 7: Relative molecular weight and dispersity of **7b**: untreated, quenched with HEA and reduced with TCEP.

	untreated		**quenched**		**reduced**	
	M_n [Da]	**Đ**	**M_n [Da]**	**Đ**	**M_n [Da]**	**Đ**
7b	549	2.29	3 380	1.65	1 290	1.13

Thiol-modified PG **7** was used as a polymeric precursor for hydrogels cross-linked via thiol-ene reaction (**chapter 3.2**).

3.1.4 Analysis of thiol-functionalized HA (HA-SH)

In contrast to pure synthetic hydrogels consisting of PG polymers only, hybrid hydrogels containing one biopolymer precursor were developed. The natural polymer HA was thiol-functionalized and used as an alternative to P(SH-*co*-G) (**6** and **7**). While the preparation and examination of those hybrid hydrogels are discussed in **chapter 3.2**, this chapter deals with the synthesis and analysis of HA-SH.

Throughout this thesis all HA-SH results and results of hybrid hydrogels with HA-SH are depicted in green.

The synthesis of HA-SH was conducted by *Sarah Bertlein* and *Verena Schill*[V] according to literature[122]. Different batches were provided, analyzed and used for hydrogel cross-linking.

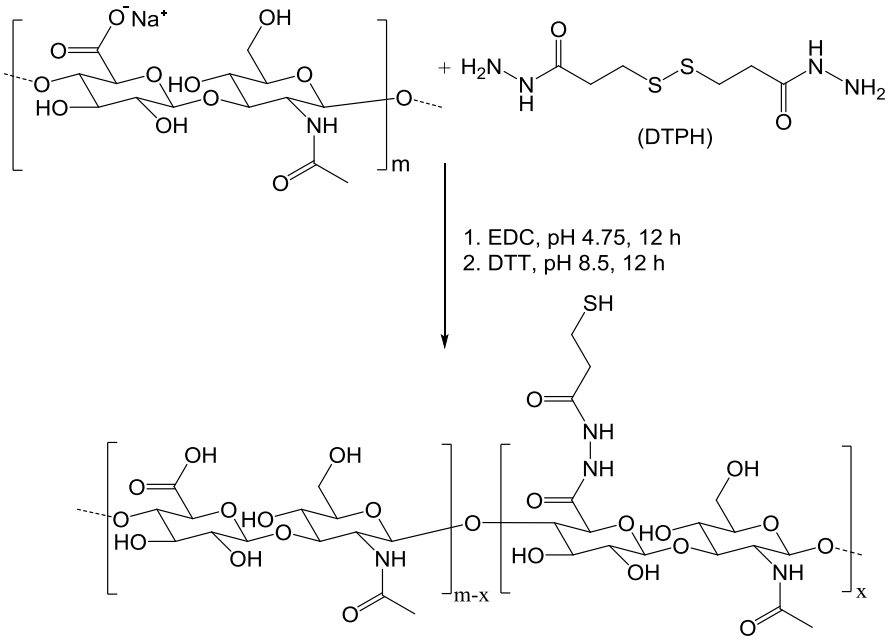

Scheme 13: Synthesis of HA-SH via EDC mediated DTPH coupling.

Thiol-modified high molecular weight (HMW) HA-SHs (1.36 MDa) were synthesized with different degree of functionality, however due to poor solubility in conjunction with high viscosities, these polymers were excluded for hydrogel formation. Low molecular weight (LMW) HA-SH batches were also synthesized with different degree of functionality. For hydrogel cross-linking the three most comparable HA-SH

[V] Both PhD students at the Department for Functional Materials in Medicine and Dentistry, University of Würzburg.

batches, in the meaning of characterization, were choosen (batch I.-III.). The desired functional degree of these three batches was 40 %. Batches which showed too high deviations in viscosity and functionalization degree were excluded.

Briefly, for synthesis of HA-SH, the carboxyl groups of LMW HA (27.3 kDa) were activated with the carbodiimide EDC and reacted with the disulfide containing dihydrazide (DTPH) yielding an intermediate gel stage, obtained via cross-linking between HA-SH polymer chains. The disulfides of the gel were subsequently reduced with DTT and thiolated HA was received (Scheme 13). For purification HA-SH was dialyzed against acidified water for 2 d, followed by dialysis against degassed water and freeze-drying. Depending on the molar ratio of HA to DTPH, the thiol content of HA-SH could be adjusted. HA-SHs with different thiol-functionalities were analyzed and examined regarding their applicability for hydrogel cross-linking and 3D printing.

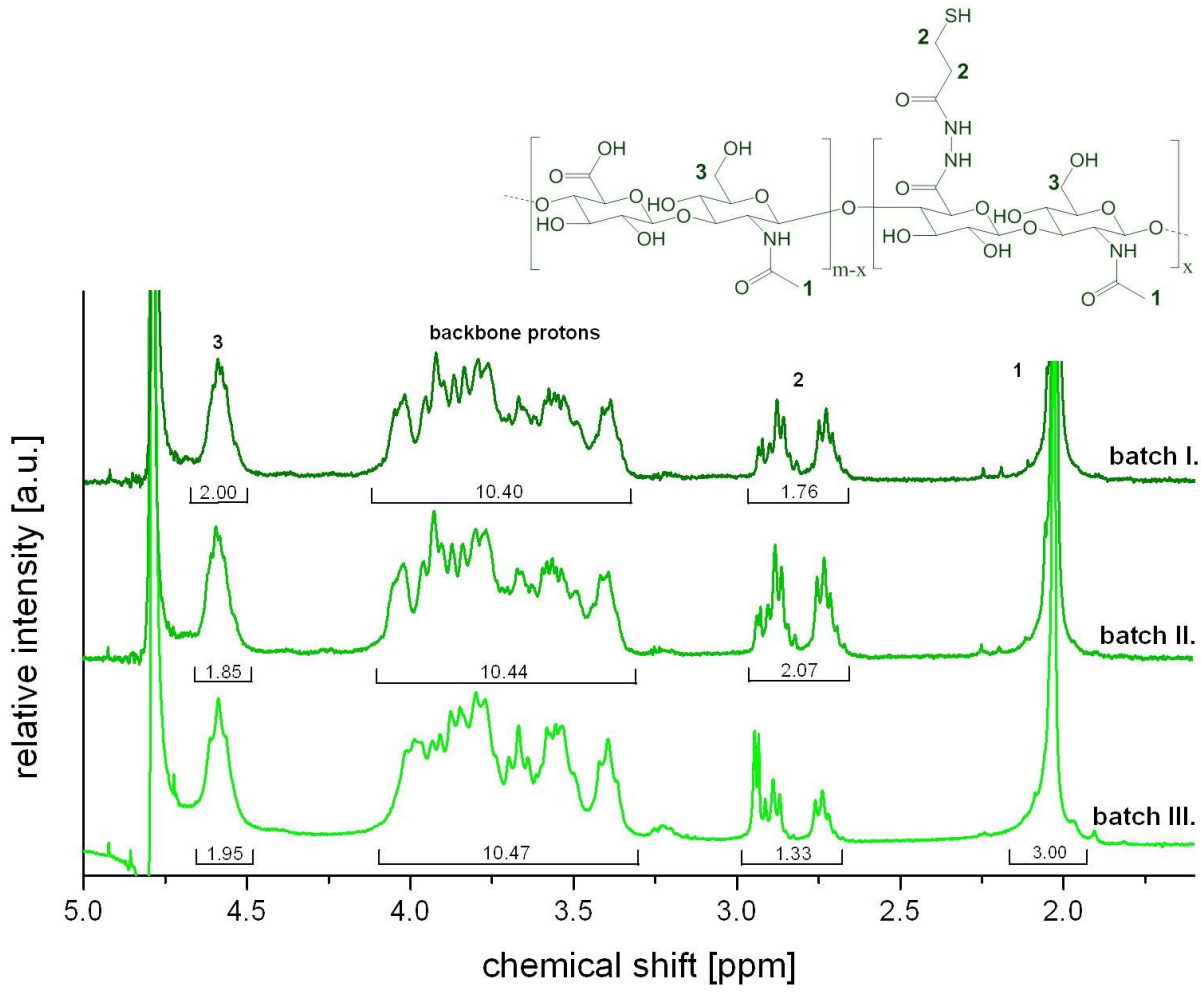

Figure 19: ^{1}H-NMR spectra of HA-SH batches with different thiol-functionality.

The degree of thiol-functionalization was determined by ^{1}H-NMR spectroscopy (Figure 19), by relating the α-protons of the HA-SH amide group (*H*-1 at 2.03 ppm) to the protons of the ethyl protons next to the thiol group (*H*-2 at 2.94-2.72 ppm). Therefore, the *H*-1 signal was used as an internal standard. The two signals at 4.58 ppm and 4.01-3.39 ppm can be assigned to the methylen group *H*-3 and the remaining backbone protons, respectively.

Table 8 shows the calculated thiol-functionality of the three HA-SH batches, which were in the range of 33 to 52 % of the available carboxyl groups.

Table 8: Degree of thiol-functionalization of used HA-SH batches.

	functionalization degree [%]
batch I.	44
batch II.	52
batch III.	33

SEC measurements were conducted to determine the relative molecular weight of functionalized HA (Table 9). Compared to most synthetic polymers, natural polymers have a broader molecular weight distribution originating from the biosynthesis. Furthermore, the relative molecular weights were obtained by using standards of the synthetic polymer PEG, which is an additional drawback of the analysis. Already the elugram of the polymeric precursor LMW HA revealed a broad distribution with a dispersity of 4.80 (Figure 20). The elugrams of the functionalized polymers showed, that the relative molecular weights of batch I. and II. were comparable and significantly smaller than the molecular weights of batch III. and the polymeric precursor. By further investigating the synthesis of those batches, it was noted that batch III. was dialyzed using less acid, indicating that dialysis with higher amounts of acid (batch I. and II.) might have led to a stronger degradation of the HA backbone and hence to smaller polymers. The effect of the synthesis on the hydrogel performance is further discussed in **chapter 3.2.2.2**.

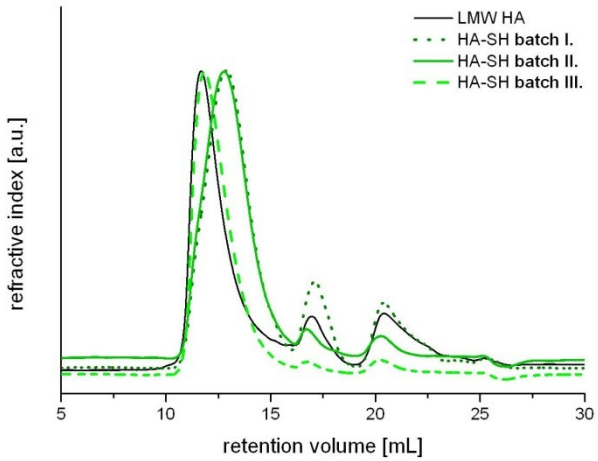

Figure 20: SEC elugram of HA-SH batches compared to LMW HA.

Table 9 summarizes the expected theoretical molecular weight with the determined molecular weights by SEC measurement.

Table 9: Molecular weights of HA-SH and HA determined by SEC measurement.

	SH-functionality [%]*	**$M_{n,\ theo.}$ [Da]**	**M_n [Da]****	**M_w [Da]****	**Đ**
LMW HA	-	27 300	11 120	53 320	4.80
batch I.	44	29 690	6 430	22 780	3.54
batch II.	52	30 080	6 560	23 700	3.59
batch III.	33	29 040	11 680	40 890	3.50

*determined by ^{1}H-NMR

**determined by water SEC (without quenching)

Since the obtained modified natural polymers showed a high batch-to-batch variation compared to the synthetic polymers, additional analysis was required to ensure the comparability of different HA-SH batches in hydrogel performance. The following analyses are only shown for the three selected HA-SH batches. These batches met the requirements for hydrogel preparation and 3D printing best and showed good comparability.

Dynamic vicosity measurements

Due to the synthesis and purification of HA-SH under acidic conditions, the backbone was partially cleaved and as a consequence of this, the viscosity as well as the molecular weight of the resulting HA-SH differed for each batch. The reproducibility of thiolated HA was challenging and, to avoid major differences in printing performance, the dynamic viscosity of the three batches was examined by falling ball viscometer before use. Therefore, 0.5 wt.% solutions of unfunctionalized LMW HA and HA-SH were prepared and measured. Higher concentrated HA solutions could not be measured due to the fact that the ball got stuck in the polymer solution.

Table 10 shows the determined viscosities of the different HA-SH batches compared to the polymeric precursor LMW HA. All viscosities of thiolated HA were significantly lower than the viscosity measured for unmodified HA. This effect can be associated to the reduction of the HA backbone during functionalization as well as to the different coiling behavior of HA-SH compared to HA. Through the introduction of thiol-groups into the backbone, the ionic character and the molecule structure was changed and molecular coiling was enhanced resulting in a lower viscosity.

The viscosities measured by falling ball viscosimetry could be directly related to 3D extrusion printing performance. It was proven that HA-SH batches with a viscosity between 1.09 and 1.50 mPa s are well suited for 3D extrusion printing using the determined polymer amount (5 wt.% in hydrogel solution) (**chapter 3.2.3**).

Table 10: Viscosities of 0.5 wt.% LMW HA and HA-SH solutions measured with a falling ball viscosimeter.

	viscosity [mPa s]
unmodified LMW HA	2.50
batch I.	1.09
batch II.	1.12
batch III.	1.44

pH value

For biological applications, cells were mixed into the hydrogel solutions and hence the pH value of the precursor solutions had to be neutral. Since HA-SH was synthesized and dialyzed under acidic conditions, the pH value of the purified polymers was prone to be acidic and thus had to be examined before use of HA-SH as cross-linking agent in hydrogels. The pH value was measured for 5 wt.% HA-SH solutions in PBS (Table 11), since this was the applied concentration of HA-SH in hybrid hydrogels. For all three HA-SH solutions an acidic pH value was measured, ranging from 2.36 (batch III.) to 2.60 (batch II.). As a consequence of that, all hybrid hydrogel precursor solutions had to be neutralized prior to cell embedding and cross-linking (**chapter 3.2.1**).

Table 11: pH values of 5 wt.% HA-SH solutions in PBS compared to unmodified HA.

	pH value
unmodified LMW HA	7.04
batch I.	2.57
batch II.	2.60
batch III.	2.36

Analysis of different HA-SH batches showed a good comparability of the three selected batches. All three batches were used as precursor polymers for thiol-ene cross-linked hydrogels. In **section 3.2.1** and **3.2.2**, the preparation as well as the examination of the hybrid hydrogels is discussed and **section 3.2.3** focuses on the printing of those gels.

3.1.5 Synthesis of peptide-functionalized PGs (P(peptide-*co*-G), 8)

Peptide-functionalized polymers can be additionally applied to interact with biopolymers via the formation of physically cross-linked hydrogels, e.g. by ionic interaction of positive charged peptides with negative charged HA (**chapter 3.3**). In order to investigate this alternative route of corss-linking, peptide-functionalized PGs (**8**) were synthesized by polymer analogue thiol-ene modification of P(AGE-*co*-G) (**5**) with cysteine terminated peptides (Scheme 14).

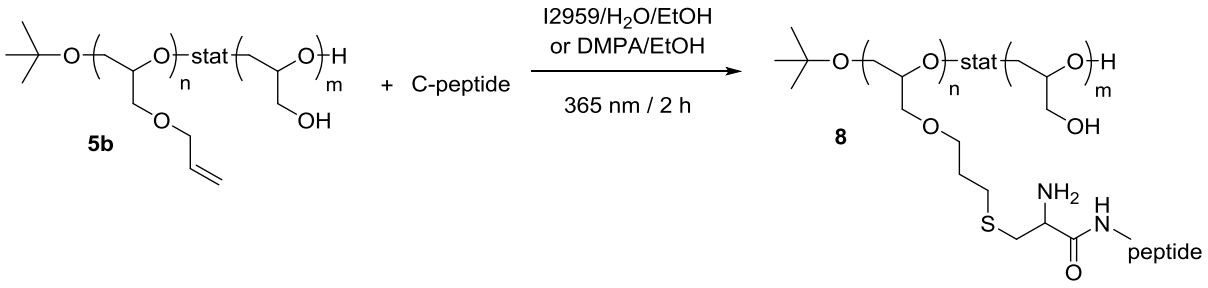

Scheme 14: Thiol-ene reaction of P(AGE-*co*-G) (**5**) with cyteine terminated peptides.

For thiol-ene reactions with allyl-functionalized PG (**5**), the peptides have to bear a free thiol group to be clickable. For all used peptides, it was therefore necessary to contain the amino acid cysteine (abbreviated as C) ideally at the beginning or the end of the peptide sequence in order to be readily accessible. Polymer **5b**, with 11 % allyl-functionality was used for all thiol-ene reactions with peptides, due to the fact that a too high content of allyl-groups (**5c**) might lead to an incomplete functionalization of P(AGE-*co*-G) (**5**), because of steric hindrance of the peptides. Whereas a too little allyl-functionality (**5a**) might yield in P(peptide-*co*-G) (**8**) with less peptides and hence less possible interactions for physical hydrogel cross-linking.
The conditions for the UV mediated reaction varied depending on the used peptide and chosen initiator. The reaction was either conducted in EtOH with DMPA or in a water-EtOH mixture with I2959 as initiator. By changing the initiator to I2959, the UV source had to be changed as well. Reactions with DMPA were examined with the LED cubes and reactions with I2959 with the UV hand lamp (**chapter 5.2.1**). For purification, the functionalized polymers were dialyzed against water and freeze-dried. Covalent binding of peptides to the polymer backbone was verified by ^{1}H-NMR and IR spectroscopy (Figure 21 and Figure 22).

Three different peptides were covalently bound to **5b**, peptide1 functioned as a model compound in order to establish the synthesis protocol, peptide2, a collagen-II (Col-II) binding peptide[148] and peptide3, a HA binding peptide[149]. Table 12 shows the used peptides and the particular conditions for the binding reaction.

Table 12: Peptides and conditions for thiol-ene reaction with **5b**.

	used peptide	**peptide abbriviation**	**M [Da]**	**condition**
8a	CGPRGQ-Orn-GVMGF-Orn	peptide1	1337	EtOH/DMAP
8b	CGWYRGRL	peptide2	1011	EtOH/DMAP
8c	RYPISRPRKRC	peptide3	1432	I2959/H_2O/EtOH

Comparison of the ^{1}H-NMR spectra of peptide-functionalized PGs **8a-c**, the polymeric precursor **5b** and the respective peptides verified the successful synthesis of **8** (Figure 21). The signals at 7.59-6.86 ppm can be assigned to the aromatic protons of the amino acids phenylalanine (abbreviated as F, peptide1, **8a**), tryptophan (abbreviated as W, peptide2, **8b**) and tyrosine (abbreviated as Y, peptide2 and peptide3, **8b-c**). The remaining protons generated broad signals at 4.35-3.86 ppm and 3.26-0.80 ppm, which were detectable in all peptide-functionalized PGs (**8a-c**) as well as in the peptide spectra. Signals at 3.71 ppm and 1.26 ppm in the spectra of **5b** and **8** can be attributed to the polymeric backbone protons and the *tert*-butyl protons, respectively.

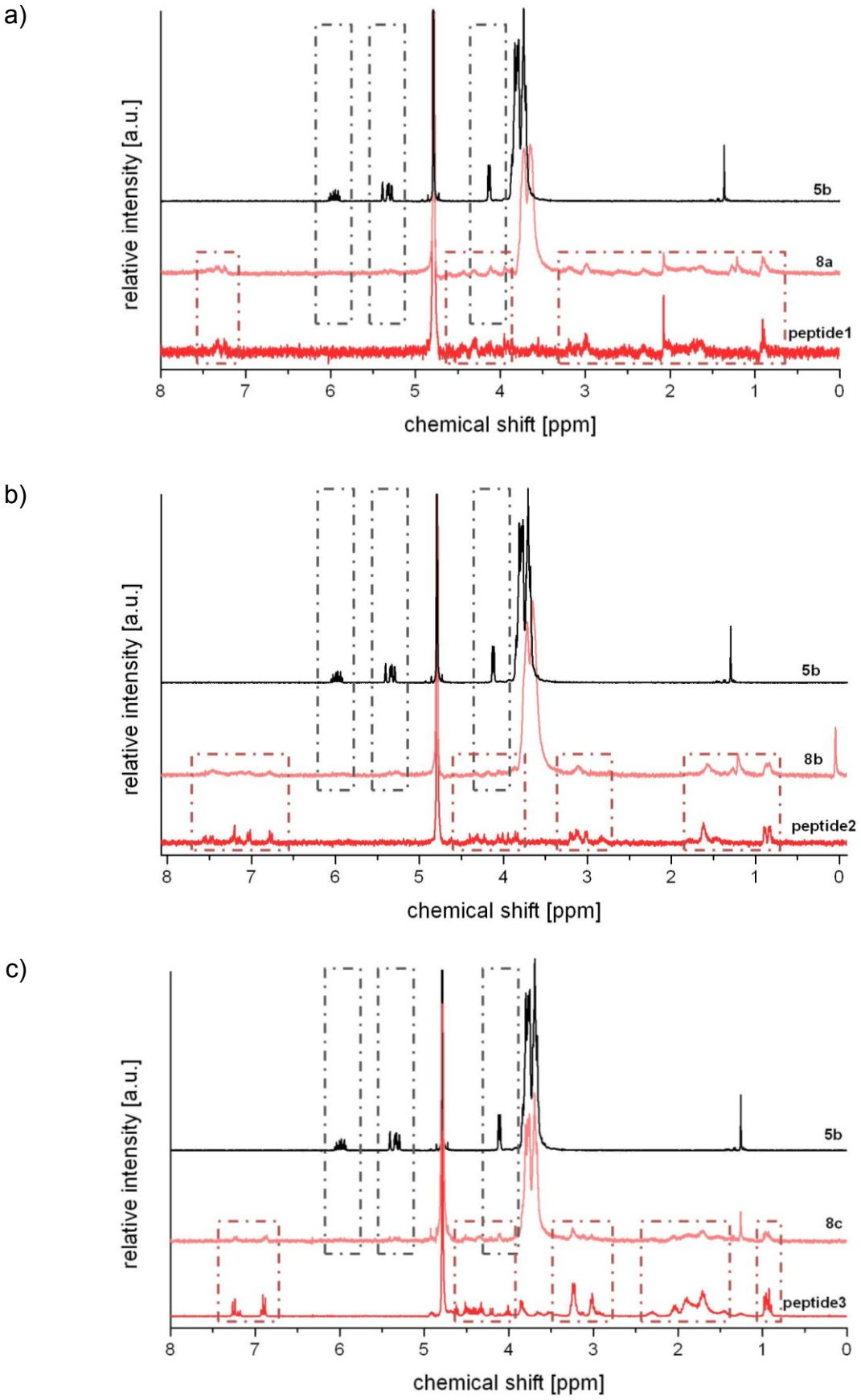

Figure 21: ^{1}H-NMR spectra of peptide-functionalized PG **8** compared with the coresponding peptide and the precursor polymer **5b**; a) **8a**, b) **8b** and c) **8c**.

Weak signals at 5.49-5.29 ppm in the spectra of **8a-c** can be assigned to unfunctionalized allyl-protons, indicating an incomplete functionalization of P(AGE-*co*-G) (**5b**). Due to the poor signal to noise ratio, integration of the peptide and allyl protons in **8** was challenging. Nevertheless, by integration of the backbone peak to 280 H (comparable to **5b**), the remaining allyl-peak could be determined as 3 H for all peptide-functionalized polymers **8a-c**. Accordingly, 4.5 out of 6 allyl-groups of **5b** were converted to peptide-groups, resulting in P(peptide$_{4.5}$-*co*-AGE$_{1.5}$-*co*-G$_{50}$). This incomplete functionalization might be revered to the lower excess of peptide (1.5:1.0 eq., peptide:allyl) compared to thiol-ene-reactions with thioacetic acid (3.5:1.0 eq., acid:allyl, **chapter 3.1.3.2**). But even with a higher amount of petide, the remaining allyl groups would likely not be functionalized due to steric hindrance. Schmitz *et al*. investigated peptide funtctionalization of poly(2-oxazoline)s by native chemical ligation using different peptide/polymer ratios (polymer:peptide molar ratio: 1:1, 1:3 and 1:6).[150] They showed that a complete peptide conjugation was impossible also when using high amounts of peptides due to static effects.

For further characterization, IR spectra of peptide-functionalized PGs **8a-c** were measured (Figure 22). In the spectra of P(peptide-*co*-G) (**8a-c**) vibrations of the peptide as well as of the polymeric precursor were detected, verifying the successful binding of peptides to the backbone of **5b**. While the peptide related vibrations of amines and amides were detected at 1640 and 1530 cm^{-1}, vibrations at 2900-2870 cm^{-1} and 1040 cm^{-1} could be assigned to –CH, –CH$_2$ and –C-O-C vibrations, respectively. The signal at 3500-3100 cm^{-1} can be attributed to hydroxyl and amine vibrations.

The successful binding of different peptides to allyl-functionalized PG (**5**) via thiol-ene chemistry proven by IR and ^{1}H-NMR measurements demonstrated the feasibility of the UV reaction for covalent peptide binding.

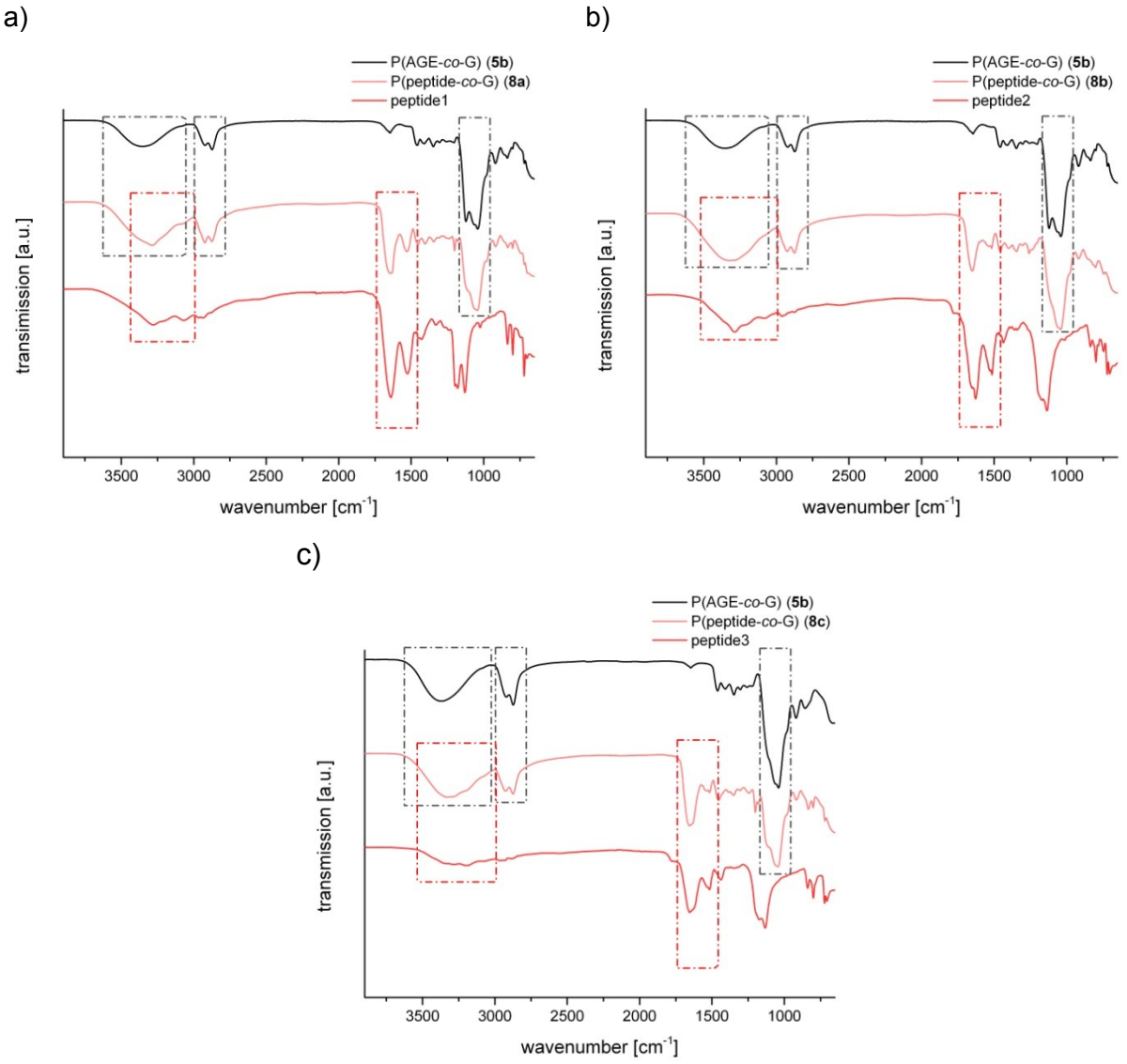

Figure 22: IR spectra of **8** compared to the precursor polymer P(AGE-*co*-G) (**5b**) and the coresponding peptide; a) **8a**, b) **8b** and c) **8c**.

Table 13: Theoretical and experimental molecular weight of **8a-c**.

	$M_{n,\ theo.}$ [Da]	$M_{n,\ exp.}$ [Da]*
8a	12 484	10 479
8b	10 527	9 012
8c	13 053	10 906

*determined by ^{1}H-NMR

The theoretical and experimental determined molecular weights are shown in Table 13. The experimental molecular weight was calculated for P(peptide$_{4.5}$-*co*-AGE$_{1.5}$-*co*-G$_{50}$), due to the fact that the ^{1}H-NMR spectra of **8a-c** showed a conversion of 4.5 AGE-groups. The incomplete functionalization can be correlated with the smaller experimental molecular weight compared to the theoretical value.

Determination of the relative molecular weight through SEC measurement was not possible, due to the tremendous interaction of the peptide-functionalized polymers **8** with the column (Figure 23). By binding of peptides to the polymer backbone, the ionic interaction and hence the coiling behavior and interaction with the column was changed and impeded a comparison of the molecular weights of **8** with PEG standards. The comparison with the polymeric precursor **5b** underlined the changed interactions with the column, due to incorporation of peptides to the side chain of the polymeric backbone.

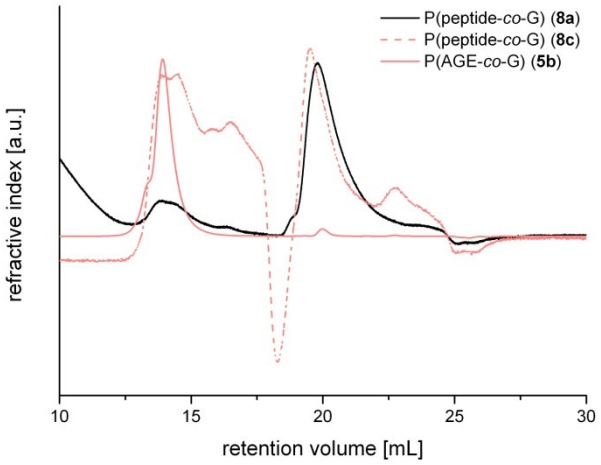

Figure 23: SEC elugram of **8a** (pale red solid line) and **8c** (pale red dashed line) compared to the polymeric precursor **5b** (black).

P(peptide-*co*-G) functionalized with peptide3 **8c** was used to determine ionic interaction between the peptide-functionalized polymer **8c** and HMW HA (**chapter 3.3**). **8b** functionalized with Col-II. binding peptide can be used for cartilage binding studies of the project Hydro-ZONES. However, this is not further discussed throughout this thesis.

3.2 Hydrogels cross-linked via thiol-ene reaction

This chapter focuses on chemically cross-linked hydrogels via thiol-ene reaction based on following polymeric precursors: allyl-functionalized PG **5**, thiol-modified PGs (**6**, **7**) and thiolated HA (HA-SH).

In the subsequent subchapters, the formation (**chapter 3.2.1**), the characterization (**chapter 3.2.2**) and the 3D printing (**chapter 3.2.3**) of these hydrogels is discussed.

3.2.1 Hydrogel formation

Hydrogel formation occurred through UV-induced thiol-ene reaction, a dimerization reaction between thiols and alkenes resulting in a thioether bond (Scheme 15). Related to hydrogel network formation, the thioether bond represents the bridge between the polymeric precursors.

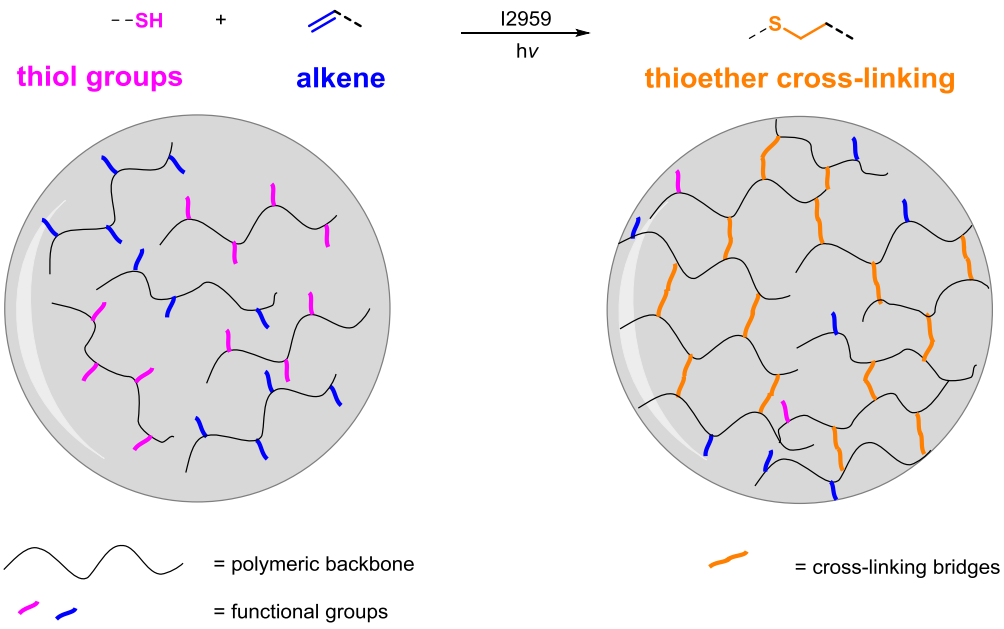

Scheme 15: Hydrogel formation via thiol-ene reaction.

Throughout this thesis, allyl-functionalized PG **5** was used as the alkene compound for thiol-ene cross-linked hydrogels. Depending on the polymeric source of the thiol component (P(SH-*co*-G) (**6**, **7**) or HA-SH) the hydrogels were categorized in synthetic

and hybrid hydrogels (Scheme 16). Through cross-linking of allyl-functional PG **5** with P(SH-*co*-G) (**6** and **7**), synthetic hydrogels were obtained, whereas cross-linking of PG **5** with thiolated HA yielded in hybrid hydrogels. For synthetic hydrogels, both degradable and non-degradble hydrogels were prepared. Hydrogels based on PG-SH_{ec} **6** with additional ester groups allowed hydrolytic degradation of the hydrogel network, in contrast to synthetic hydrogels based on PG-SH_{ef} **7**.

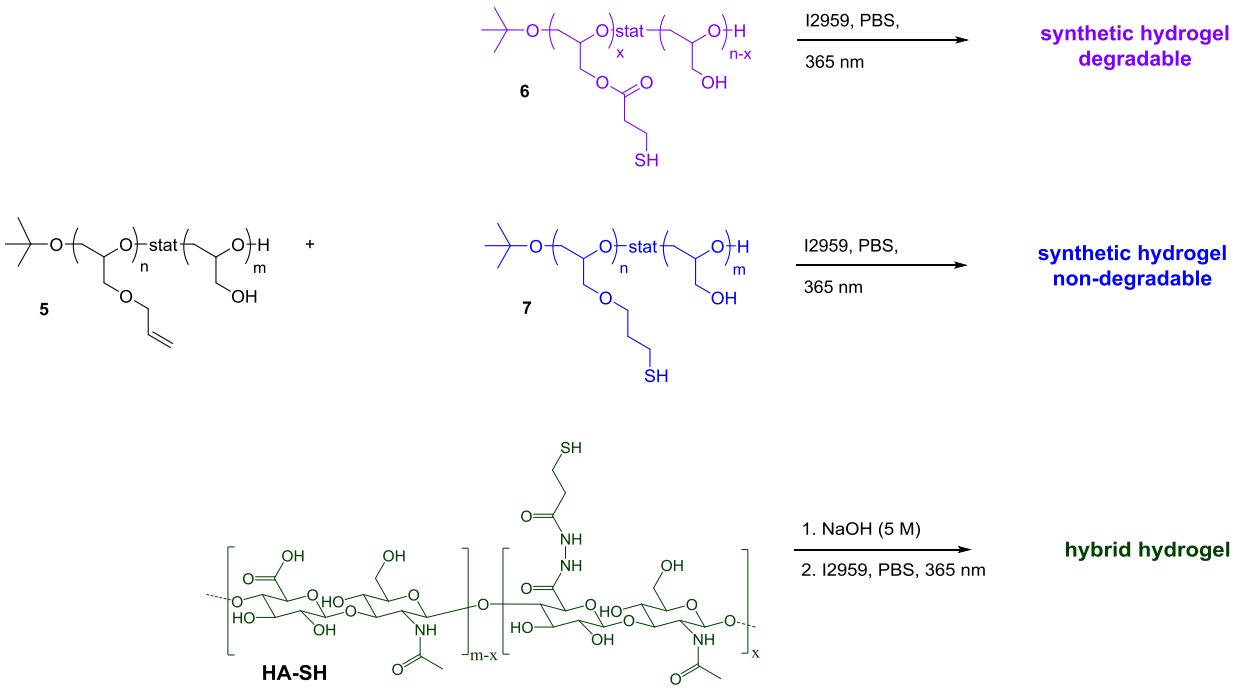

Scheme 16: Thiol-ene reaction between allyl-functionalized PG **5** and thiolated polymers **6**, **7** and HA-SH with the resulting hydrogel systems.

While thiol-ene reactions for polymer analogue functionalization of PG **5** were mostly conducted in EtOH with DMPA as initiator (**chapter 3.1.3.2**), the application of the hydrogels as cell carriers required PBS as a solvent for hydrogel cross-linking and hence a replacement of the photoinitiator DMPA with I2959. I2959 is a commonly used photoinitiatro for hydrogel cross-linking in the field of biofabrication, as it is well tolerated by many cell types over a large concentration range.[108]

For hydrogel preparation, thiol- and allyl-functionalized polymers were dissolved in PBS with an equimolar ratio of functional groups and mixed with the photoinitiator I2959. In contrast to synthetic hydrogel solutions, hybrid hydrogel precursor solutions were acidic (**chapter 3.1.4**) and thus had to be neutralized with 5 M NaOH before cross-linking. The hydrogel precursor solution was transferred into cylindrical molds

(h = 2 mm, Ø 6 mm, 57 µL) and irradiated with UV light for 10 min (365 nm, UV hand lamp).

In order to avoid later cell damage the photoinitiator concentration was kept to a minimum of 0.05 wt.% in all gel systems. The amount of polymeric precursors was dependent on the used thiolated polymers, since natural and synthetic polymers differ in solubility as well as viscosity, a lower amount of cross-linking polymers was applied for hybrid hydrogel systems. In Table 14, the general compositions and cross-linking conditions for the three different systems are listed.

Table 14: Hydrogel cross-linking conditions.

	polymers	polymer amount [wt.%]	initiator concentration [wt.%]	UV irradiation time [min]
synthetic hydrogel *degradable*	**5** + **6**	15	0.05	10
synthetic hydrogel *non-degradable*	**5** + **7**	15	0.05	10
hybrid hydrogel	**5** + HA-SH	10	0.05	10

Depending on the desired application of the hydrogel system, the properties could be tailored by variation of the compositions and cross-linking conditions. Since these hydrogels were part of the EU project HydroZONES,[VI] which aimed to develop hierarchically structured hydrogels for cartilage regeneration, the developed gels had to fulfill several requirements. One major aim was the printability by estrusion of the hydrogel precursor solutions to allow the fabrication of layer-by-layer constructed scaffolds. For printability, the hydrogel precursor solution had to be viscous enough and thus the viscosity of the hydrogel solution had to be increased by addition of HMW HA (**chapter 3.2.3**). However, the pivotal factor for the application in cartilage regeneration is the required cytocompatibility of the hydrogels. Therefore, after characterization and development of the hydrogels, the hydrogels were evaluated *in vitro* and *in vivo* together with collaboration partners of the HydroZONES consortium

[VI] Seventh Framework Programme FP7/2007-2013 under grant agreement n°309962.

(**Appendix**). For these *in vitro* and *in vivo* experiments, cells had to be encapsulated into the hydrogels, by mixing the cells into the precursor solution prior to cross-linking.

The following **chapter 3.2.2** focuses on the characterization of the hydrogels associated with the influence of different factors, for example additives and UV irradiation time.

3.2.2 Hydrogel characterization

Two major hydrogel characteristics, swelling and mechanical behavior, describe the hydrogel network and are discussed in **chapter 3.2.2.1** and **3.2.2.2**. Further characteristics as diffusion and biological suitability are presented in **chapter 3.2.2.3** and the **Appendix**.

3.2.2.1 Swelling studies

By investigating the swelling behavior, the swelling equilibrium and the maximum water uptake is determined and hence information about the network density are obtained. For swelling studies, molded hydrogels (h = 2 mm, Ø 6 mm, 57 µL) were prepared, incubated in PBS at 37 °C and weighed at specific time points over a period of five weeks.

Synthetic hydrogel system

The swelling profiles of non-degradable and degradable synthetic hydrogels are depicted in Figure 24a. Both systems showed comparable swelling within the first 24 h of incubation, however, after one week the swelling behavior of the systems started to differ. The non-degradable system reached equilibrium swelling after two weeks of incubation by release of the sol fraction (~ 20 % of the original dry polymer weight) and showed no swelling over time. In contrast to that, the degradable system gained wet weight after one week incubation, since the ester bonds of the cross-linked polymer PG-SH_{ec} **6** were hydrolytically cleaved and the network was continuously degraded, resulting in a decreased network density. Due to the degradation and the decrease in density, the hydrogel could imbibe more water and thus gained more wet weight resulting in a complete dissolution after five weeks. By lyophilisation of the supernatant, the hydrolyzed precursor polymers could be regained and the obtained weight was in agreement with the theoretical dry weight of the applied polymers.
The comparison of the two synthetic systems demonstrated the influence of the ester group of PG-SH_{ec} **6** on swelling behavior and degradation.

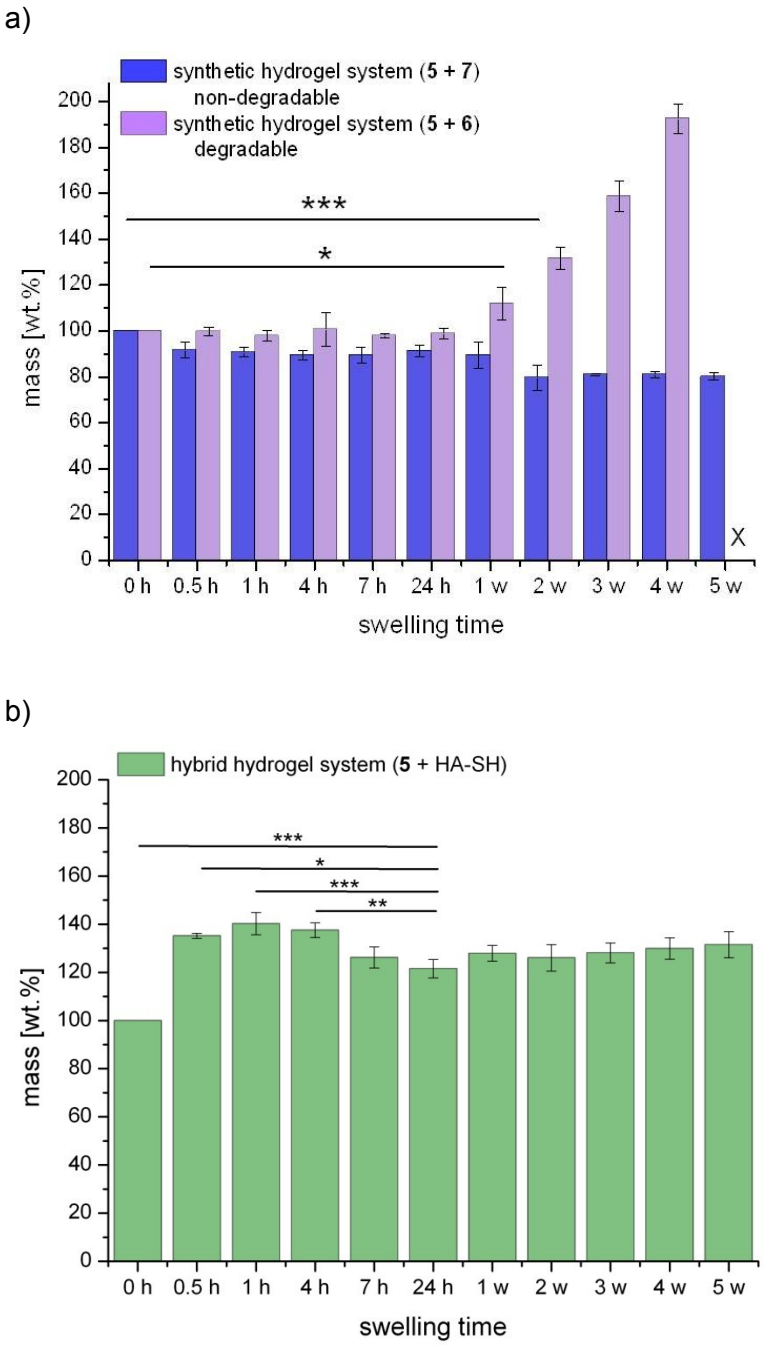

Figure 24: Swelling behavior of a) non-degradable (**5** + **7**) and degradable (**5** + **6**) synthetic hydrogels (15 wt.% polymer content, 0.05 wt.% I2959 concentration, 10 min UV irradiation) and b) hybrid hydrogels (**5** + HA-SH) (10 wt.% polymer content, 0.05 wt.% I2959 concentration, 10 min UV irradiation). The statistics are shown for the critical points in the respective diagrams, on the one hand the reached equilibrium (a) non-degradable system and (b) and on the other hand the beginning of the degradation degradable system in (a).

Hybrid hydrogel system

The impact of the polymer origin on the swelling behavior can be seen by comparison of the swelling profiles of the synthetic hydrogels with the profile of the hybrid hydrogel (Figure 24). The hybrid hydrogels swelled in the first hour up to 140 ± 4.6 %, whereas the synthetic hydrogels showed no initial swelling. This effect can be directly associated with the exchange of the thiol-component. The biopolymer HA has a hydrophilic nature and thus binds large amounts of water, in addition cross-linking with HA-SH instead of P(SH-*co*-G) (**6**, **7**) required a decrease in polymer concentration due to solubility and viscosity issues, resulting in hydrogels with a less dense network. This led to a higher water absorbance of the hybrid hydrogel network and hence a higher swelling equilibrium of 122 ± 3.8% was reached for hybrid hydrogels after 24 h incubation. The statistic deviations depicted in Figure 24b show, that there is a difference in mass up to 24 h swelling time and no significant difference after these 24 h. Therefore, the following mechanical tests (**chapter 3.2.2.2**) were conducted at swelling equilibrium after 24 h incubation.

Swelling behavior of hydrogels with additive HMW HA

One major goal of this thesis was to achieve printability of the developed hydrogel solutions. Therefore, it was necessary to increase the initial viscosities of the hydrogel precursor solutions by addition of HMW HA prior to cross-linking. Besides viscosity, the swelling behavior was also affected by the incorporation of non-bound HA. This influence on synthetic and hybrid hydrogels was evaluated with different amounts of HA, since the concentration of the HMW thickener had to be adjusted to the subsequent biological application and the 3D printing requirements of the respective system (**chapter 3.2.3**). Thus, the study was conducted with additional 3.5 wt.% (synthetic system) and 1.0 wt.% (hybrid system) HMW HA (Figure 25). The study revealed that regardless of the amount of additional HA and regardless of the used system, the incorporation of HMW HA influenced the swelling behavior of both systems equally. In the first hour, hydrogels with HMW HA showed a strong initial swelling up to ~ 200 wt.% referred to the start weight, followed by a mass decrease within the first 24 h/1 w. After 24 h (hybrid system) and 1 w (synthetic system) the equilibrium swelling of the hydrogels with additional HMW HA was comparable to the systems without supplemented HA.

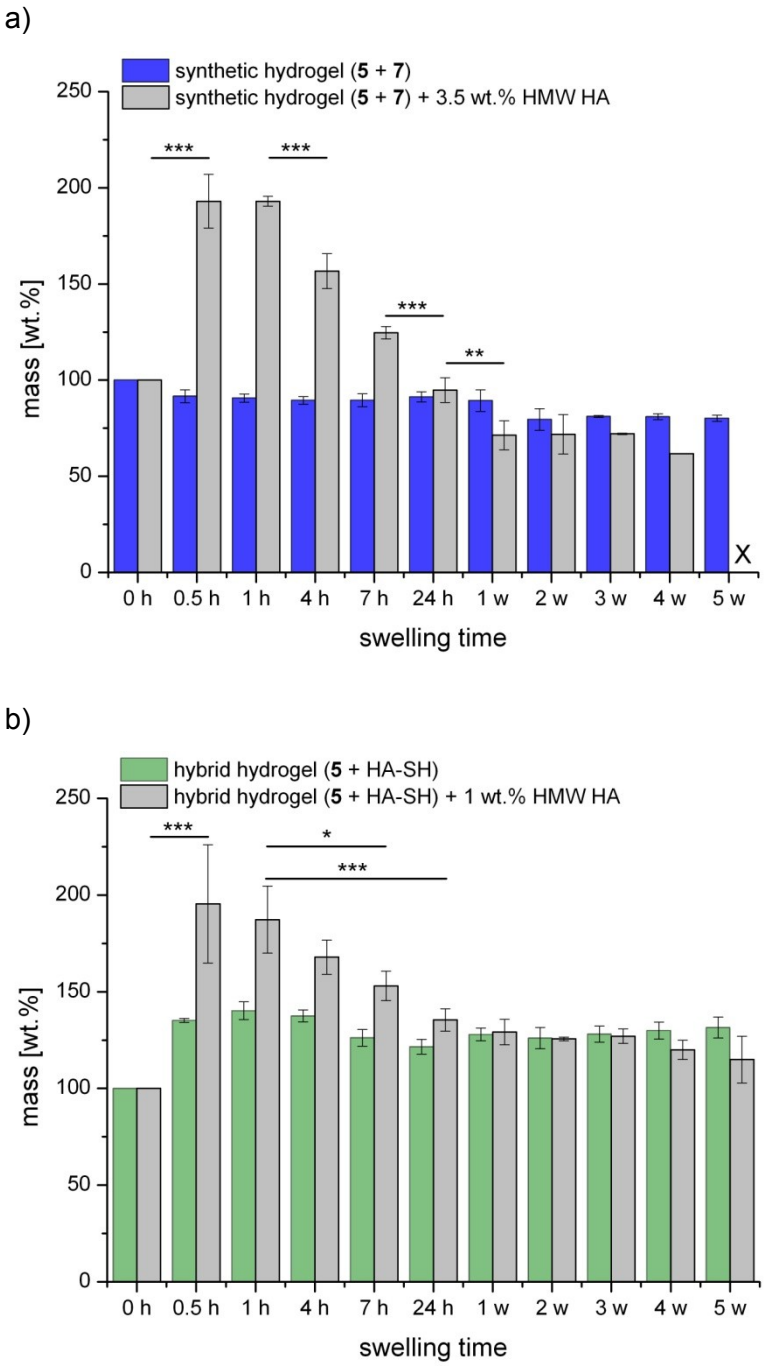

Figure 25: Swelling profiles of a) synthetic and b) hybrid hydrogels with and without additional HMW HA. The statistics are shown for the hydrogels with additional HMW HA at the decisive points of the measurement: initial swelling and reached equilibrium.

The swelling profiles of hydrogels with HMW HA demonstrated that the unbound HA had only an influence on the initial swelling and not on the swelling equilibrium of the hydrogels. As previously discussed, the water uptake in the first hour can be related to the hydrophilic nature of HA, whereas the mass loss might led to the presumption that the non-bound HA is released out of the network within the first 24 h. Therefore,

additional diffusion measurements with embedded fluorescently-labeled HMW HA (800 kDa) were conducted to determine the release of unbound HA out of the network (**chapter 3.2.2.3**). These measurements showed that the labeled HMA HA was not released out of the network as it was expected from the swelling measurements. Additionally, the supernatant was examined during the swelling measurements and HMW HA could not be detected in the lyophilizate. Thus the decrease in mass in the first 24 h was attriubted to the dissolution behavior of HA instead of release of unbound HA. After complete dissolution the HA molecules relaxate which led to a syneresis effect.

Although both systems showed comparable changes in swelling behavior by addition of non-bound HA, the synthetic hydrogels with supplemented HA appeared softer, assuming a less dense network, resulting in hydrogels which were destroyed after 4 w of measurement. The influence of the additional HMW HA on the stiffness was investigated by mechanical testing of the hydrogels and is discussed in the following **subchapter 3.2.2.2**.

3.2.2.2 Mechanical testing and swelling ratio

The mechanical properties of the hydrogels were examined, to determine the influence of different parameters on the hydrogel stiffness and hence the network density. Therefore, unconfined compression tests of cylindrical hydrogels (h = 2 mm, Ø 6 mm, 57 µL) with varying parameters, such as UV irradiation time, polymer concentration and swelling time were implemented. The stiffness of the hydrogels, the so-called Young's modulus, was given by the slope of the true stress-strain curve in the linear elastic range (strain: 0-10 %). Additional to the mechanical tests, the swelling ratio (SR), the quotient of the swollen weight (W_s) and the dried weight (W_d), was calculated for the used hydrogels. For these SR measurements, the hydrogels were weighed before the mechanical testing (W_s), freeze-dried after the testing and weighed again (W_d).

The results of the synthetic and hybrid hydrogels are first discussed separately, as the hybrid hydrogel implied batch-to-batch variations and hence requested the examination of an additional parameter. At the end of this subchapter, the results of both systems are summarized and compared.

Synthetic hydrogel system

The first mechanical study shows the influence of the swelling time on hydrogel stiffness and SR (Figure 26). For each time point, triplets of non-degradable and degradable hydrogels were prepared, incubated in PBS at 37 °C and measured. In the first 24 h, both hydrogel systems showed no significant difference in SR and Young's modulus. Furthermore, the stiffness was constant over this time period with an average value of 78.9 ± 15.1 kPa for the non-degradable system and 95.5 ± 19.1 kPa for the degradable system. The same applies for the SR within the first 24 h of incubation, for the non-degradable system a mean value of 6.8 ± 0.4 and for the degradable system a mean value of 6.6 ± 0.4 was calculated. However, the measurements after 4 w of incubation demonstrated the differences between both systems. The Young's modulus (99.4 ± 20.0 kPa) and the SR (7.2 ± 0.6) of the non-degradable hydrogel was comparable with the values of the first 24 h, whereas, as the ester bonds of the degradable system were hydrolytically cleaved, the network

density of the degradable hydrogel decreased, followed by a significantly decreased stiffness (9.7 ± 0.6 kPa) combined with an increased SR (17.5 ± 0.9).

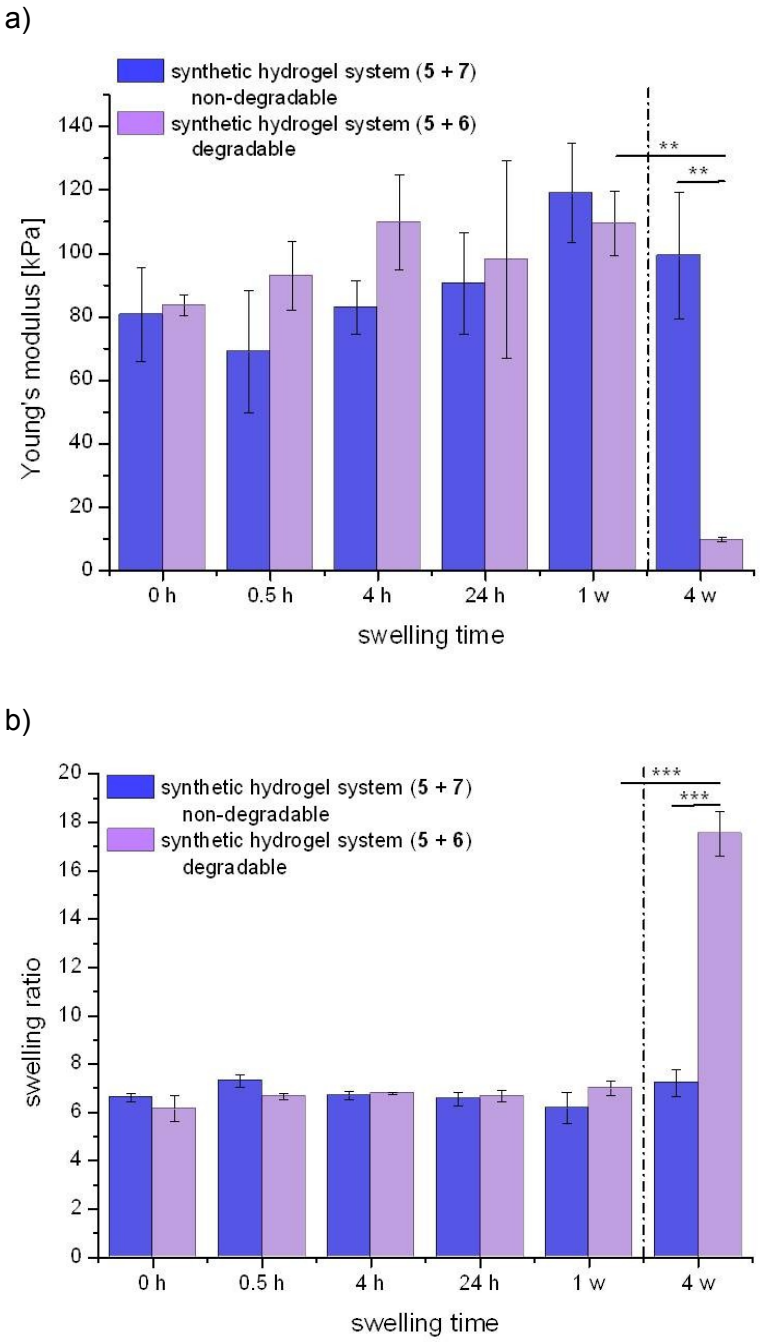

Figure 26: Influence of swelling time in PBS on hydrogel stiffness and SR, shown for non-degradable (blue) and degradable (purple) synthetic hydrogels (15 wt.% polymer concentration, 0.05 wt.% I2959 concentration, 10 min UV irradiation). The statistical difference between the 4 w measurement (degradable system) and the earlier time points were all comparable and are shown as an example for the comparison between 4 w and 24 h.

Summarizing the results of the SR and the mechanical examinations, it was determined that the non-degradable and degradable synthetic hydrogels were comparable during the first 24 h of incubation concerning stiffness and SR. Therefore, the influence of further parameters was evaluated with non-degradable hydrogels after an incubation time of 4 h.

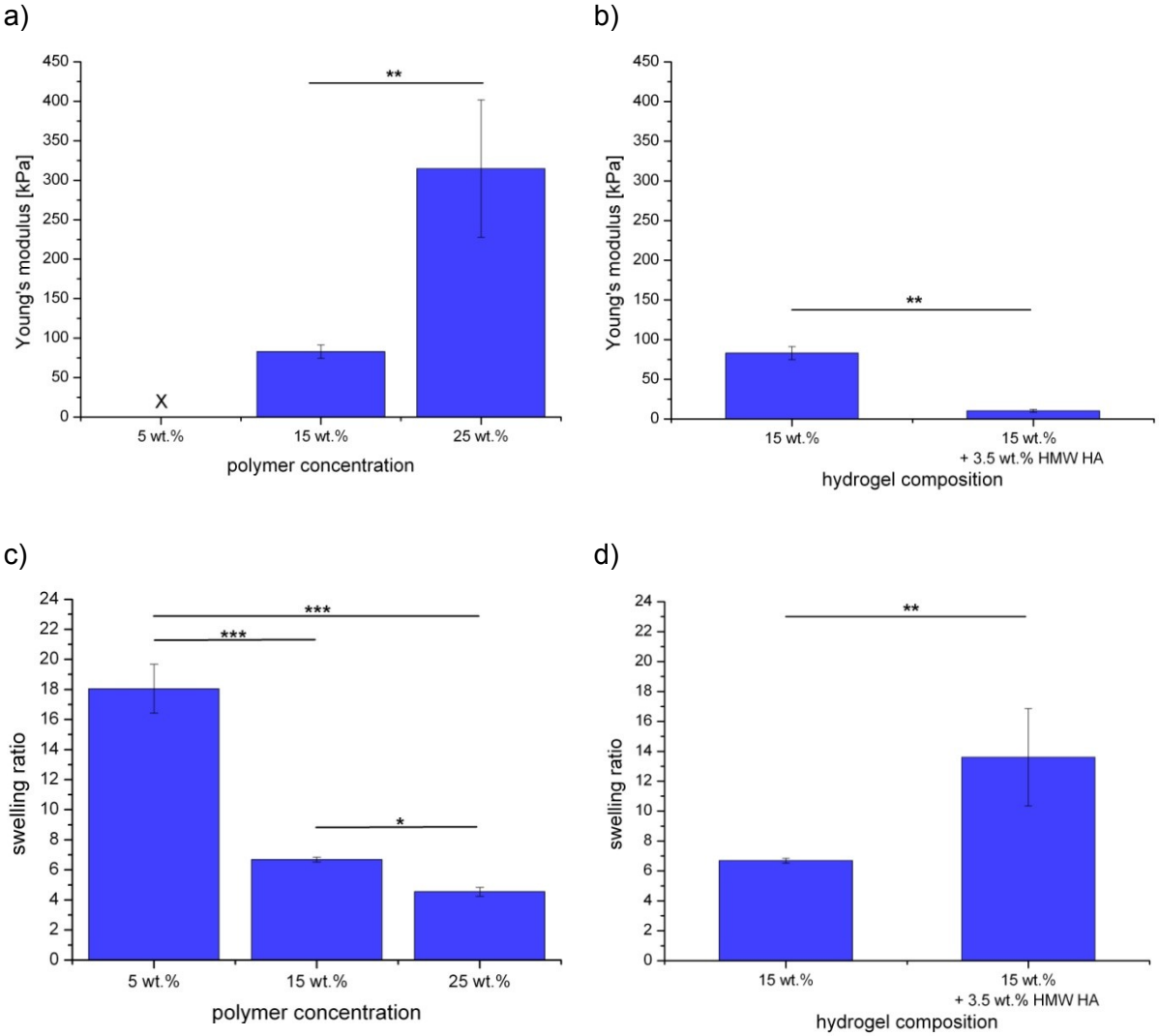

Figure 27: Influence of polymer content (a + c) and addition of 3.5 wt.% HMW HA (b + d) on stiffness and SR of non-degradable synthetic hydrogels (**5** + **7**; 10 min UV irradiation, 0.05 wt.% I2959 concentration).

To investigate the influence of polymer amount on stiffness and SR, triplets of hydrogels with 5, 15 and 25 wt.% polymer concentration were prepared and measured (Figure 27a/c). As the hydrogel network is formed by cross-linking of the

functional groups of the polymeric precursors, the concentration of these polymers has a huge influence on the network density.

Hydrogels with an increased concentration of 25 wt.% were almost four times stiffer (314.7 ± 87.0 kPa) compared to hydrogels with a polymer concentration of 15 wt.% (83.0 ± 8.4 kPa), whereas hydrogels with only 5 wt.% polymer amount were too weak for the mechanical measurements (Figure 27a). The reverse trend was observed for the SR, with increased polymer content the SR decreases from 18.1 ± 1.6 (5 wt.% hydrogels) to 4.6 ± 0.3 (25 wt.% hydrogels), due to the fact that hydrogel networks with a higher polymer concentration can incorporate less water (Figure 27c). The relationship between polymer concentration and Young's modulus was previously evaluated for diverse hydrogel systems.[16, 19, 104, 105, 151] In agreement with the herein presented study, they demonstrated an increased stiffness combined with a decreased SR by increasing the polymer concentration.

Apart from the influence of cross-linkable polymers, the impact of additional unbound HA was also investigated (Figure 27b/d). Incorporation of 3.5 wt.% HMW HA to 15 wt.% synthetic hydrogels yielded in gels with a significant lower Young's modulus (10.2 ± 1.8) along with an increased SR (13.6 ± 0.3). The significant decrease in hydrogel stiffness is in accordance with a less dense network, which led to the conclusion, that the non-bound HA hampered the hydrogel cross-linking. This is in line with the observation during swelling measurements (**chapter 3.2.2.1**), where the gels appeared softer and were destroyed after 5 w of incubation. Hydrogels with a looser network can absorb more water, resulting in hydrogels with an higher SR. Additionally, as discussed before, the incorporation of the hydrophilic natural polymer HA led to a higher water uptake mainly in the first hour of incubation, which strongly influences the initial swelling and hence also the SR.

As the cross-linking reaction is triggered through radicals generated by UV light, the influence of UV irradiation time as well as the influence of UV intensity on Young's modulus and SR was investigated. For the UV irradiation dependency study, non-degradable synthetic hydrogels with 15 wt.% polymer concentration were cross-linked for 5, 10 and 15 min with the UV hand lamp (1 mW cm^{-2}) (Figure 28a/c). The stiffest hydrogels with a value of 122.5 ± 17.4 kPa were obtained for the longest

irradiation time, whereas the UV irradiation of 5 min led to hydrogels with a less dense network and hence an decreased Young's modulus of 62.6 ± 6.9 kPa. A comparable effect of UV exposure time on hydrogel stiffness and SR was demonstrated for gelatin-methacrylamide (gelMA) and norbornene-functionalized HA hydrogels.[16, 105]

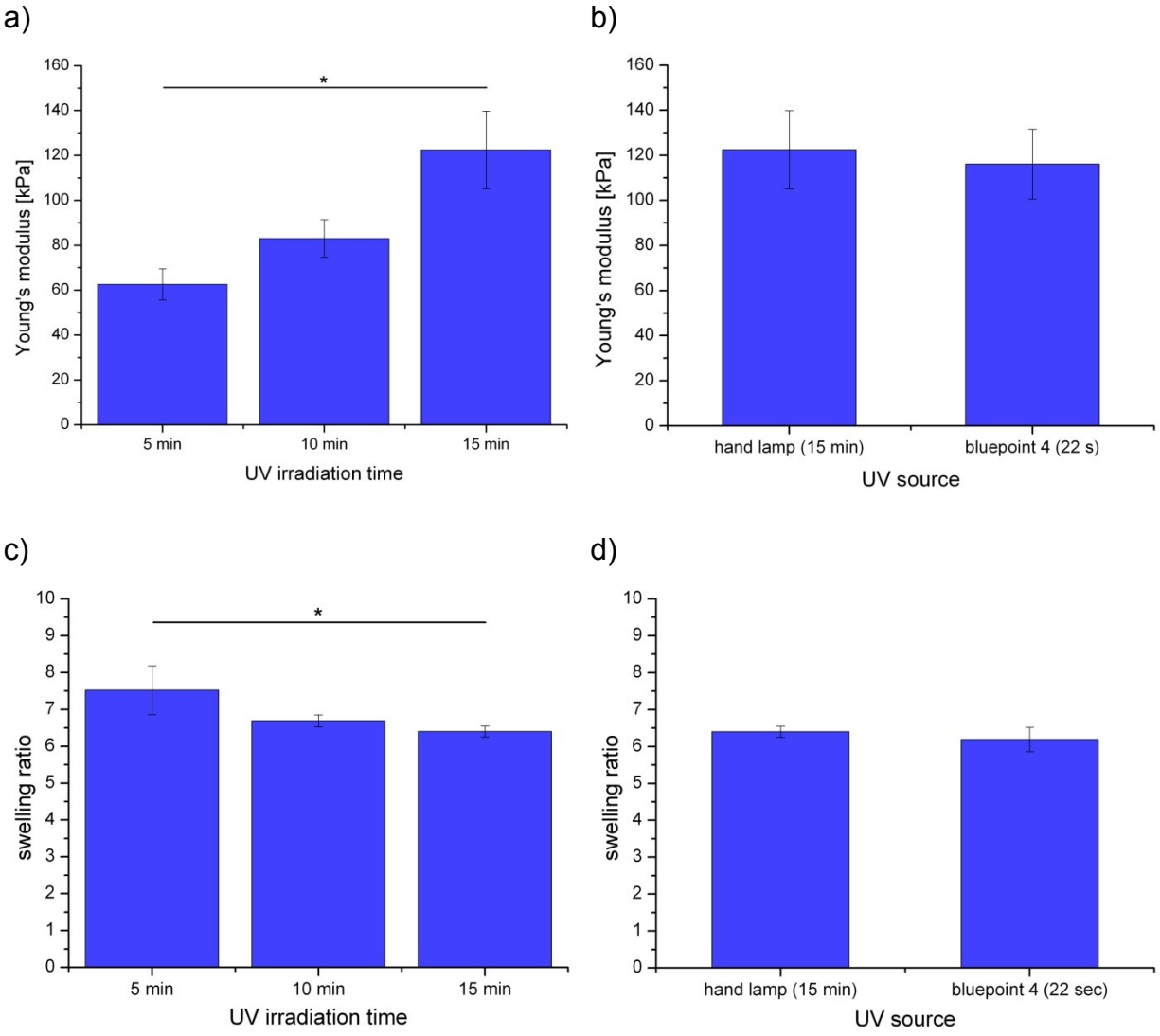

Figure 28: Influence of UV irradiation time (a + c) and UV source (b + d) on Young's modulus and SR of non-degradable synthetic hydrogels (**5** + **7**; 15 wt.% polymer concentration, 0.05 wt.% I2959 concentration).

Considering the application of the hydrogels, the low intensity UV source was well suited for biological applications, since cells can be harmed by UV light and the intensity in addition to the irradiation time should be adjusted to a minimum.

Nevertheless, 3D printing required a high intensity UV source, to ensure fast cross-linking directly after hydrogel solution deposition. Therefore, a second UV light (bluepoint 4) with a higher intensity of 130 mW cm^{-2} was used for cross-linking the printed constructs. To investigate the influence of the high intense UV source on stiffness and SR, the molded hydrogels were cross-linked with the bluepoint 4 lamp and the results were compared with the values obtained for gels prepared with the less intense UV hand lamp (Figure 28b/d). Since the molded hydrogels have a height of 2 mm and a printed construct with this height is cross-linked for 22 s, the casted gels were irradiated for this period. The Young's modulus (116.1 ± 15.5 kPa) and the SR (6.2 ± 0.3) of these hydrogels were comparable to the stiffness and SR of hydrogels cross-linked for 15 min with the less intense UV lamp.

Hybrid hydrogel system

The influence of different parameters on the stiffness and SR was also examined for hybrid hydrogels which include the biopolymer HA-SH as the thiol component of the hydrogel. All measurements, with the exception of the time-dependent study, were conducted after 24 h of incubation since the swelling profile of hybrid hydrogels showed equilibrium swelling at this time point.

As already discussed in **chapter 3.1.4**, the major disadvantage of the used modified biopolymers is their batch-to-batch variation followed by subsequent differences in hydrogel performance. Therefore, the analysis of different HA-SH batches presented in **chapter 3.1.4** aimed to determine comparable batches. Three different HA-SH batches, abbreviated as batch I. – III., were found to be comparable and used for further hydrogel preparations, characterizations and applications.
Even though the batches were well comparable in their polymer analysis (SEC, NMR, pH value and viscosity), mechanical and SR measurements revealed differences between hydrogels prepared with varying batches (Figure 29). While hydrogels prepared with batch II. resulted in the stiffest gels with a Young's modulus of 126.8 ± 27.2 kPa and a SR of 11.8 ± 0.6, gels prepared with batch I. had a significant lower Young's modulus of 46.6 ± 5.0 kPa combined with a higher SR of 14.9 ± 1.6. The stiffness of hydrogels prepared with batch III. (55.8 ± 9.2 kPa) was comparable to the stiffness of batch I. related gels, but the gels differed in their swelling behavior

and thus in their SR. Generally, the SRs of the hydrogels were not comparable and swelling behavior differed for each batch.

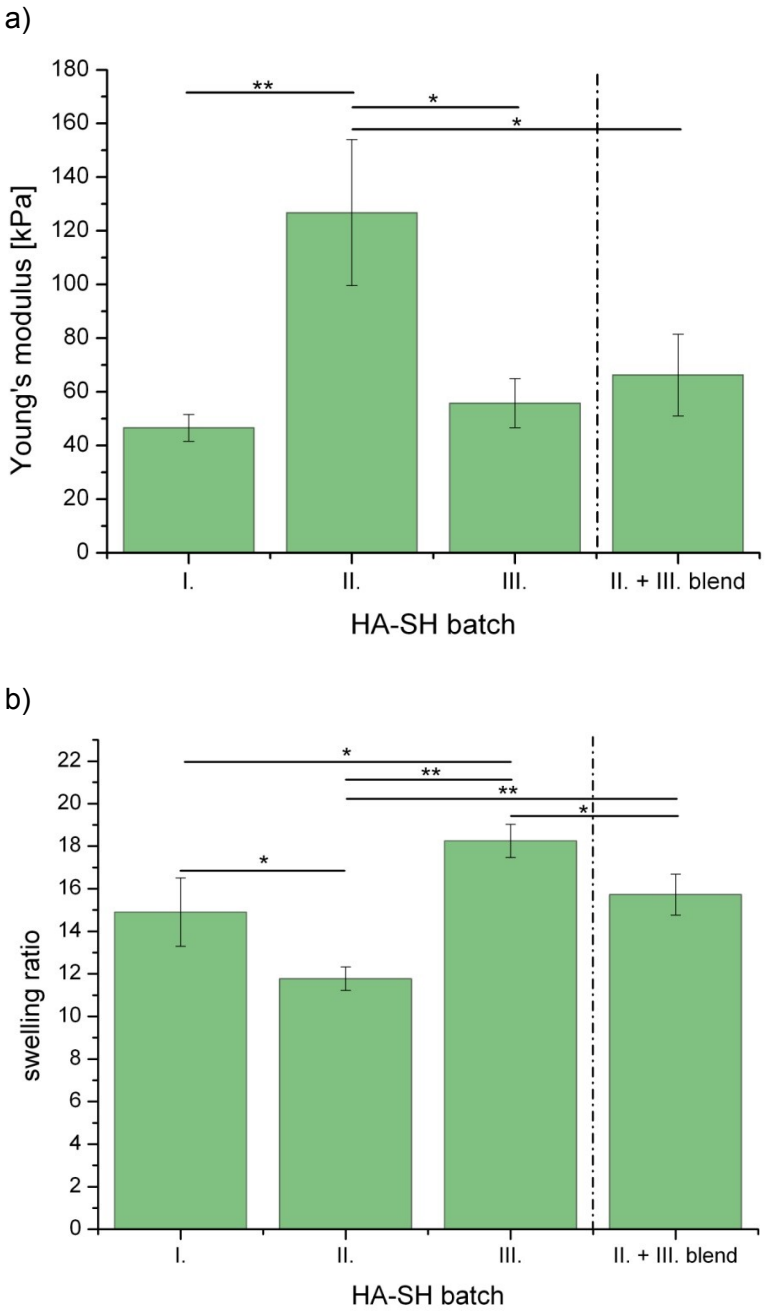

Figure 29: Young's modulus (a) and SR (b) depending on the used HA-SH batch. Hybrid hydrogels (**5** + HA-SH): 10 wt.% polymer concentration, 0.05 wt.% I2959 concentration, 24 h swelling time and 10 min UV irradiation time.

As hydrogels prepared with batch I. were widely used for biological applications by partners of the EU project and batch I. was running out, it was necessary to find an

adequate replacement. Mechanical as well as SR measurements obtained that neither batch II. nor batch III. were suitable to replace batch I., since hydrogels related to batch II. were too stiff and hydrogels related to batch III. swelled too strong. As a consequence of that, a blend batch combining batch II. and III. (50:50) was mixed and used for hydrogel preparation. Stiffness and SR of hydrogels cross-linked with the blend batch, showed no significant difference to batch I. gels and thus the blend batch was used as a substitute for batch I.
In the following figures, the used batch is always given in the graphs.

Next, time dependent Young's modulus and SR measurements were conducted with hybrid hydrogels. Therefore, triplets of hybrid gels were incubated in PBS at 37 °C for 0.5 h, 4 h, 7 h, 24 h, 1 w, 2 w, 3 w, 4 w and 5 w and the stiffness as well as the SR was determined for each time point (Figure 30).
A decreased Young's modulus and an increased SR were measured in the first 4 h of incubation, since the gels swelled initially in this time period, which was already observed in the swelling study (**chapter 3.2.2.1**). Than after 7 h of incubation a Young's modulus equilibrium was reached. The average stiffness of the hydrogels in the first 4 h was 29.1 ± 9.8 kPa, while the average equilibrium stiffness between 7 h and 5 w increased up to 48.1 ± 16.2 kPa. Compared to synthetic hydrogels, the standard deviations of the measured Young's modulus were significantly higher for hybrid gels due to the fact that by incorporation of the natural based polymer HA-SH the resulting hydrogel solutions and thus the hydrogel network density was more inhomogeneous. For the SR, an equilibrium between 7 h and 3 w was measured, with an average value of 15.3 ± 0.9. After 4 w an increased SR of 19.1 ± 1.6 was measured, which suggests a less dense network and thus the presumption of a partial hydrogel degradation.

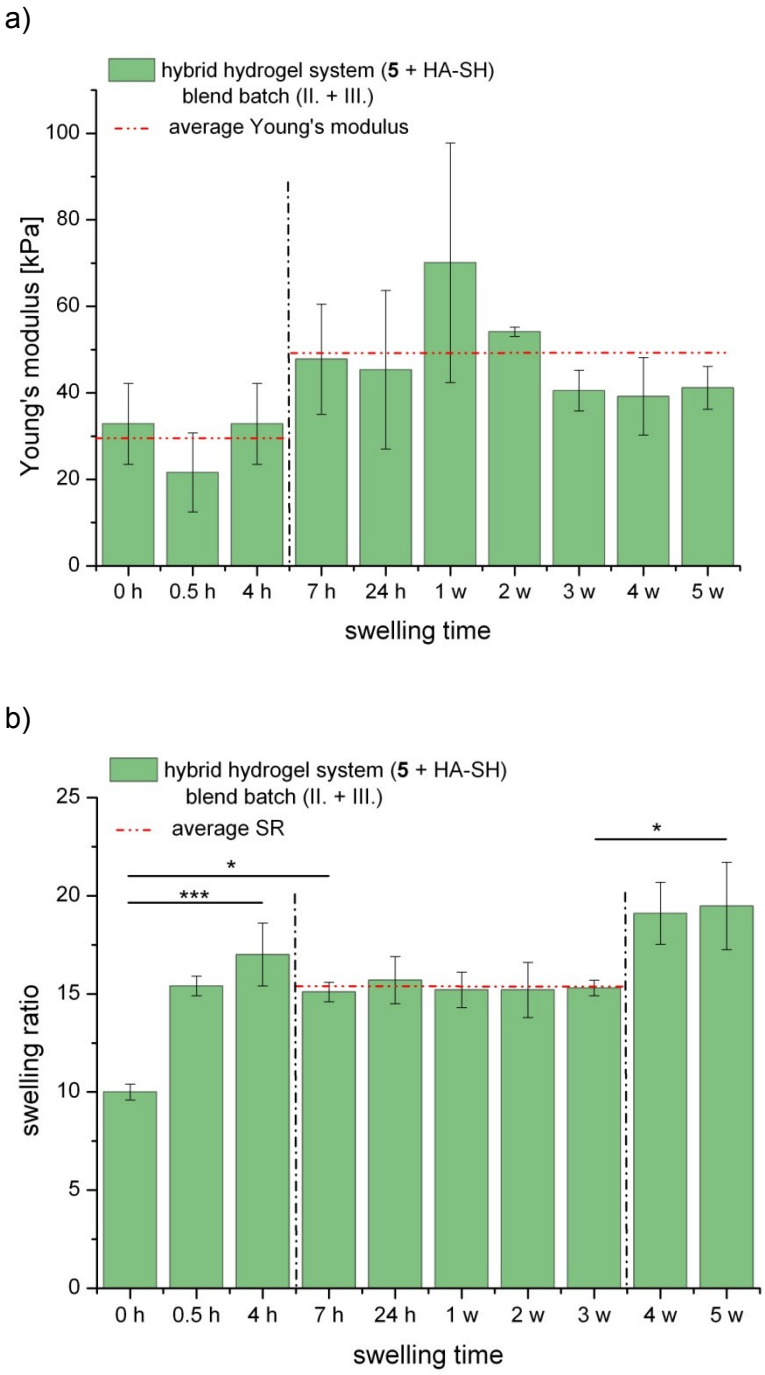

Figure 30: Influence of swelling time on Young's modulus and SR of hybrid hydrogels (10 wt.% polymer concentration, 0.05 wt.% I2959 concentration and 10 min UV irradiation).

As already shown for the synthetic hydrogels, the concentration of cross-linkable polymers has a huge influence on the stiffness and SR of the hydrogels (Figure 31a/c).

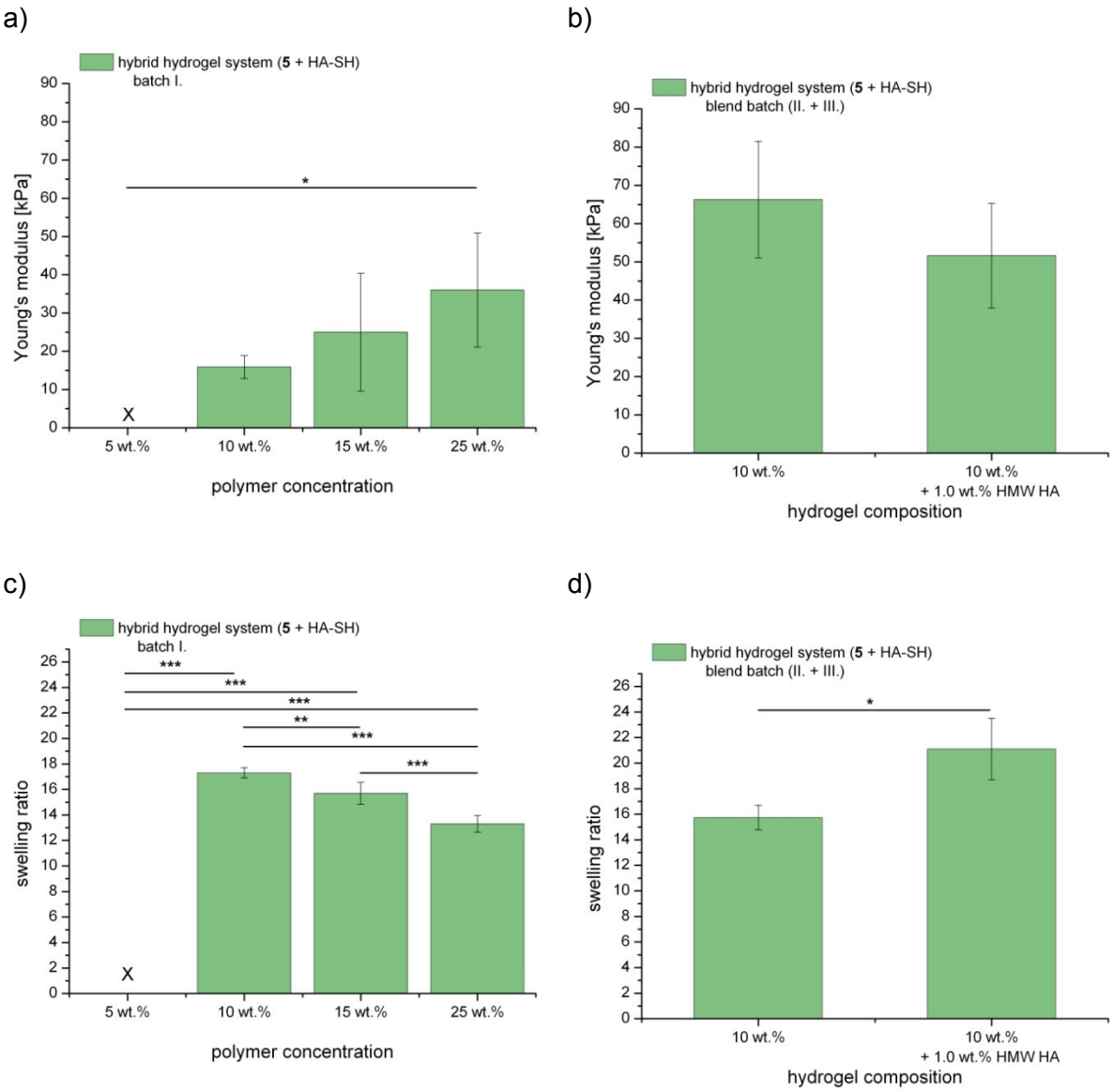

Figure 31: Influence of polymer concentration (a and c, 5 min UV irradiation) and hydrogel composition (b and d, 10 min UV irradiation) on hybrid hydrogels (0.05 wt.% I2959 concentration).

With higher polymer concentrations the network density increased which is in accordance with an increasing stiffness and decreasing SR. This relation between polymer concentration and swelling/stiffness was already demonstrated for the

synthetic hydrogel system as well as for other hydrogel systems in previous studies.[16, 19, 104, 105, 151]

Besides the expected trend, it was striking, that the standard deviation increased up to 60 % for hydrogels with a higher polymer concentration than 10 wt.%. An increased polymer content resulted in inhomogeneous polymer solutions having hydrogels with inhomogeneous networks as a consequence. Due to these solubility issues and the related problems with varying physical characteristics, hybrid gels were prepared with 10 wt.% instead of 15 wt.% polymer concentration compared to synthetic gels.

To investigate the influence of additional non-bound HMW HA on SR and Young's modulus of hybrid hydrogels, 10 wt.% hydrogel solutions were supplemented with 1 wt.% HMW HA (Figure 31b/d). The stiffness of hydrogels with additional HMW HA was with a value of 51.6 ± 13.7 kPa slightly lower compared to the stiffness of hydrogels without non-bound HA (66.3 ± 15.3 kPa) and the SR for hydrogels with incorporated HMW HA increased from 15.7 ± 1.0 (without HMW HA) up to 21.1 ± 2.4 (with HMW HA). The increased SR and the slightly decreased stiffness led to the conclusion that the network density of hybrid hydrogels with additional HA was decreased. However, compared to the huge impact of HMW HA on the SR and stiffness of synthetic gels, the influence on the hybrid system was rather low, which can be explained by the amount of additional HA which was added to the different hydrogel solutions. Since hybrid hydrogels were supplemented with only 1 wt.% HMW HA instead of 3.5 wt.% HA, less polymeric chains of HMW HA were present during hydrogel cross-linking and hence the network building was less disturbed by supplemented HA. Thus, the hydrogel network density of hybrid hydrogels was less influenced and changed by addition of non-bound HA. Furthermore, the hybrid system already includes the hydrophilic polymer HA-SH and the initial swelling is without supplementary HA already higher as for the synthetic system and thus the differences in swelling between with and without additional HA is smaller.

The influence of UV irradiation time was also examined for hybrid hydrogels (Figure 32a/c). After 10 min of UV irradiation, the Young's modulus reached a plateau at 35.4 ± 6.0 kPa and further irradiation for 5 min resulted in gels with comparable stiffness (36.4 ± 4.9 kPa) as well as comparable SR of 13.6 ± 0.3 (10 min) and

14.8 ± 1.7 (15 min). The results are comparable to previous studies from literature.[16, 105]

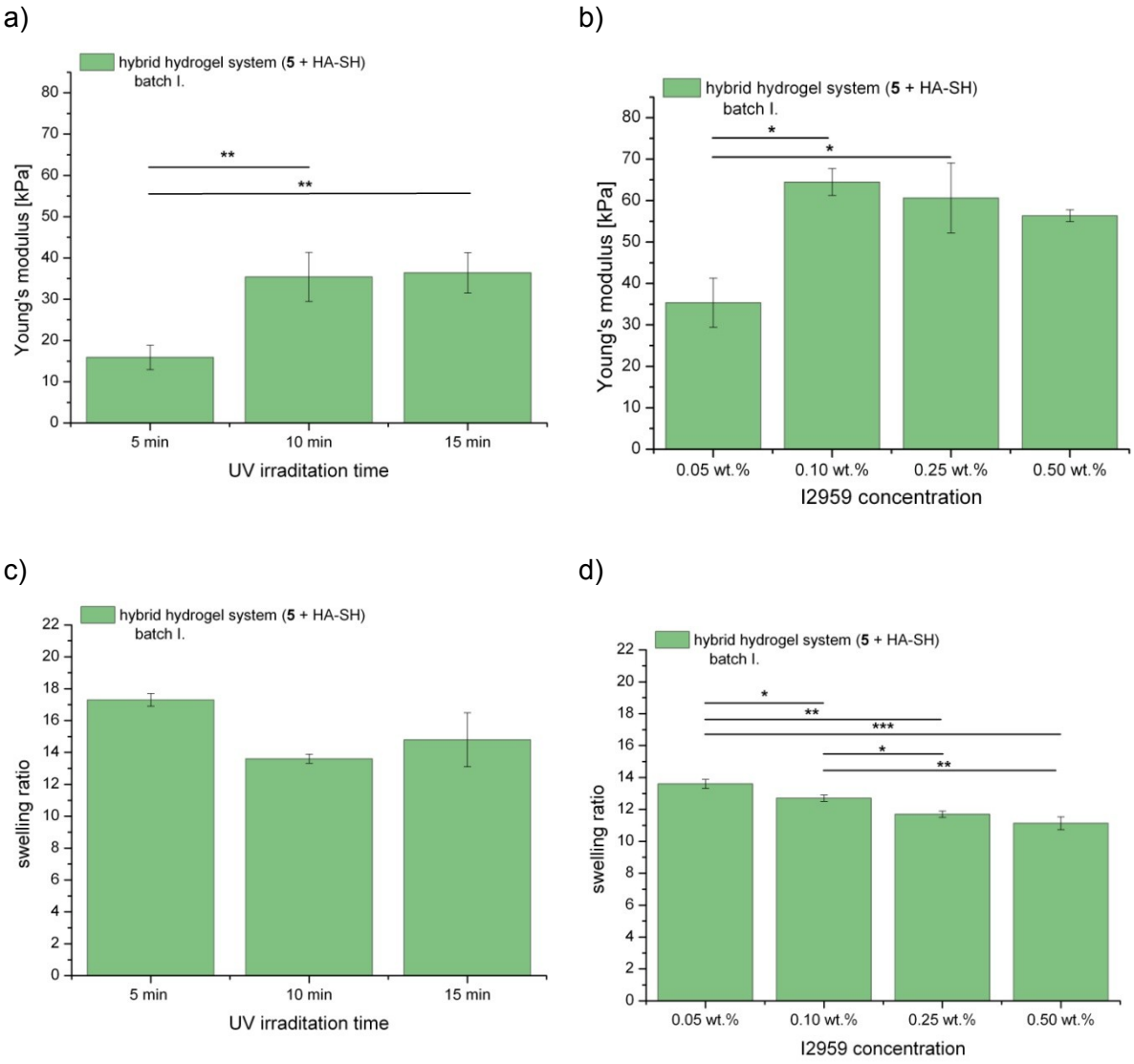

Figure 32: Young's modulus and SR of hybrid hydrogels (10 wt.% polymer concentration) dependent on UV irradiation time (a and c, 0.05 wt.% I2959 concentration) and on I2959 concentration (b and d, 10 min UV irradiation time).

As a final parameter, the photoinitiator concentration was varied and the impact on hydrogel stiffness and SR was examined. Therefore, hybrid hydrogels with 0.05, 0.10, 0.25 and 0.50 wt.% I2959 concentration were prepared and measured (Figure 32b/d). A Young's modulus maximum of 64.5 ± 3.3 kPa was measured for hydrogels with 0.10 wt.% photoinitiator, implying that further addition of I2959 did not result in stiffer gels. As the amount of photoinitiator and hence the amount of free radicals has

a huge influence on cell survival during hydrogel network building, the I2959 concentration was kept to a minimum (0.05 wt.% in biological applied gels) in order to avoid severe cell damage.

Comparison of synthetic and hybrid hydrogel system

The mechanical and SR measurements of hybrid and synthetic hydrogels generally followed the same trends. However, the exchange of the thiol-compound P(SH-*co*-G) (**6**, **7**) with the functional biopolymer HA-SH for hybrid hydrogels involved two major drawbacks: firstly, high batch-to-batch variations and secondly, inhomogeneous solutions resulting in hydrogels with different physical properties and thus measurements with higher standard deviations. Due to the differences in solubility, homogeneity and polymer source of synthetic and hybrid hydrogels, the measuring conditions differed in part, for example incubation time (4 h synthetic hydrogel, 24 h hybrid hydrogel) and basic polymer concentration (15 wt.% synthetic hydrogel, 10 wt.% hybrid hydrogel), which makes a comparison of the obtained values even more difficult.

Therefore, the overview table of Young's modulus and SR in dependency of UV irradiation and polymer concentration only aims for a general comparison of both systems (Table 15).

Summarizing all results, it was noticed, that hybrid hydrogels have higher SR and lower Young's modulus compared to synthetic hydrogels. The increased SR and the decreased stiffness of hybrid hydrogels can be related to a less dense network, which can absorb more water. For both systems, an increased polymer concentration resulted in measurements with higher standard deviations, as by addition of higher amounts of cross-linkable polymers the inhomogeneity of the built network increased. Furthermore, a decreased stiffness was measured for both systems after addition of non-bound HMW HA. However, as already discussed above, the Young's modulus decrease for hybrid hydrogels was significantly lower because of the considerably smaller amount of supplemented HMW HA.

Table 15: Overview of Young's modulus and SR of hybrid and synthetic hydrogels in dependency of UV irradiation and SR (all hydrogels with 0.05 wt.% I2959 concentration).

hydrogel composition	polymer amount [wt.%]	UV exposure time [min]	Young's modulus [kPa]	swelling ratio
synthetic hydrogel *degradable* (**5** + **6**)	15	10	109 ± 15.0	6.8 ± 0.1
synthetic hydrogel *non-degradable* (**5** + **7**)	15	5	62.6 ± 6.9	7.5 ± 0.7
	15	10	83.0 ± 8.4	6.7 ± 0.2
	15	15	122.5 ± 17.4	6.4 ± 0.2
	15	22 s*	116.1 ± 15.5	6.2 ± 0.3
	5	10	X	18.1 ± 1.6
	25	10	314.7 ± 87.0	4.6 ± 0.3
+ 3.5 wt.% HMW HA	15	10	10.2 ± 1.8	13.6 ± 3.3
hybrid hydrogel (**5** + HA-SH)	10	5	15.9 ± 3.0	17.3 ± 0.4
	10	*10*	*35.4 ± 6.0*	*13.6 ± 0.3*
	10	15	36.4 ± 4.9	14.8 ± 1.7
	5	5	X	X
	10	5	15.9 ± 3.0	17.3 ± 0.4
	15	5	25.0 ± 15.4	15.7 ± 0.9
	25	5	36.0 ± 14.9	13.3 ± 0.7
	10	10	66.3 ± 15.2	15.7 ± 1.0
+ 1.0 wt.% HMW HA	10	10	51.6 ± 13.7	21.1 ± 2.4

X not measureable

*UV source: bluepoint 4

The values highlighted in red, show the Young's modulus and SR for the standard hydrogel composition and conditions, meaning the established conditions for 3D printing and biological applications. In the case of the hybrid hydrogels, however, it was noted that the values of the standard composition varied slightly from measurement to measurement (italic-marked in Table 15) and also in dependency of the used batch.

Table 16 presents the different values measured for the same condition (10 min UV irradiation, 24 h incubation in PBS) and composition (10 wt.% polymer concentration, 0.05 wt.% I2959 concentration). Besides the already discussed batch dependency of Young's modulus and SR, slight differences were measured for the same batch during different measurements. This difference can be attributed to the incorporation of the natural based polymer HA-SH and the associated more inhomogeneous network. Taking all single measurements into account, an average Young's modulus of 41.0 ± 7.9 kPa was obtained for batch I. and an average stiffness of 55.8 ± 18.9 kPa for the blend batch.

Table 16: Young's modulus and SR for hybrid hydrogels with 10 wt.% polymer concentration, 0.05 wt.% I2959 concentration and 10 min UV irradiation after 24 h incubation in PBS.

measurement	**used HA-SH batch**	**Young's modulus [kPa]**	**swelling ratio**
batch-dependent	I.	46.6 ± 5.0	14.9 ± 1.6
	II.	126.8 ± 27.2	11.8 ± 0.6
	III.	55.8 ± 9.2	18.3 ± 0.8
	blend (II. + III)	66.3 ± 15.3	15.7 ± 1.0
time-dependent	blend (II. + III)	45.3 ± 18.3	15.7 ± 1.2
UV-dependent	I.	35.4 ± 6.0	13.6 ± 0.3

3.2.2.3 Diffusion studies

Two different diffusion measurement experiments were carried out with hydrogels: firstly, an experiment with embedded fluorescently labeled polymers (charged and uncharged) in hydrogels to investigate the diffusion out of the gels and secondly, hydrogels with fluorescently labeled polymer solutions of different molecular weights, which were placed onto the gels to examine the molecular weight dependent diffusion through the gels. The two experiments will be discussed separately throughout this chapter.

Since hybrid hydrogels proved to be more feasible for biological applications (**appendix**), diffusion measurements, in contrast to the basic mechanical (**chapter 3.2.2.2**) and swelling studies (**chapter 3.2.2.1**), were mainly implemented with hybrid hydrogels. All measurements of the hybrid hydrogel were performed with the HA-SH blend batch.

Diffusion of fluorescence dyes out of hydrogels

The swelling profiles of hydrogels with additional HMW HA showed an significant initial swelling, followed by a mass decrease until the swelling equilibrium was reached after 24 h (**chapter 3.2.2.1**), which led to the assumption that the unbound HMW HA was released from the network during the first 24 h. In order to investigate the release of non-bound molecules from the hydrogel network, two fluorescently labelled biomolecules with different molecular weights, 4 kDa fluorescein isothiocyanate-dextran (FITC-dextran) and 800 kDa fluorescein HA (F-HA), were introduced into the gels prior to cross-linking. The hydrogels with the embedded polymer bound dyes were incubated in PBS at 37 °C and the fluorescence of the incubation solution was measured at certain time points.

Due to the sensitivity of dyes, the stability of the fluorescence dyes under the present experimental conditions had to be examined before the actual measurements. The preliminary tests showed, that although the dyes were stable in PBS and against UV irradiation, they reacted significantly with the photoinitiator I2959 (Table 17). By addition of I2959, the intensity of the dye decreased already after 3 min of UV irradiation. It was concluded that the exact concentration of fluorescent polymers still

present in hydrogels after cross-linking reaction could not be determined and thus no quantitative results can be achieved by diffusion measurements with embedded molecules. Furthermore, solubility issues of F-HA were observed during preparation of the hydrogel solutions. Therefore, the absolute concentration before cross-linking could not be determined for these solutions, which impeded the interpretation of the F-HA results.
Nevertheless, the diffusion measurements gave general qualitative information about the release of unbound molecules out of the hydrogel network.

Table 17: Sensitivity of fluorescein dye to UV light with and without photoinitiator addition.

	FITC-dextran + UV light			**FITC-dextran + UV light + I2959**		
fluorescence intensity	2240	824	585	14	12	11
FITC-dextran concentration (%)	100	50	33	100	50	33

LMW FITC-dextran (4 kDa) and HMW F-HA (800 kDa) were incorporated into hybrid hydrogels with and without additional HMW HA (1 wt.%) and the release differences between these systems as well as dyes was measured (Figure 33).
The release curves of the two systems showed no significant differences, in both cases, no burst release of the unbound fluorescence dyes was measured. As already discussed, the exact percentage of released molecules could not be determined, since the dyes partially reacted with the photoinitiator during cross-linking and thus a comparison of the two systems concerning the amounts of released polymers was not possible. The fluorescence measurements showed, however, that the dye molecules were incorporated into the network in such a way that no burst release was determined and that the dyes diffused out of the gel rather slowly over time.
In contrast to the release curve of FITC-dextran, the release curve of F-HA showed a slight increase in the absolute release in the first 24 h. In fact, due to the significantly higher molecular weight of F-HA compared to FITC-dextran, a correspondingly slower release of F-HA was expected, since the long polymer chains should be higher entangled in the hydrogel network. This observation can be explained by

repulsion between identical charged F-HA and HA-SH resulting in a slightly higher release in the first few hours.

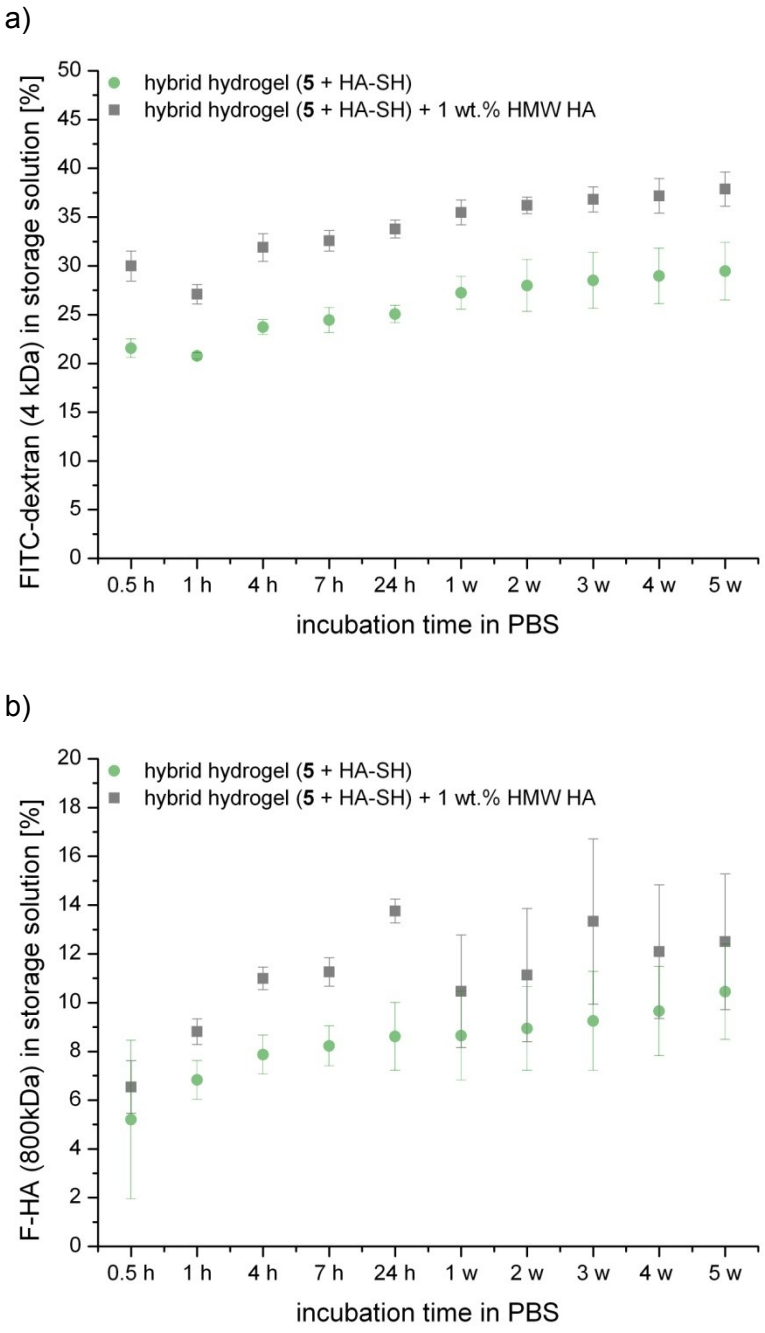

Figure 33: Diffusion of embedded unbound a) FITC-dextran (4 kDa) and b) F-HA (800 kDa) out of hybrid hydrogels with (grey) and without (green) additional HMW HA (10 wt.% polymer concentration, 0.05 wt.% I2959, 10 min UV irradiation).

HMW F-HA was also incorporated into non-degradable synthetic hydrogels and the release curve was compared to the curve of the hybrid hydrogel system (Figure 34).

While the release curves of synthetic and hybrid gels were comparable in the first 24 h, a significant increase in released F-HA was measured for the synthetic gel after 1 w of incubation. Due to the same charge of HA-SH and F-HA, a higher release of F-HA was expected for hybrid hydrogels. However, the measurements of synthetic gels revealed, that the charge repulsions had a subordinate role concerning release of F-HA.

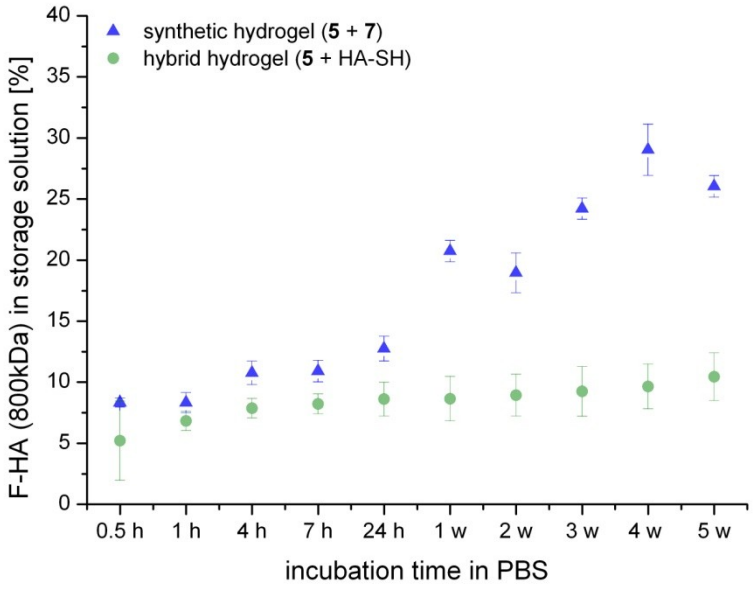

Figure 34: Diffusion of incorporated F-HA (800 kDa) out of hybrid (green) and synthetic (blue) hydrogels.

Diffusion of fluorescence labelled polymers through hydrogels

In order to receive information about the mesh size of the hydrogels, solutions of FITC-dextran with different molecular weights (4 kDa, 40 kDa, 500 kDa and 2 MDa) were prepared and the diffusion of these polymers through hydrogels was examined. To measure diffusion through gels a customized experimental setup was selected: hydrogels were prepared in a cell sieve (8 µm pores) and the sieve was stored in 24 well-plates in PBS solution. The FITC-dextran solutions were pipetted onto the gel and the fluorescence of the PBS storage solution was measured at specific times. Cell sieves without hydrogels were used as positive controls, to determine the amount of polymers which diffuse through the sieve alone. The measured fluorescence of the PBS storage solutions at different time points were then related to the positive control.

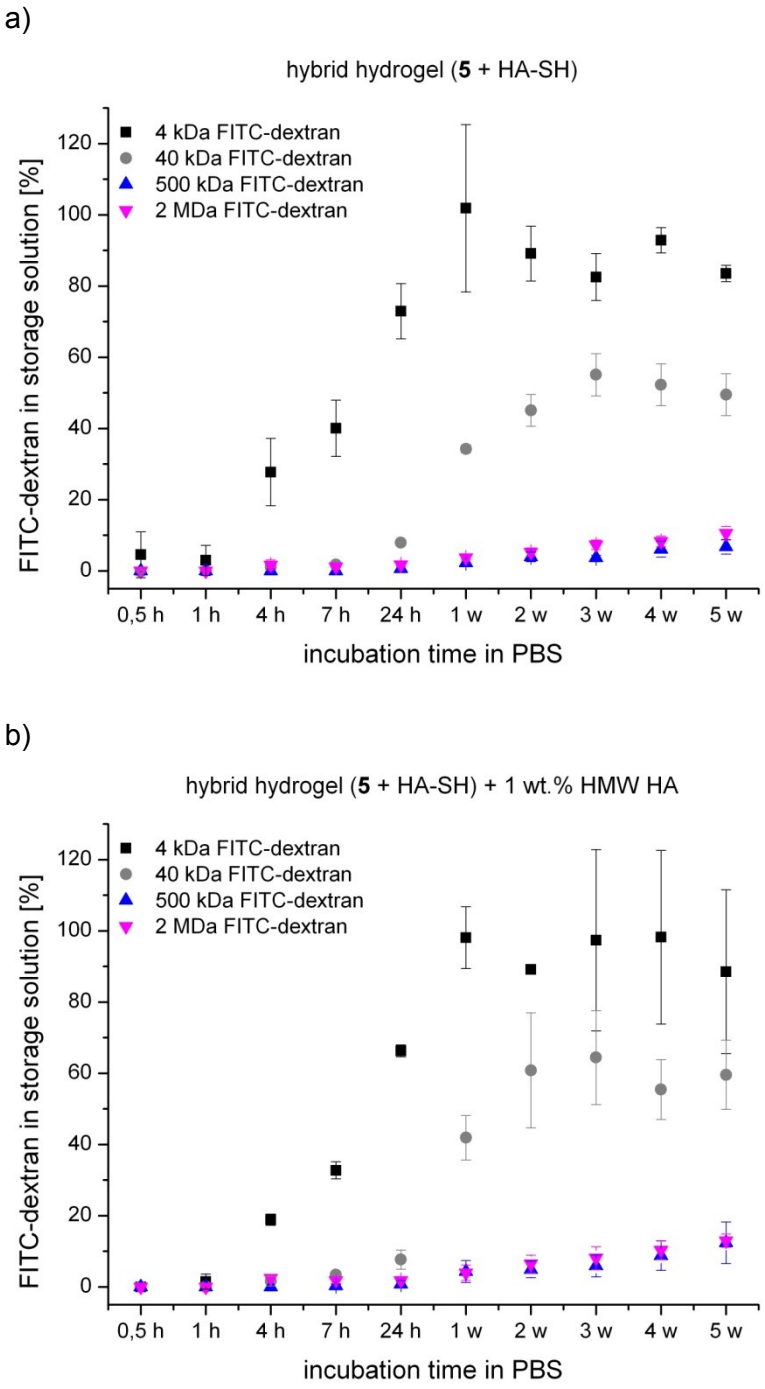

Figure 35: Diffusion of FITC-dextran (4 kDa, 40 kDa, 500 kDa and 2 MDa) out of hybrid hydrogels a) without and b) with additional 1 wt.% HMW HA.

The diffusion of different molecular weight FITC-dextran through hybrid hydrogels with and without additional 1 wt.% HMW HA is shown in Figure 35. The FITC-dextran with the smallest molecular weight, 4 kDa, diffused completely through both hydrogel systems within the first week of incubation. 40 kDa FITC-dextran diffused more slowly through the gels and reached a diffusion plateau after 2 w (with HMW HA) and

3 w (without HMW HA) of incubation in PBS. Compared to the 4 kDa FITC-dextran only around 55 % of 40 kDa FITC-dextran diffused through the gel into the storage solution. For the two HMW dyes, 500 kDa and 2 MDa FITC-dextran, an amount of only 5-10 % dye in PBS was measured, which suggests that the HMW dextrans were too large to diffuse through the network of hybrid gels in the studied time frame.

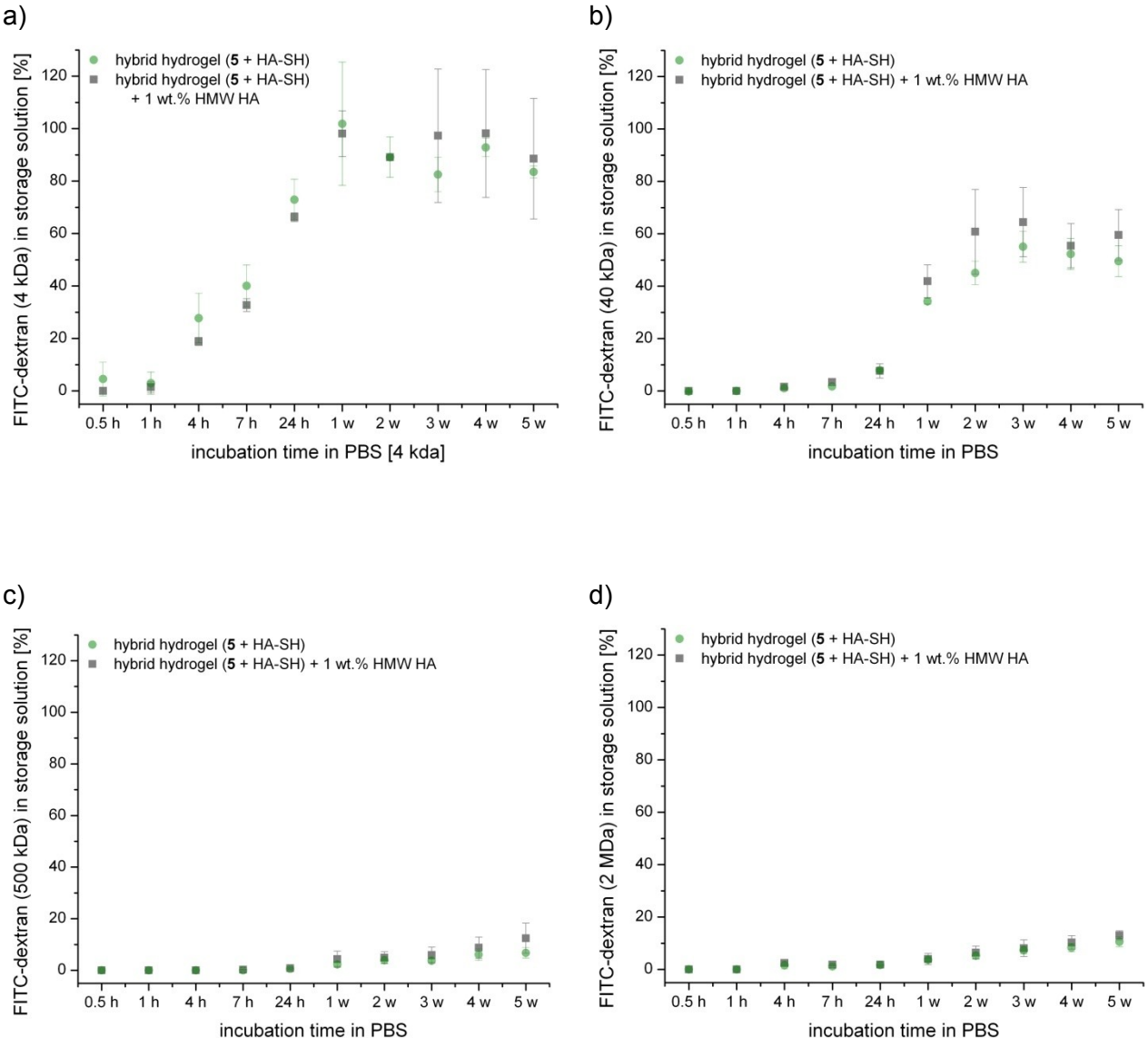

Figure 36: Comparison of diffusion of FITC-dextran through hybrid hydrogels with (grey) and without (green) additional HMW HA, a) with 4 kDa, b) with 40 kDa, c) with 500 kDa and d) with 2 MDa FITC-dextrans.

The direct comparison of hybrid hydrogels with and without additional HMW HA showed that the introduction of the unbound HA had no significant influence on the diffusion of the different FITC-dextran (Figure 36). Thus, the mesh size of the two

systems could also be compared, in relation to the measured range. However, mechanical measurements of hybrid hydrogels with and without supplemented HMW HA showed small differences in stiffness and SR between the two (**chapter 3.2.2.2**), which can be attributed to differences in the networks not relevant for the diffusion of the macromolecules.

In addition to the mesh size of the hydrogels, the diffusion measurements gave further information about possible applications of the hydrogels as carriers for active drug substances. The different molecular weights of FITC-dextran can be brought into correlation with drugs and/or matrix components produced by cells within the gels. Finally the size of the active substances determines, which active substances can be released by the hybrid gel and which cannot diffuse out and will stay locally entrapped till the degradation of the hydrogels.

3.2.3 3D Printing

After physical and biological evaluation of the developed thiol-ene cross-linked hydrogels, the printability of these gels was examined. First, the hydrogel composition and cross-linking conditions had to be adjusted in order to obtain printable polymer solutions resulting in scaffolds with high resolution. In a next step, the hydrogel composition was further altered and hydrogel printing was combined with printing of a thermoplastic to meet the requirements of printing robust scaffolds with high cell support. The two approaches are discussed separately throughout this chapter.

All hydrogel solutions for printing were prepared as described before, however, with the difference that the solutions were centrifuged before being transferred into the printing syringe to avoid air bubbles which could cause inconstant material flow.

3.2.3.1 Printing of hydrogel solutions

Extrusion based 3D printing allows the fabrication of scaffolds in a layer-by-layer fashion via deposition of strands through a nozzle. Therefore, printing solutions, so-called inks, must fulfill following requirement. They have to have vioscoelastic properties that ensure dispensing material strands instead of droplets. Furthermore, the printed construct should maintain their shape after deposition to exclude deterioration of the scaffold resolution.[1, 3, 35]

The developed hydrogels, both hybrid and synthetic, were not suitable for printing without thickening agents, since strand deposition was not possible. The same issue was already observed for gelMA and dextran based hydrogels.[16, 128, 152] To overcome this problem, HA or collagen I were supplemented to the gelMA/dextran solutions to increase their viscosities. A study on gelMA demonstrated the tailorable adaption of the viscoelastic properties of gelMA solutions by addition of HMW HA.[16] Through supplementation of the gelMA solution with HA, the viscosity was increased and the solution could be deposited in strands. In addition to the possibility of tailoring the viscoelasticity of hydrogel solutions with HA, the use of HA as thickening agent has further advantages for latter cell applications. HA is major component of the ECM and has beneficial effects on chondrogenic differentiation of hMSCs.[153-155] Due to this

advantage, HMW HA has also been used for the systems developed throughout this thesis to improve printability of the polymer solutions. The fast cross-linking of the polymeric solution and thus the maintenance of the printed structure was ensured by irradiation with the high-intensity UV lamp (bluepoint 4), which enabled cross-linking within seconds.

a)

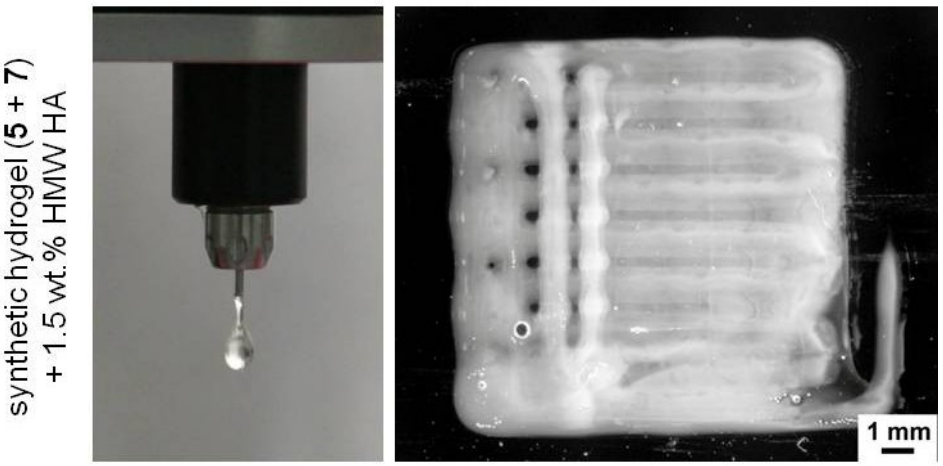

b)

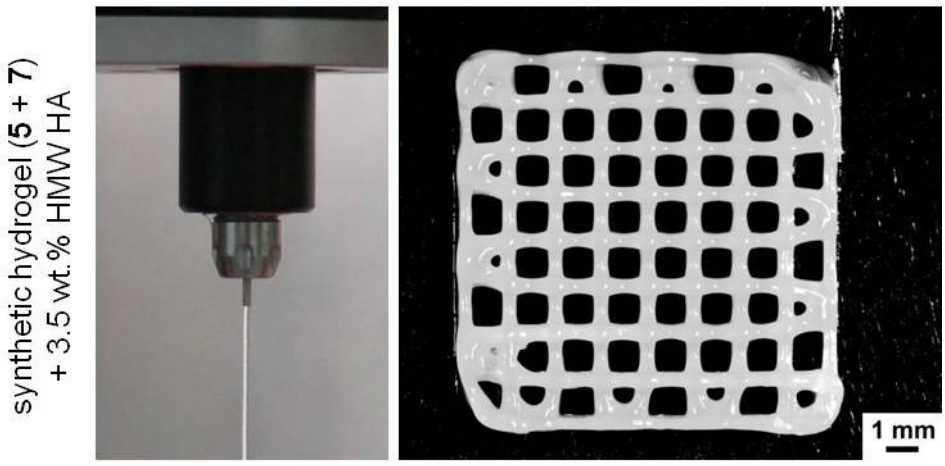

Figure 37: 3D printing of synthetic hydrogel solution (**5** + **7**, 15 wt.% polymer concentration) and the resulting scaffolds with a) 1.5 wt.% additional HMW HA and b) 3.5 wt.% additional HMW HA. Printing parameters: scaffold size: 12 mm x 12 mm, strand-to-strand distance: 1.5 mm, inner needle diameter: 0.45 mm, UV irradiation: 2 s each layer, a) 2 layers and b) 12 layers.

The influence of the amount of additional HMW HA on the viscostiy and thus on the deposition of the synthetic hydrogel solution (non-degradable) is shown in Figure 37. The addition of 1.5 wt.% HMW HA resulted in polymeric solutions which formed droplets upon ejection (Figure 37a), whereas by addition of 3.5 wt.% HMW HA the solutions were deposited as fibers (Figure 37b). The direct relationship between droplet versus fiber deposition and printing fidelity could be seen in the resulting constructs. The polymeric solution with only 1.5 wt.% additional HMW allowed printing of one layer, however, the printing of a second layer failed (Figure 37a). By contrast the polymeric solution with an increased amount of HMW HA (3.5 wt.%) enabled printing of a 12 layered scaffold with high shape fidelity (Figure 37b). Each layer was cross-linked for 2 s with UV light directly after deposition to maintain the shape of the construct.

Variation of needle diameter and strand-to-strand distance

In addition to the viscosity of the solution, there are several other parameters which influence the printing results, such as needle diameter and strand-to-strand distance. To investigate the effect of these parameters on printing fidelity, the synthetic hydrogel solution with additional 3.5 wt.% HMW HA was printed with varying parameters and the resulting scaffolds were compared.

First, the hydrogel solutions were printed with nozzles with inner needle diameters of 0.30 mm and 0.45 mm, respectively (Figure 38). Printing of the hydrogel solution through the nozzle with an inner needle diameter of 0.45 mm was feasible with a pressure of 1.5 bar (Figure 38a). Using the needle with the larger inner diameter enabled printing of a 20 layered construct (construct height: 3.90 mm) with high shape fidelity and high resolution without structural collapse. By replacing the needle tip with a needle with a smaller inner diameter (0.30 mm), the pressure had to be increased up to 3.2 bar, which simultaneously led to a higher material deposition (Figure 38b). As a result of this, the printed scaffold showed a decreased resolution and decreased shape fidelity. These printing settings allowed printing of a construct with 8 layers with a scaffold height of 1.36 mm. A reduced pressure did not enable the printing of thinner fibers, but resulted in a stop of the material flow.

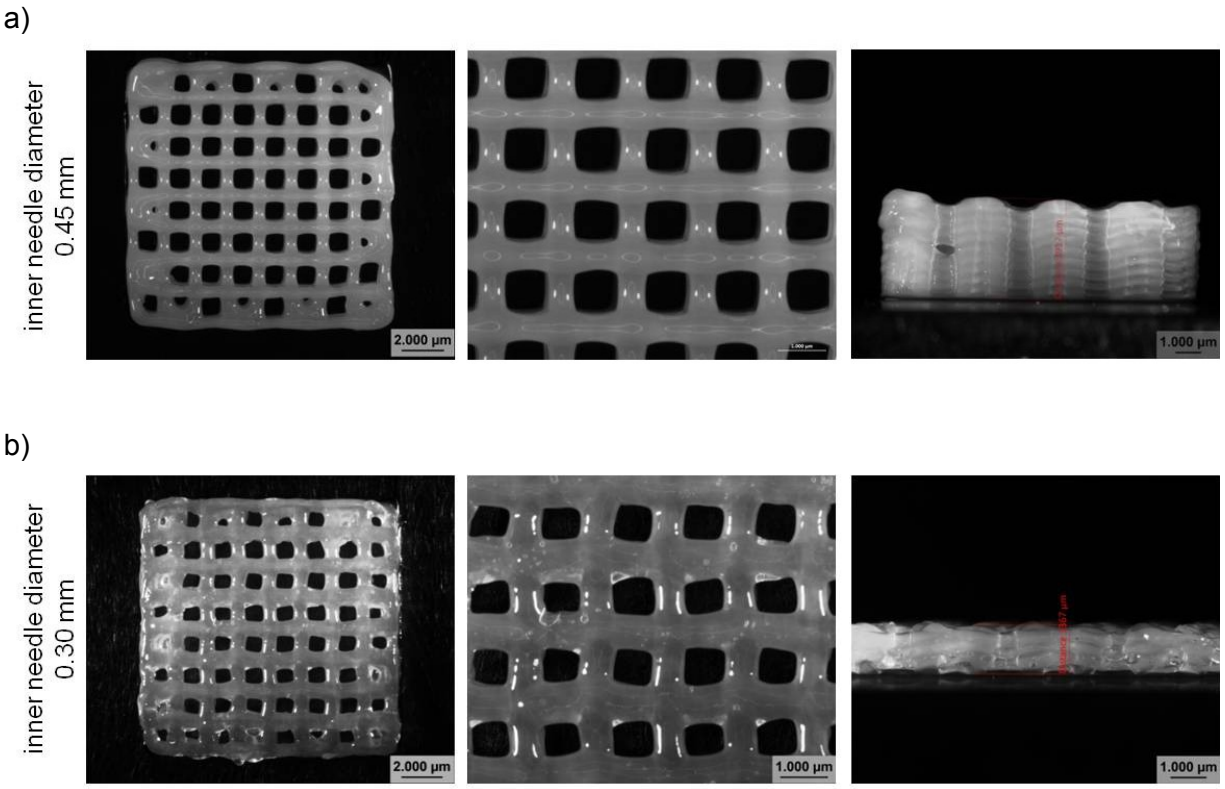

Figure 38: Synthetic hydrogel solutions with additional HA (**5** + **7**, 15 wt.% polymer concentration + 3.5 wt.% HMW HA) printed with a inner needle diameter of a) 0.45 mm and b) 0.30 mm. Printing parameters: scaffold size: 12 mm x 12 mm, strand-to-strand distance: 1.5 mm, UV irradiation: 2 s each layer, a) 20 layers (height: 3.90 mm) and b) 8 layers (height: 1.36 mm).

Furthermore, the hydrogel solutions were printed with varying strand-to-strand distances, in order to evaluate the influence of the fiber distances on the constructs shape fidelity (Figure 39). Although the hydrogel solutions were printed with the same inner needle diameter (0.45 mm), the pressure had to be reduced to 1.3 bar with a reduced strand-to-strand distance of 1.0 mm, in order to avoid that the strands fuse (Figure 39b, top). Additionally, when printing with a strand-to-strand distance of 1.0 mm the hydrogel solution was irradiated continuously during printing to avoid the confluence of the strands. The changed settings enabled printing of constructs with high shape fidelity and resolution, however, the reduced pressure caused partial strut breakup during the printing process (Figure 39b, top left). An slightly increased pressure (1.5 bar) resulted in less strut breakup, but with the consequence that the strands fused and thus the resolution of the scaffold decreased extremely (Figure 39b, bottom). It was not possible to adjust the pressure in such a way that, on the

one hand, the breaking of the fibers and, on the other hand, the confluence of the strands was avoided.

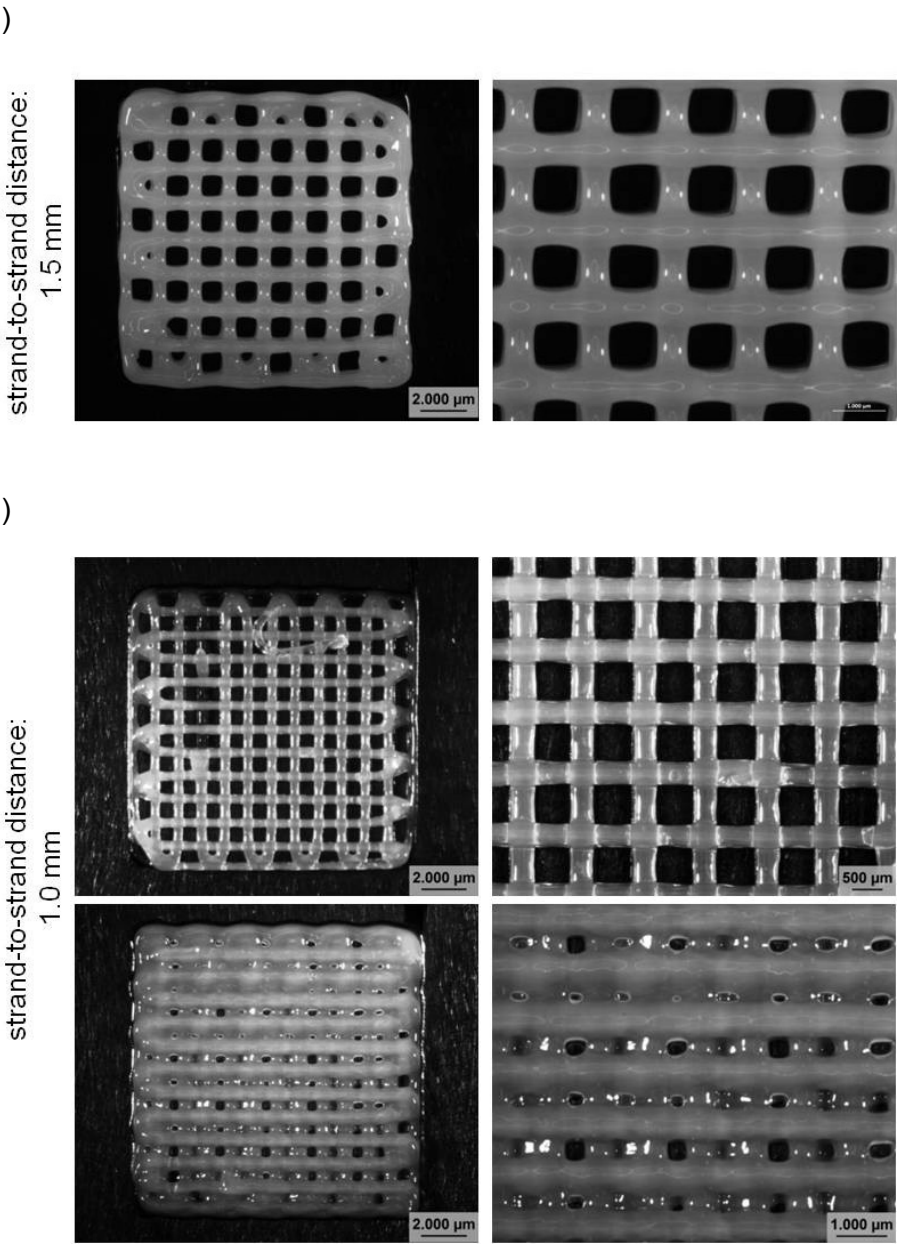

Figure 39: Synthetic hydrogel solutions with additional HA (**5** + **7**, 15 wt.% polymer concentration + 3.5 wt.% HMW HA) printed with a strand-to-strand distance of a) 1.5 mm and b) 1.0 mm. Printing parameters: scaffold size: 12 mm x 12 mm, inner needle diameter: 0.45 mm, UV irradiation: a) 2 s each layer and b) continuously during printing, layers: a) 20 layers and b) 4 layers, pressure: a) 1.5 bar and b) top: 1.3 bar, bottom: 1.5 bar.

Summarizing the results of the investigations of the different printing conditions, the scaffolds with the highest shape fidelity were obtained with a nozzle with an inner needle diameter of 0.45 mm and a strand-to-strand distance of 1.5 mm.

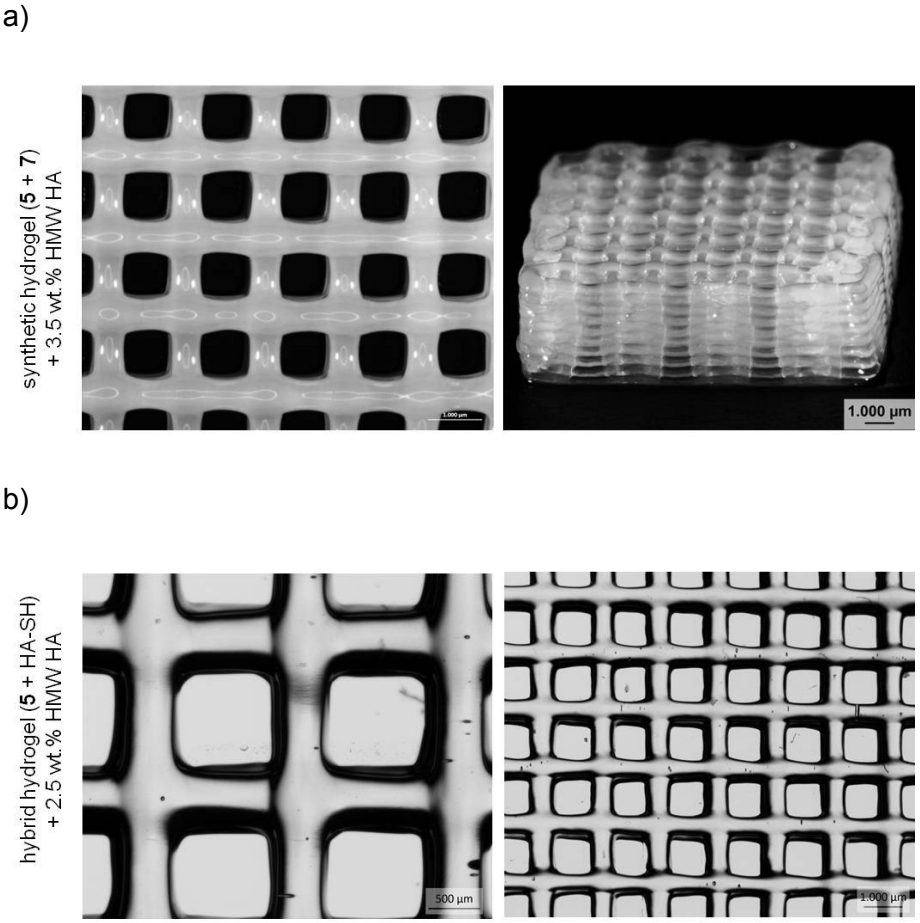

Figure 40: Comparison of synthetic and hybrid hydrogel printing. a) synthetic hydrogel (5 + 7, 15 wt.% polymer concentration + 3.5 wt.% HMW HA) and b) hybrid hydrogel (5 + HA-SH, 10 wt.% polymer concentration + 2.5 wt.% HMW HA). Printing parameters: scaffold size: a) 12 mm x 12 mm and b) 21 mm x 21 mm, inner needle diameter: 0.45 mm, UV irradiation: a) 2 s each layer and b) continuously during printing, layers: a) 20 layers and b) 10 layers, pressure: a) 1.5 bar and b) 2-3 bar.

The printing of hybrid hydrogel solutions (**5** + HA-SH (blend batch)) was also investigated (Figure 40b). As shown for synthetic hydrogels, additional HMW HA had to be supplemented to the precursor solution in order to enable extrusion of strands instead of droplets. Since the viscosity of solutions depend on polymer concentration as well as on the molecular weight of these polymers, the inital viscosity of the hybrid hydrogel solution without additional HMW HA was already slightly higher compared

to the synthetic hydrogel solution, because of the exchange of the thiol-component PG-SH_{ef} (**7**) for the higher molecular weight HA-SH. Therefore, the addition of already 2.5 wt.% HMW HA to the hybrid hydrogel solution was sufficient to achieve successful strand deposition.

Printing of the hybrid hydrogel solution was conducted with the same printing settings as for the synthetic hydrogels (inner needle diameter: 0.45 mm, strand-to-strand distance: 1.5 mm), as the use of a smaller needle diameter resulted in clogging of the needle and a smaller strand-to-strand distance resulted in strand fusion and thus in reduced shape fidelity. These settings allowed printing of hybrid hydrogel constructs with up to 10 layers (Figure 40b). For printing of hybrid hydrogel solutions the pressure had to be adjusted between 2 to 3 bar.
The aforementioned inhomogeneity of the hybrid hydrogel solution (**chapter 3.2.2.2**) also had an influence on the printability of the hybrid system. The pressure had to be adapted to the current flow of the solution during the entire printing process, as the material flow changed over time. Since the flow of the hybrid hydrogel solution was not constant and had to be adjusted manually, a reproducible printing of hybrid hydrogel constructs was challenging. In contrast to that, the synthetic solution was deposited as a consistent strand at a pressure of 1.5 bar and thus the printing of synthetic solutions was reproducible and resulted always in scaffolds with the same height and resolution (20 layer, height: 3.90 mm) (Figure 40a).

The rheological evaluation of the two printable hydrogel formulations is depicted in Figure 41. Shear viscosity and recovery tests were performed to investigate the rheological properties of the printing solutions. The rotational shear viscosity measurements revealed shear thinning behavior, meaning viscosity decrease with shear rate increase, of both polymeric solutions (Figure 41a) and b) left). The rheological properties of the solutions implied printability under investigated pressure.[51] The extend of relative reduction in viscosity is dependent on the molecular weight of the polymer and the polymer concentration. This influence was previously evaluated for alginate solutions and dextran based hydrogels.[31, 52] For both systems it was demonstrated, that with increased concentration and molecular weight the relative reduction in viscosity was increased.

Recovery tests were performed in order to evaluate the ability of the solution to recover after an implemented high shear rate, which can be associated with applied pressure during printing. Thus, the goal of this test was to mimic the shear conditions during/after printing to characterize the recovery behavior in the context of bioprinting. Comparable rheological tests were previously examined for PEG based hydrogels.[156] For these test, the printing solutions were alternately rotated with a high (5 s^{-1}) and low (0.01 s^{-1}) shear rate. For both hydrogels it could be demonstrated, that the hydrogel solutions recover after each shear change.
Both measurements indicate that the used hydrogel solutions are printable.

a)

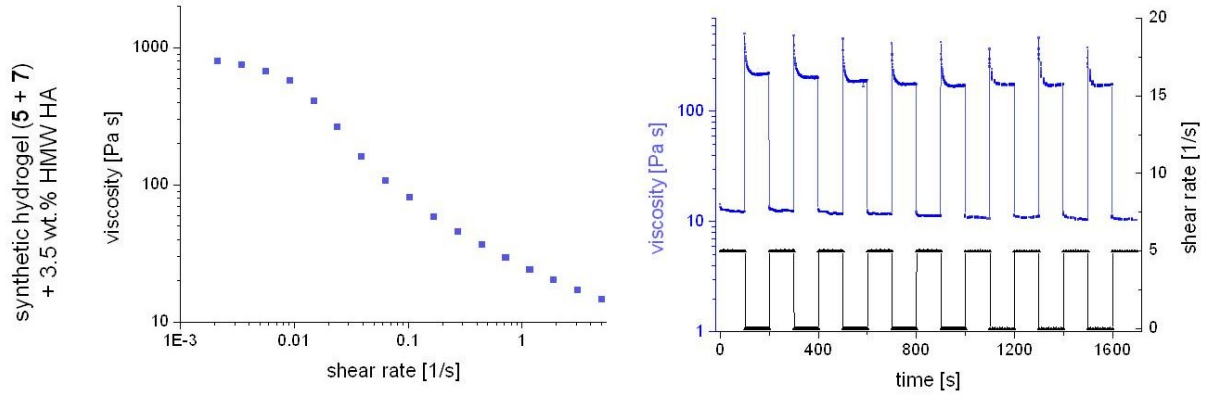

b)

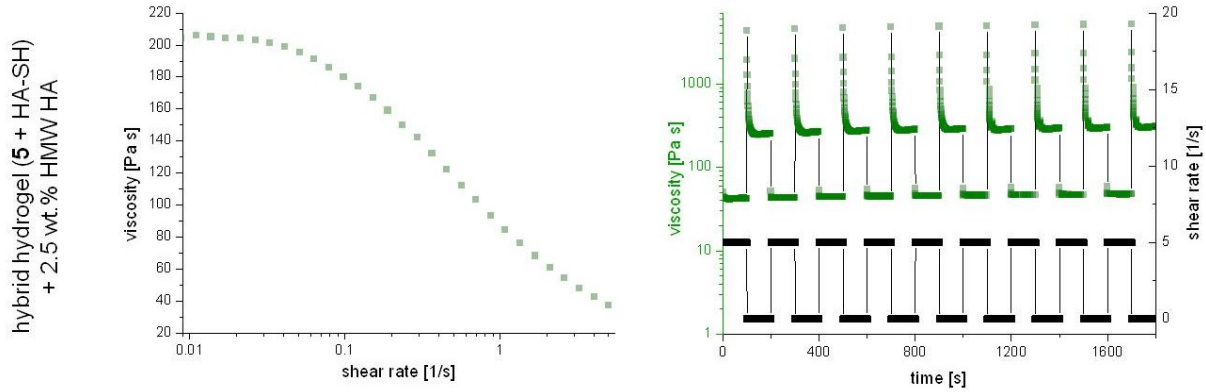

Figure 41: Rheological analysis of synthetic (a) and hybrid (b) hydrogel solutions: Rotational shear-viscosity measurement (left) and recovery test under rotation (right).

In this section it was demonstrated that both hydrogel systems were printable after adjusting the viscoelastic properties of the precursor solutions with HMW HA. The obtained constructs showed good resolution and high shape fidelity. Nevertheless, the mechanical stability of these constructs had to be increased to enable their use in the EU-project HydroZONES[VII] as cartilage regeneration construct (**Appendix**). A common approach to yield stiffer hydrogels and thus enhanced stability of printed constructs, was to increase the polymer concentration of the precursor solution.[1] However, with increased cross-linking density the matrix formation of encapsulated cells was reduced and thus the use of the hydrogel as a bio-ink is declined.[1, 49, 50] Therefore, this thesis aimed to enhance stability of the printed constructs with an alternative printing approach, which is discussed in the following section.

3.2.3.2 Double printing of hydrogel solutions with PCL

To enable printing of constructs with increased mechanical stability, without further increasing the polymer concentration, the hydrogel solutions were double printed with the thermoplastic poly(ε-caprolactone) (PCL). By this reinforcement strategy, the contradictive biological and physical requirements of bio-inks could be circumvented, since it allows printing of less viscous hydrogel solutions between supporting robust PCL strands. The double printing approach was previously applied for gelMA and alginate hydrogels.[16, 61] The alginate-PCL double printing study showed, that the stiffness of double printed constructs were comparable to the stiffness of PCL-only scaffolds, which were in the range of cartilage (4.1 MPa).[61, 157]

For double printing, molten PCL and the hydrogel solution were alternately printed. First a PCL layer was deposited and second the hydrogel solution was deposited in between the PCL strands. The subsequent layers were printed in the same manner, always in a 90° angle to the previous one. The hybrid hydrogel system was used as a bio-ink, since it has been demonstrated that it is the more promising system for the desired application (**Appendix**). Due to the fact that the biological evaluation revealed a slightly less robust chondrogenic differentiation of hMSCs (**Appendix**) for the hybrid hydrogel system with additional HMW HA (1 wt.%), the amount of HMW HA was further reduced to 0.5 wt.% for double printing (Figure 42, top). However, by

[VII] Seventh Framework Programme FP7/2007-2013 under grant agreement n°309962.

decreasing the amount of supplemented HMW HA, the attachment of the PCL layers was simultaneously decreased, since the reduced viscosity of the bio-ink solution led to spreading of the hydrogel solution over the PCL layer and consequently less coherence of the termoplast. Therefore, double printing was conducted with hybrid hydrogels with 1.0 wt.% additional HMW HA, accepting a slightly reduced chondrogenic differentiation of MSCs to the benefit of better attachment of the PCL layers. Thereby, stable constructs with high shape fidelity could be obtained (Figure 42, bottom).

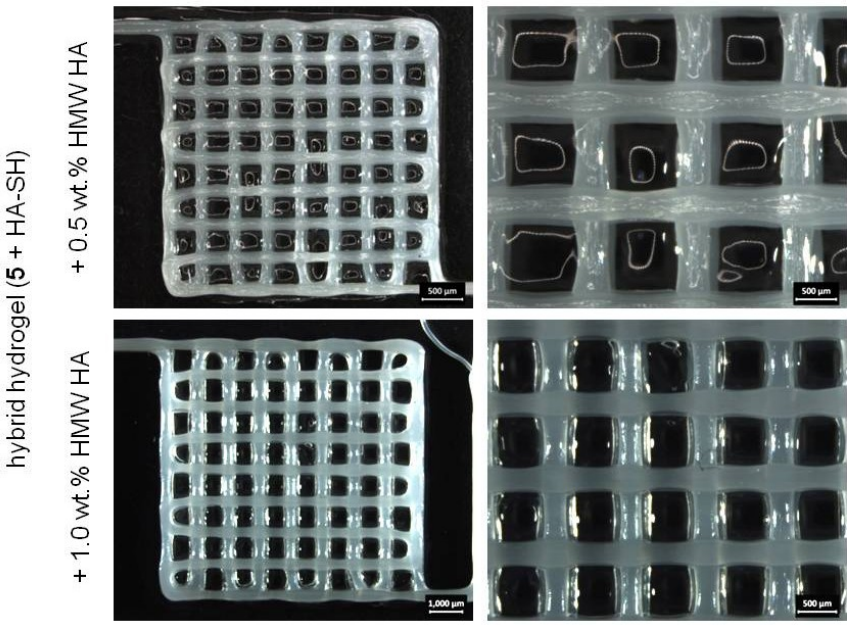

Figure 42: Double printing of PCL with the hybrid hydrogel system (10 wt.% polymer concentration, HA-SH blend batch) with different amounts of additional HMW HA top: 0.5 wt.% and bottom: 1.0 wt.%. Printing parameters: scaffold size: 12 mm x 12 mm, layers: four, UV irradiation: 8 s after printing of the whole construct, pressure: top: 0.5 bar and bottom: 1.0 bar.

This study demonstrated that the double printing approach enables the printing of hydrogel solutions with lower viscosities and thus allows the application of a wide range of hydrogels for printing. This makes double printing a powerful tool for the field of biofabrication.

To investigate the influence of the printing process on cell viability, hMSCs were embedded into the hybrid hydrogel printing solution and extruded through the printer

nozzle (Figure 43, bottom). The cell survival was compared to hMSCs embedded in casted gels (Figure 43, top). This cell experiment revealed that embedded hMSCs survive the printing process and furthermore that the cell survival of hMSCs embedded in cast and printed gels were comparable after 21 d in culture (Figure 43, right). The feasibility of the printing process for cell survival was also shown previously in literature for chondrocytes in methacrylated poly(N-(2-hydroxypropyl) methacrylamide-mono/dilactate)-PEG based hydrogels supplemented with methacrylated polysaccharides.[128] In this study, they could show printing of chondrocytes without affecting their cell viability.

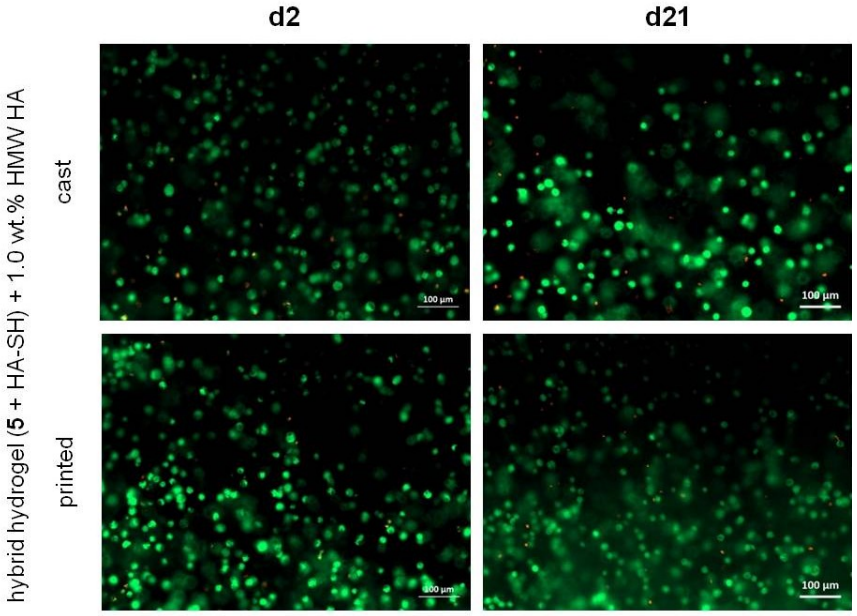

Figure 43: Live/dead assay of hMSCs embedded in hybrid hydrogels with additional 1 wt.% HMW HA, top: casted and bottom: printed. Viable cells are depicted in green (labelled with calcein acetoxymethyl ester) and dead cells are depicted in red (labelled with ethidium homodimer III). Scale bars represent 100 µm. Live/dead assay was evaluated by *Thomas Böck*.[158]

In addition to the double printing strategy, an alternative reinforcement method was developed, in which the PCL and hydrogel part were separated. First a pure PCL construct was printed, which was subsequently infused with a hydrogel solution. The separation of the PCL printing was associated with advantages and disadvantages. One major disadvantage of this method was that although the hydrogel solution could be introduced zonally into the PCL plug, it was not possible to obtain the same

precision as with hydrogel printing, since printing allows the highly accurate and precise deposition of material, which could not be imitated by manual filling of the PCL plugs. However, the separation PCL printing approach facilitated the *in vivo* application of the reinforced hydrogel constructs, due to the fact, that it allows the fabrication of PCL enhanced scaffolds directly in the facilities of the particular cooperation partners, by using prefabricated PCL plugs and infusing them on-site with the desired hydrogel solution. Therefore, the PCL constructs infused with hydrogels were used by cooperation partners[VIII] of the HydroZONES consortium, in order to investigate the use of PCL-hydrogel constructs *in vivo*.[159]

Figure 44 depicts a pure PCL construct and a construct infused with the hybrid hydrogel. Depending on the application of the cooperation partner, the scaffold size and height of the PCL plugs could be adjusted.

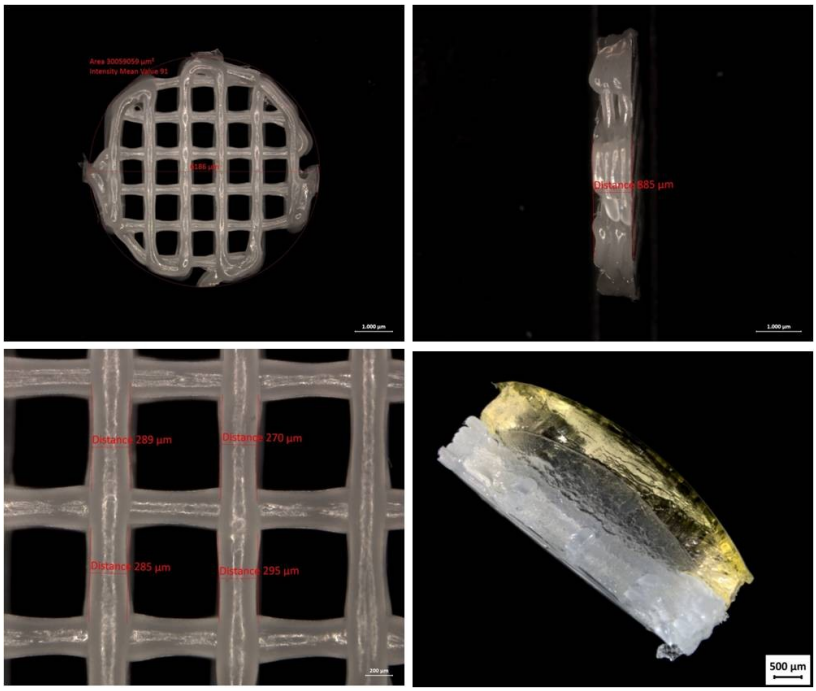

Figure 44: PCL plug with 1.0 mm strand-to-strand distance, 6 mm diameter, 0,9 mm height. Infused with hybrid hydrogel (bottom right), coloured with FITC-dextran (40 kDa).

Throughout this 3D printing chapter, it was shown that the developed hydrogel solutions were printable with and without supporting thermoplastic. In both cases, non-bound HMW HA was supplemented to the hydrogel solutions in order to adjust

[VIII] Irina Mancini, Regenerative Medicine Utrecht, Utrecht University;
Friederike Bothe, Research Centre for Experimental Orthopaedics, University Hospital Heidelberg.

the viscoelastic properties. Furthermore, it could be demonstrated, that embedded hMSCs survive the printing process and thus, that the established hydrogel solution was suitable for use as a bioink. The addition of PCL reinforcement scaffolds, as plugs or in the double printing approach, finally led to constructs which are suitable for application as cartilage regeneration scaffolds.

3.3 Hydrogels cross-linked via ionic interactions

In addition to the chemically cross-linked hydrogels presented in **chapter 3.2**, it was also investigated if accordingly modified PG can also be used to form weaker physical hydrogels via ionic interactions. For this proof of principle study, a hybrid hydrogel system based on functionalized PG and HMW HA was produced. Peptide-modified PG **8c** served as PG component, since it was functionalized with the HA-binding peptide RYPISRPRKRC (peptide3, **chapter 3.1.5**) which was reported to bind to the negatively charged HA via ionic interactions.[149]

In this chapter, the physical-ionic interactions between peptide-functionalized PG **8c** and HMW HA are discussed.
Compared to chemical cross-linking, the physical cross-linking provides weak non-permanent bonds between the polymer chains which can be displayed through rheological investigations. Thus, shear-viscosity and recovery measurements of P(peptide-*co*-G) (**8c**) / HMW HA solutions were carried out using a rheometer.

3.3.1 Rheological evaluation of HMW HA solutions

First, a rheological screening of HMW HA solutions with different polymer concentrations was conducted, in order to determine the initial concentration of the HA solution before mixing with P(peptide-*co*-G) (**8c**) and furthermore to define the measurement conditions (Figure 45). Therefore, HMW HA solutions with polymer concentrations of 0.5 to 3.5 wt.% were prepared and shear-viscosity and recovery measurements were implemented. It was demonstrated that the viscosity of all HA solutions decreased with increasing shear rate, also referred to as shear thinning behavior (Figure 45a). The shear-viscosity measurements also revealed that the relative viscosity decrease increases with increasing polymer concentration. This effect of polymer concentration on shear thinning behavior was previously also detected for alginate solutions and dextran based hydrogels.[31, 52] During these measurements, it was further observed that the solutions were pressed out of the measurement plates at shear rates above 100 s^{-1}. Therefore, the highest shear rate for subsequent recovery studies was set to 100 s^{-1} and further shear-viscosity measurements with P(peptide-*co*-G) (**8c**) were performed only up to shear rates of 100 s^{-1}.

a)

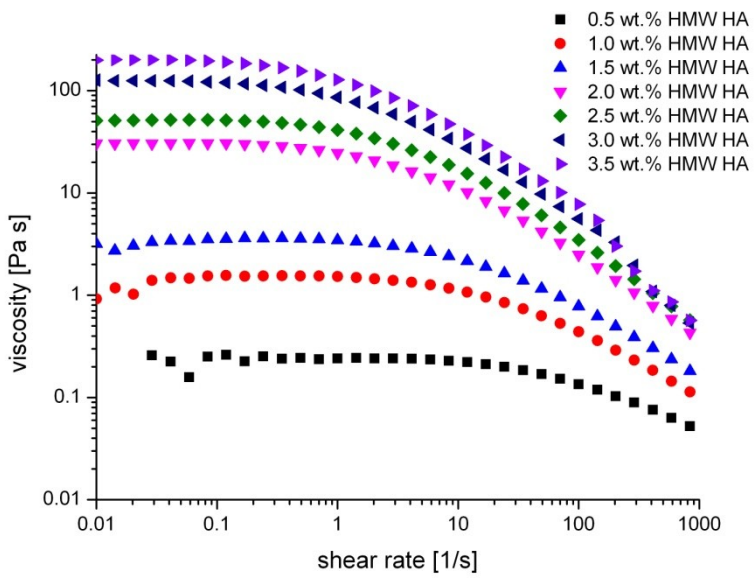

b)

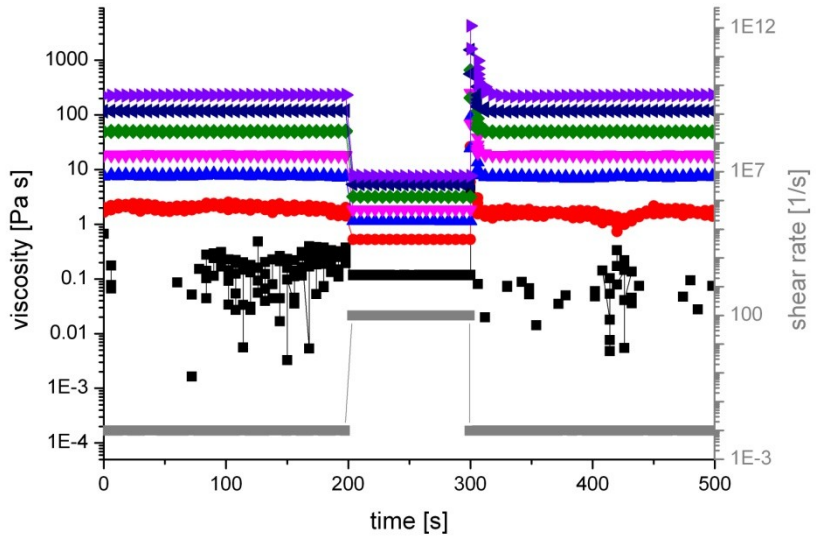

Figure 45: Rheological investigations of HMW HA solutions (polymer concentration: 0.5-3.5 wt.%). a) shear-viscosity test with a shear ramp ranging from 0.01 s^{-1} to 1000 s^{-1} and b) recovery test under rotation with a high shear rate of 100 s^{-1} and a low shear rates of 0.01 s^{-1}. The legend given in a) also applies to measurements shown in b).

The recovery measurements of HA solutions with different polymer concentrations gave information about the recover abilities of the solutions after an implemented shear change (Figure 45b). These measurements are used primarily to determine the suitability of the prepared solutions for 3D printing, since the change in shear rate mimics the conditions during printing (**chapter 3.2.3.1**). However, they were also

used to determine the solutions which are stable enough under shear change and thus to define possible precursor solutions possible precursor solutions for the further cross-linked physical hydrogels.
HA solutions with a polymer concentration above 1.5 wt.% showed good recovery properties, whereas the viscosities of solutions below 1.5 wt.% extremely fluctuated at a shear rate of 0.01 s^{-1}.

After evaluating both measurements, HMW HA solution with 2 wt.% polymer concentration was chosen as precursor solution for hydrogel cross-linking with P(peptide-*co*-G) (**8c**). This polymer concentration was preferred, since the solution showed high recovery properties and shear thinning behavior. Furthermore, the use of higher concentrated solutions was excluded, as it was expected that the impact of ionic interactions would be more challenging to detect in these solutions and a potential cell culture might be hampered by the high polymer content.

3.3.2 Rheological evaluation of P(peptide-*co*-G) (8c)/HMW HA solution

After the concentration of the HA solution was determined, peptide-functionalized PG **8c** was mixed into the solution and the influence of **8c** on the rheological properties of the HA solution was evaluated (Figure 46). Therefore, the two components were mixed with a 1:1 negative/positive charge ratio in different solvent. Demineralized water was used as alternative solvent, since the ions in PBS probably will hamper the interaction between the positively charged amino acids in P(peptide-*co*-G) (**8c**) and the negatively charged HA. This solvent effect was previously shown also for other HA based hydrogels cross-linked via ionic interactions.[95]
In addition, the HMW HA solution was mixed with the precursor polymer of **8c**, P(AGE-*co*-G) (**5b**), to distinguish the influence of increased polymer amount from ionic interactions.
The measurements demonstrated that the viscosity and shear thinning behavior of the 2 wt.% HA solution significantly increased by addition of peptide-functionalized PG **8c**. In contrast, the addition of the same amount of precursor polymer **5b** resulted only in a lesser increase. The higher increase in viscosity can be attributed to the ionic interactions between the peptides attached to the PG backbone of **8c** and the carboxylic acid functions of HA.

a)

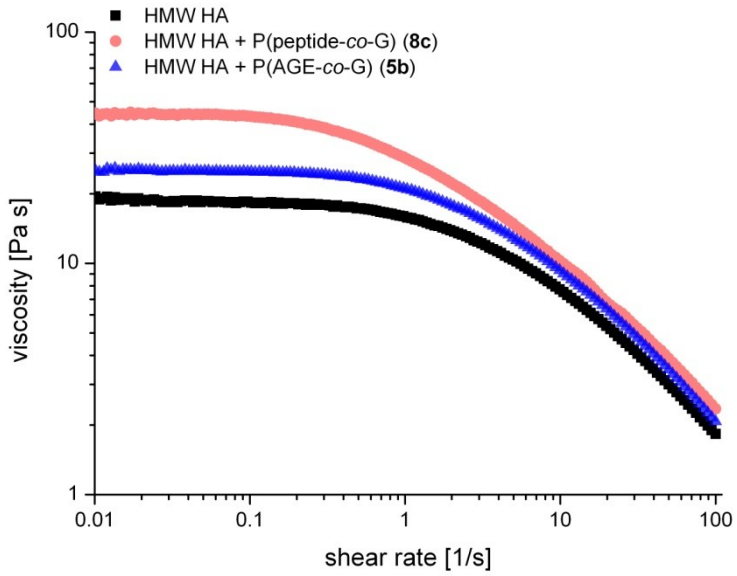

b)

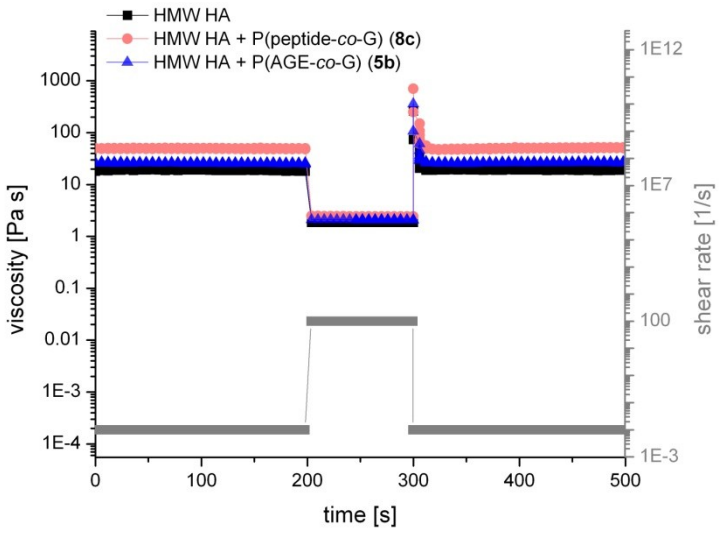

Figure 46: Rheological evaluation of 2 wt.% HMW HA solution mixed with P(peptide-*co*-G) (**8c**) and P(AGE-*co*-G), 1:1 charge ratio of HA/**8c**. a) shear-viscosity test with a shear ramp ranging from 0.01 s^{-1} to 100 $s^{-1}$and b) recovery test under rotation with a high shear rate of 100 s^{-1} and a low shear rates of 0.01 s^{-1}.

As comparison, the shear-viscosity study was also carried out in PBS, in order to investigate the influence of the solvent on the physical interactions between peptide-functionalized PG **8c** and HA (Figure 47). These measurements revealed that the

viscosity of HMW HA was not significantly increased by addition of P(peptide-*co*-G) (**8c**) and hence demonstrated that the interactions between the peptides and HA were most likely hampered by the ions contained in the isotone PBS.

In general, a less pronounced shear thinning behavior was measured for both solutions. This effect can also be ascribed to the aforementioned shielded charges of the polymers. The ions of the PBS solutions interact with the charged molecules (**8c** and HA) and thus reduce the repulsion and interaction of the charged polymers.

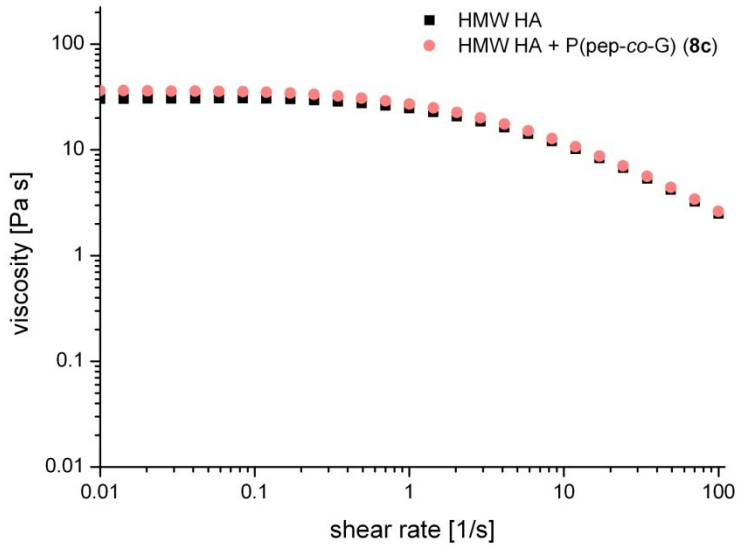

Figure 47: Shear-viscosity measurements of 2 wt.% HMW HA solution and 2 wt.% HMW HA solution mixed with P(peptide-*co*-G) (**8c**) (1:1 charge ratio) with PBS as solvent.

In summary, this proof of principle study has provided a first insight into the application of peptide-functionalized PG in physical gels. The introduction of a HA-binding peptide into the polymeric backbone opened the possibility for the formation of alternative hybrid gels with HA or the enhancement of the gel stability after printing. Nevertheless, due to the weak physical interactions, the detection of these interactions was difficult and fabrication of robust hydrogels was hampered. For cell culture experiments the use of ion free solutions, like isotone glucose would also be necessary.

To improve the mechanical stability and thus enhance the stiffness of physical gels, the gels need to be chemically post-cross-linked in order to obtain stable products. Since the used peptide-functionalized polymer (**8c**) features unconverted allyl-

groups, a post-cross-linking via thiol-ene reaction would be possible in this case. This approach would combine both cross-linking strategies presented throughout this thesis and could be investigated in future to achieve enhanced shape fidelity.

Chapter 4

Summary / Zusammenfassung

4.1 Summary

The aim of the work was the development of thiol-ene cross-linked hydrogels based on functionalized poly(glycidol)s (PG) and hyaluronic acid (HA) for extrusion based 3D bioprinting. **Additionally**, the functionalization of the synthesized PG with peptides and the suitability of these polymers for physically cross-linked gels were investigated, in a proof of principle study in order to demonstrate the versatile use of PG polymers in hydrogel development.

First, the precursor polymers of the different hydrogel systems were synthesized (**chapter 3.1**). For thiol-ene cross-linked hydogels, linear allyl-functionalized PG (P(AGE-*co*-G), **5**) and three different thiol-(SH-)functionalized polymers, ester-containing PG-SH (PG-SH_{ec}, **6**), ester-free PG-SH (PG-SH_{ef}, **7**) and HA-SH[IX] were synthesized and analysed, The degree of functionalization of these polymers was adjustable and thus polymers with different SH (**6**: 14 %, **7**: 10 % and 18 %, HA-SH: 33-52 %) and allyl (**5**: 5 %, 11 % and 20 %) content were prepared. The successful polymer synthesis was verified by ^{1}H-NMR and SEC measurements. The presence of thiol groups in PG-SH_{ec} (**6**) and PG-SH_{ef} (**7**) was further confirmed by Raman spectroscopy. Since the natural polymer based HA-SH showed high batch-to-batch variations, especially with regard to their viscosity, they were further analysed by dynamic viscosity and pH measurements. These measurements demonstrated adequate comparability of the three selected HA-SH batches.
For physically cross-linked hydrogels, peptide-functionalized PG (P(peptide-*co*-G), **8**), was synthesized through polymer analogue thiol-ene modification of P(AGE-*co*-G) (**5**). The successful covalent binding of three different peptides was proven by ^{1}H-NMR and IR spectroscopy. The ^{1}H-NMR spectra revealed a conversion of 75 % allyl groups to the respective peptide thioethers.

Subsequently, thiol-ene cross-linked hydrogels were prepared with the synthesized thiol- and allyl-functionalized polymers (**chapter 3.2**). Depending on the origin of the used polymers, two different systems were obtained: on the one hand synthetic hydrogels consisting of PG-$SH_{ec/ef}$ (**6** or **7**) and P(AGE-*co*-G) (**5**) and on the other hand hybrid gels, consisting of HA-SH and P(AGE-*co*-G) (**5**). In synthetic gels, the

[IX] Different HA-SH batches were provided from *Sarah Bertlein* and *Verena Schill* (both of the Department for Functional Materials in Medicine and Dentistry, University of Würzburg) and used throughout this thesis for hydrogel preparation and polymer analysis.

degradability of the gels was determined by the applied PG-SH (**6** or **7**). The use of PG-SH_{ec} (**6**) resulted in hydrolytically degradable hydrogels, whereas the cross-linking with PG-SH_{ef} (**7**) resulted in non-degradable gels.
The physical properties of these different hydrogel systems were determined by swelling, mechanical and diffusion studies and subsequently compared among each other. In swelling studies the differences of degradable and non-degradable synthetic hydrogels as well as the differences of synthetic compared to hybrid hydrogels were demonstrated. It was displayed that both synthetic gels showed no swelling in the first 24 h of incubation, whereas hybrid gels exhibited strong initial swelling of up to 140 ± 4.6 % (mass-% all referred to the start weight). In addition, the studies revealed an equilibrium swelling for non-degradable synthetic hydrogels after 2 w of incubation (~ 80 %) and for hybrid gels after 24 h of incubation (~ 120 %). In contrast, the degradability of ester-containing (PG-SH_{ec}, **6**) synthetic gels was demonstrated, since the hydrogel network of these gels was completely dissolved after 5 w of incubation.
Unbound high molecular weight (HMW) HA was additionally incorporated into the bioink as a thickening agent. Its influence on swelling was also demonstrated, whereby for all systems, a strong initial swelling (~ 200 %) with subsequent mass decrease up to equilibrium swelling was observed. The equilibrium swelling was comparable to those of the systems without additional HA. The initial swelling of hybrid gels as well as gels supplemented with non-bound HMW HA could be attributed to the hydrophilic nature of HA.

Next, the stiffness and the swelling ratios (SR) of the established hydrogel systems were examined in dependency of different parameters, such as incubation time, polymer concentration and UV irradiation. In general, these measurements revealed the same trends for synthetic and hybrid hydrogels: an increased polymer concentration as well as prolonged UV irradiation led to an increased network density. Moreover, it was demonstrated that the incorporation of additional non-bound HMW HA hampered the hydrogel cross-linking resulting in gels with decreased stiffness and increased SR. This effect was strongly dependent on the amount of additional HMW HA.
The impact of the HA-SH batch on the resulting hydrogel properties was also proven by mechanical measurements. Even though only comparable HA-SH batches were used for hydrogel formation, the mechanical stiffness of the hybrid hydrogels varied strongly depending on these batches (from 46.6 kPa (batch I.) to 126.8 kPa (batch

II.)). Comparing the physical properties of hybrid and synthetic hydrogels, it was found that the properties of hybrid hydrogels were less reproducible. This could be ascribed to the higher batch-to-batch variations of the modified natural polymers as well as the more inhomogeneous solutions.

The diffusion of different molecular weight fluorescein isothiocyanate-dextran (FITC-dextran) through hybrid hydrogels (with/without HMW HA) gave information about the mesh size of these gels. The introduction of non-bound HMW HA (1.0 wt.%) had no significant influence on the diffusion speed of the different FITC-dextrans. The smallest FITC-dextran (4 kDa) completely diffused through both hydrogel systems within the first week, whereas only 55 % of 40 kDa and 5-10 % HMW FITC-dextrans (500 kDa and 2 MDa) could diffuse through the networks.

The applicability of synthetic and hybrid hydrogels for cartilage regeneration purpose was investigated through by biological examinations. It was proven that both gels support the survival of embedded human mesenchymal stromal cells (hMSCs) (21/28 d *in vitro* culture), however, the chondrogenic differentiation was significantly improved in hybrid hydrogels compared to synthetic gels. The addition of non-bound HMW HA resulted in a slightly less distinct chondrogenesis.

Lastly the printability of the established hydrogel systems was examined. Therefore, the viscoelastic properties of the hydrogel solutions were adjusted by incorporation of non-bound HMW HA (synthetic gel: + 3.5 wt.% HA, hybrid gel: + 2.5 wt.% HA). Rheological measurements verified shear thinning and recovery properties of the printing solutions. Both systems could be successfully printed with high resolution and high shape fidelity. Comparing synthetic and hybrid gels concerning printability, synthetic gels showed good reproducibility, whereas the reproducible printing of hybrid gels was challenging due to the aforementioned inhomogeneity of the hybrid solution which caused inconstant flow.

The introduction of the double printing approach with reinforcing PCL allowed printing of hydrogel solutions with lower viscosities. As a consequence, the amount of additional HMW HA necessary for printing could be reduced allowing successful printing of hybrid hydrogel solutions with embedded cells. It was demonstrated that the integrated cells survived the printing process with high viability measured after

21 d. Moreover, by this reinforcing technique, robust hydrogel-containing constructs were fabricated.

In addition to thiol-ene cross-linked hydrogels, hydrogel cross-linking via ionic interactions was investigated with a hybrid hydrogel based on HMW HA and peptide-functionalized PG **8c** (**chapter 3.3**). Rheological measurements revealed an increase in the viscosity of a 2 wt.% HMW HA solution by the addition of peptide-functionalized PG **8c**. The increase in viscosity could be attributed to the ionic interactions between the positively charge PG **8c** and the negatively charge HMW HA. Furthermore, it was demonstrated that these interactions are strongly dependent on the used solvent.

In conclusion, throughout this thesis thiol-ene chemistry and PG were introduced as promising cross-linking reaction and polymer precursor for the field of biofabrication. Furthermore, the differences of hybrid and synthetic hydrogels as well as chemically and physically cross-linked hydrogels were demonstrated.
In the future, the presented cross-linking method as well as polymers could be applied for many other systems and the advantages of the different approaches could be combined. For example, physically cross-linked gels could be mechanically stabilized by chemical post-cross-linking and the synthetic hydrogels could be endowed with biological moieties to enable their biological applicability.
Moreover, the double printing approach was demonstrated to be a promising tool for the fabrication of robust hydrogel-containing constructs. It opens the possibility of printing hydrogels that were not printable yet, due to too low viscosities.

4.2 Zusammenfassung

Ziel der Arbeit war die Entwicklung von Thiol-En-vernetzten Hydrogelen basierend auf funktionalisierten Poly(glyzidolen) (PG) und Hyaluronsäure (HA) für das extrusionsbasierte 3D-Biodrucken. Um die vielseitigen Anwendungsmöglichkeiten von PG-Polymeren für die Hydrogelentwicklung zu zeigen, wurde **darüber hinaus**, in einer *Proof-of-Principle*-Studie, PG mit Peptiden funktionalisiert und die Eignung dieser Polymere für die Herstellung von physikalisch vernetzten Gelen untersucht.

Zunächst wurden die Vorläuferpolymere für die verschiedenen Hydrogelsysteme synthetisiert (**Kapitel 3.1**). Für die Thiol-En-vernetzten Hydrogele wurde lineares Allyl-funktionalisiertes PG (P(AGE-*co*-G), **5**) und drei verschiedene Thiol-(SH-)funktionalisierte Polymere, Ester haltiges PG-SH (PG-SH_{ec}, **6**), Ester freies PG-SH (PG-SH_{ef}, **7**) und HA-SH^{X} synthetisiert und analysiert. Dabei war der Funktionalisierungsgrad dieser Polymere einstellbar und es wurden Polymere mit unterschiedlichen Anteilen an SH (**6**: 14 %, **7**: 10 % und 18 %, HA-SH: 33-52 %) und Allyl (**5**: 5 %, 11 % und 20 %) hergestellt. Die erfolgreiche Polymersynthese wurde durch ^{1}H-NMR und SEC Messungen verifiziert. Des Weiteren wurde die Anwesenheit von Thiolgruppen in PG-SH_{ec} (**6**) und PG-SH_{ef} (**7**) durch Raman-Spektroskopie bestätigt. Da das natürlich basierte HA-SH hohe Chargen-zu-Chargen-Variationen aufwies, insbesondere bezüglich der Viskosität, wurden diese Polymere zusätzlich mittels dynamischen Viskositäts- und pH-Messungen analysiert. Diese Messungen zeigten eine adäquate Vergleichbarkeit der drei ausgewählten HA-SH Chargen.
Für physikalisch vernetzte Hydrogele wurde Peptid-funktionalisierte PGs (P(Peptid-*co*-G), **8**) mittels polymeranaloger Thiol-En-Modifikation von P(AGE-*co*-G) (**5b**) synthetisiert. Die erfolgreiche kovalente Anbindung von drei verschiedenen Peptiden wurde durch ^{1}H-NMR- und IR-Spektroskopie bestätigt. Die ^{1}H-NMR-Spektren zeigten, dass 75% der Allyl-Gruppen zu Peptiden umgesetzt wurden.

Anschließend wurden Thiol-En-vernetzte Hydrogele auf Basis der synthetisierten Thiol- und Allyl-funktionalisierten Polymeren hergestellt (**Kapitel 3.2**). Je nach Ursprung der verwendeten Polymere wurden zwei verschiedene Systeme erhalten: einerseits synthetische Hydrogele bestehend aus PG-$SH_{ec/ef}$ (**6** oder **7**) und P(AGE-*co*-G) (**5**) und andererseits hybride Gele, bestehend aus HA-SH und P(AGE-*co*-G)

[X] Verschiedene HA-SH Chargen wurden von *Sarah Bertlein* und *Verena Schill* (beide vom Department for Functional Materials in Medicine and Dentistry, University of Würzburg) bereitgestellt und in dieser Arbeit für die Hydrogelherstellung und Polymeranalyse verwendet.

(**5**). Bei den synthetischen Gelen wurde die Abbaubarkeit der Gele durch das verwendete PG-SH (**6** oder **7**) bestimmt. Die Verwendung von PG-SH_{ec} (**6**) resultierte in hydrolytisch abbaubaren Hydrogelen, während die Vernetzung mit PG-SH_{ef} (**7**) zu nicht abbaubaren Gelen führte.
Die physikalischen Eigenschaften der verschiedenen Hydrogelsysteme wurden mittels Quell-, mechanischen und Diffusionsexperimenten bestimmt und anschließend miteinander verglichen. Die Quellungsstudien zeigten die Unterschiede von abbaubaren und nicht abbaubaren synthetischen Hydrogelen, sowie die Unterschiede von synthetischen gegenüber hybriden Hydrogelen. Es stellte sich heraus, dass beide synthetischen Gele in den ersten 24 h Inkubation nicht quollen, wohingegen hybride Gele eine starke initiale Quellung von bis zu 140 ± 4,6 % (Massen-% alle bezogen auf das Startgewicht) zeigten. Darüber hinaus zeigten die Studien einen Gleichgewichtsquellzustand für nicht abbaubare synthetische Hydrogele nach 2 w Inkubationszeit (~ 80 %) und für Hybridgele nach etwa 24 h Inkubationszeit (~ 120 %). Auf der anderen Seite wurde die Abbaubarkeit von Ester haltigen (PG-SH_{ec}, **6**) synthetischen Gelen nachgewiesen, da sich das Hydrogel-Netzwerk dieser Gele nach 5 w Inkubation vollständig auflöste.
Nicht gebundene, hochmolekulare (HMW) HA wurde als Verdickungsmittel zusätzlich in die Biotinten eigebracht. Ihr Einfluss auf die Quellung wurde ebenfalls untersucht, wobei bei allen Systemen wurde starke Anfangsquellung (~ 200 %) mit anschließender Massenabnahme bis hin zur Gleichgewichtsquellung beobachtet wurde. Der Gleichgewichtszustand der Quellung war vergleichbar mit demjenigen der Systeme ohne zusätzliche HA. Das initiale Quellen von Hybridgelen sowie Gelen, die mit nicht gebundener HMW HA ergänzt wurden, konnte der hydrophilen Natur von HA zugeschrieben werden.

Als nächstes wurden die Steifigkeit und das Quellverhältnis (SR) der etablierten Hydrogelsysteme in Abhängigkeit von verschiedenen Parametern wie Inkubationszeit, Polymerkonzentration und UV-Bestrahlung untersucht. Im Allgemeinen zeigten diese Messungen für synthetische und hybride Hydrogele die gleichen Trends: eine erhöhte Polymerkonzentration sowie eine verlängerte UV-Bestrahlung führten zu einer erhöhten Netzwerkdichte. Darüber hinaus wurde gezeigt, dass das Einbringen zusätzlicher, nicht gebundener HMW HA die Hydrogelvernetzung behinderte, was zu Gelen mit verringerter Steifigkeit und

erhöhtem SR führte. Dieser Effekt war stark abhängig von der Menge an zusätzlich eingebrachter HMW HA.
Die Auswirkung der HA-SH-Charge auf die resultierenden Hydrogeleigenschaften wurde ebenfalls durch mechanische Messungen aufgezeigt. Obwohl nur vergleichbare HA-SH-Chargen für die Hydrogelbildung verwendet wurden, variierte die mechanische Steifigkeit der Hybridhydrogele stark in Abhängigkeit von den verwendeten Chargen (von 46,6 kPa (Charge I.) bis 126,8 kPa (Charge II.)).
Beim Vergleich der physikalischen Eigenschaften von hybriden und synthetischen Hydrogelen wurde festgestellt, dass die Steifigkeit und das Quellverhalten von hybriden Hydrogelen weniger reproduzierbar waren. Dies konnte auf die höheren Chargen-zu-Chargen-Variationen von natürlichen Polymeren sowie auf die inhomogeneren Lösungen zurückgeführt werden.

Die Diffusion von Fluorescein-Isothiocyanat-Dextran (FITC-Dextran) mit unterschiedlichem Molekulargewichten durch hybride Hydrogele (mit/ohne HMW HA) lieferte Informationen über die Maschengröße dieser Gele. Das Einbringen von nicht gebundener HMW HA (1,0 Gew.-%) hatte dabei keinen signifikanten Einfluss auf die Diffusionsgeschwindigkeit der verschiedenen FITC-Dextrane. Das kleinste FITC-Dextran (4 kDa) diffundierte innerhalb der ersten Woche vollständig durch beide Hydrogelsysteme, während nur 55 % der 40 kDa und 5-10 % HMW FITC-Dextrane (500 kDa und 2 MDa) durch die Netzwerke diffundieren konnten.

Die Anwendbarkeit von synthetischen und hybriden Hydrogelen für Knorpelregenerationszwecke wurde durch biologische Experimente untersucht. Es wurde bewiesen, dass beide Gele das Überleben von eingebetteten humanen mesenchymalen Stromazellen (hMSCs) unterstützen (21/28 d *in vitro* Kultur), jedoch war die chondrogene Differenzierung in hybriden Hydrogelen im Vergleich zu synthetischen Gelen signifikant verbessert. Die Zugabe von nicht gebundenem HMW HA führte zu einer etwas weniger ausgeprägten Chondrogenese.

Zuletzt wurde die Druckbarkeit der etablierten Hydrogelsysteme untersucht. Dafür wurden die viskoelastischen Eigenschaften der Hydrogellösungen durch das Einbringen von nicht gebundener HMW HA (synthetisches Gel: + 3,5 Gew.-% HA, hybrides Gel: + 2,5 Gew.-% HA) eingestellt. Rheologische Messungen bestätigten die scherverdünnenden und die Wiederherstellungseigenschaften der Drucklösungen. Beide Systeme konnten erfolgreich mit hoher Auflösung und hoher

Formgenauigkeit gedruckt werden. Beim Vergleich von synthetischen und hybriden Gelen bezüglich der Druckbarkeit erwies sich das Drucken von synthetischen Gele als sehr gut reproduzierbar, während das reproduzierbare Drucken von hybriden Gelen aufgrund der oben erwähnten Inhomogenität der Hybridlösungen erschwert wurde, da diese einen unregelmäßigen Fluss der Lösung erzeugte.

Die Einführung des Doppeldruck-Konzeptes mit verstärkendem PCL ermöglichte das Drucken von Hydrogellösungen mit niedrigeren Viskositäten. Infolgedessen konnte die für den Druck notwendige Menge an HMW HA reduziert und hybride Hydrogellösungen mit eingebetteten Zellen erfolgreich gedruckt werden. Es wurde gezeigt, dass die integrierten Zellen den Druckprozess mit hoher Vitalität überlebten (gemessen nach 21 d). Darüber hinaus wurden mit dieser Verstärkungstechnik robuste Hydrogel-enthaltende Konstrukte hergestellt.

Zusätzlich zu den Thiol-En-vernetzten Hydrogelen wurde die Hydrogelvernetzung mittels elektrostatischen Wechselwirkungen mit einem hybriden Gel auf der Basis von HMW HA und Peptid-funktionalisiertem PG **8c** untersucht (**Kapitel 3.3**). Rheologische Messungen ergaben eine Erhöhung der Viskosität einer 2 wt.% HMW HA Lösungen durch die Zugabe von Peptid-funktionalisiertem PG **8c**. Der Viskositätsanstieg konnte auf die elektrostatischen Wechselwirkungen zwischen dem positiv geladenen PG **8c** und der negativ geladenen HMW HA zurückgeführt werden. Des Weiteren wurde gezeigt, dass diese Wechselwirkungen stark vom verwendeten Lösungsmittel abhängen.

Zusammenfassend wurde in dieser Arbeit die Thiol-En-Chemie und PG als vielversprechende Vernetzungsreaktion bzw. Polymervorstufe für die Biofabrikation eingeführt. Des Weiteren wurden die Unterschiede von hybriden und synthetischen Hydrogelen sowie von chemisch und physikalisch vernetzten Hydrogelen aufgezeigt. **In Zukunft** könnte die vorgestellte Vernetzungsmethode sowie die Polymere für viele andere Systeme angewandt und die Vorteile der einzelnen Ansätze kombiniert werden. Beispielsweise könnten physikalisch vernetzte Gele durch eine chemische Nachvernetzung mechanisch stabilisiert werden und die synthetischen Gele mit biologischen Komponenten funktionalisiert werden um ihre biologische Anwendbarkeit zu ermöglichen.
Darüber hinaus wurde gezeigt, dass das Doppeldruck-Konzept eine vielversprechende Methode für die Herstellung von robusten Hydrogel-enthaltenden

Konstrukten ist. Es eröffnet die Möglichkeit, Hydrogele zu drucken, die aufgrund zu geringer Viskositäten bis jetzt nicht druckbar waren.

Chapter 5

Experimental section

Parts of this chapter have previously been published and are adapted with permission from:

S. Stichler, T. Böck, N. Paxton, S. Bertlein, R. Levato, V. Schill, W. Smolan, J. Malda, J. Teßmar, T Blunk, J. Groll, Double printing of hyaluronic acid/poly(glycidol) hybrid hydrogels with poly(ε-caprolactone) for MSC chondrogenesis, *Biofabrication* **2017**, doi: 10.1088/1758-5090/aa8cb7.

S. Stichler, S. Bertlein, J. Teßmar, T. Jüngst, J. Groll, Thiol-ene Cross-Linkable Hydrogels as Bioinks for Biofabrication, *Macromol. Symp*. **2017**, *372*, 102-107.

S. Stichler, T. Jüngst, M. Schamel, I. Zilkowski, M. Kuhlmann, T. Böck, T. Blunk, J. Teßmar, J. Groll, Thiol-ene clickable poly(glycidol) hydrogels for biofabrication, *Ann. Biomed. Eng*. **2017**, *45*, 273-285.

5.1 Materials

The monomers allyl glycidyl ether (AGE) (≥ 99 %, Sigma-Aldrich, St. Louis, MO, USA) and ethoxy ethyl glycidyl ether (EEGE) (synthesis described under 5.3.1) were purfied via drying over calcium hydride (CaH_2) (92 %, ABCR, Karlsruhe, Germany) and fractional distillation under reduced pressure and Ar atmosphere. The purified monomers were stored in a glovebox (model: GS046711, Glovebox Systemtechnik, Malsch, Germany) under N_2 atmosphere before use. For the preparation of phosphate buffered saline (PBS), sodium chloride (NaCl) (8.00 g, 136 mmol), potassium dihydrogen phosphate (KH_2PO_4) (200 mg, 1.47 mmol), sodium phosphate dibasic dodecahydrate (Na_2HPO_4 x 12 H_2O) (2.80 g, 7.82 mmol) and potassium chloride (KCl) (200 mg, 2.68 mmol) were mixed and dissolved in 1 L Milli-Q water (all salts from Merck, Darmstadt, Germany). Deionized water was taken from the Milli-Q system (arim®pro, Sartorious, Göttingen, Germany).

The peptides RYPISRPRKRC (98 %) and CGWYRGRL (98 %) were purchased from GeneCust (Ellange, Luxembourg) and the peptides CGF-Orn-GERGPP (98 %) and CGPRGQ-Orn-GVMGF-Orn (98 %) were pruchased from jpt (Berlin, Germany).

Fluorescence-labelled polymers, fluorescein isothiocyanate-dextran (FITC-dextran) with different molecular weights (4 kDa, 40 kDa, 500 kDa and 2 MDa) and fluorescein hyaluronic acid (F-HA) (> 95 %, 800 kDa) were purchased from Sigma-Aldrich (St. Louis, MO, USA) and used for time-dependent diffusion measurements.

N,N'-dicyclohexylcarbodiimide (DCC) (99 %), 2,2-dimethoxy-2-phenylacetophenon (DMPA) (99 %), 4-(dimethylamino)pyridine (DMAP) (≥ 99 %), dimethylformamide (DMF) (> 99.8 %), 3,3'-dithiodipropionic acid (DTPA) (99 %), ethyl vinyl ether (99 %, KOH stabilized), glycidol (96 %), 2-hydroxyethyl acrylate (HEA) (96 %), potassium *tert*-butoxide (KO*t*Bu) (1 M in THF), sodium hydroxide (NaOH) (> 98 %), thioacetic acid (96 %), *p*-toluenesulfonic acid monohydrate (*p*TsOH) (> 98.5 %), triethylamine (≥ 99 %) and tris(2-carboxyethyl)phosphine hydrochloride (TCEP) (≥ 98 %) were purchased from Sigma-Aldrich (St. Louis, MO, USA) and used as received. Diethylether (Staub Co., Nürnberg, Germany), ethanol (EtOH) (99 %, TH Geyer, Renningen, Germany), hydrochloric acid (HCl) (32 %, Merck, Darmstadt, Germany), 2-hydroxy-1-[4-(hydroxyethoxy)-phenyl]-2-methyl-1-propanone (I2959) (BASF, Ludwigshafen, Germany), poly(ε-caprolactone) (PCL) (Purac Purasorb PC12, Corbion-Purac, Amsterdam, the Netherlands), tetrahydrofuran (THF) (Fisher Scientific, Schwerte, Germany), sodium hydrogen carbonate ($NaHCO_3$) (Merck,

Darmstadt, Germany) and sodium sulfate (Na_2SO_4) (Merck, Darmstadt, Germany) were used as received. The deuterated solvents deuterium oxide (D_2O) and deuterated chloroform ($CDCl_3$) for NMR measurements were purchased from Deutero GmbH (Kastellaun, Germany).

Hyaluronic acids (HA) with two different molecular weights (27.3 kDa and 1.36 MDa) were purchased as sodium salts from BaccaraRose (Alpen, Germany). The high molecular weight (HMW) HA was used as an additive for 3D printing and the low molecular weight (LMW) HA was used for further functionalization. Thiol-functionalized HA (HA-SH) was synthesized by *Sarah Bertlein*[XI] and *Verena Schill*[XII] during their doctoral dissertations according to literature[122]. Different HA-SH batches were provided for hydrogel preparation and analysis.

[XI] Department for Functional Materials in Medicine and Dentistry, University of Würzburg.

[XII] Department for Functional Materials in Medicine and Dentistry, University of Würzburg.

5.2 Methods

5.2.1 UV reactions

Devices:
- UV hand lamp with filter (254 and 365 nm; 1 mW cm^{-2}) (A. Hartenstein, Wuerzburg, Germany)
- UV LED cubes (365 nm; 4 x 77 mW cm^{-2}) (Polymerschmiede, Aachen, Germany)
- bluepoint 4 (300–650 nm; 130 mW cm^{-2}) (Dr. Hoenle AG, Munich, Germany)

The high intensity bluepoint 4 UV light was used for fast cross-linking of the hydrogel solution after printing.

P(AGE-*co*-G) (**5**) functionalization with thiols and peptides was realized via UV induced thiol-ene reaction for 2 h. The UV source was dependent on the photoinitiator-solvent combination. Thiol-ene reactions in EtOH with DMPA as the photoinitiator were implemented with the LED cubes, while reactions in deionized water with I2959 as the initiator were conducted with the UV hand lamp (365 nm setting).

5.2.2 Polymer purification

5.2.2.1 Dialysis

All water soluble polymers were dialysed against deionised water (Milli-Q). Therefore Biotech Cellulose Ester dialysis membranes (spectrumlabs.com, Rancho Dominquez, CA, USA) with different MW-cut-offs of 1000 or 3500 (for P(peptide-*co*-G) (**8**) purification) Da were used. The dialysis water was changed five times a day, every 2 h. Thiol-functionalized PGs **6**, **7** were dialysed against degassed water (2 h Ar flow/2 L water) to prevent oxidation.

5.2.2.2 Lyophilization

Device: Alpha 1-2 LD (Christ, Osterode am Harz, Germany)
Polymer solutions were freeze-dried to remove water.

5.2.3 Polymer characterization

5.2.3.1 NMR spectroscopy

Device: 300 MHz Bruker Biospin spectrometer (Bruker, Billerica, MA, USA)
The shown chemical shifts were referred to the particular solvent peak which was set as an internal reference (D_2O: δ = 4.79 ppm and $CDCl_3$: δ = 7.26 ppm). Signal multiplicities were abbreviated with s (singlet) and m (multiplet). The protons of the synthesized products were numbered and referred to the corresponding signal.
Allyl respective thiol peaks were set in relation to significant backbone peaks to determine the allyl- respective thiol-functionality of P(AGE-*co*-G) (**5**), P(SH-*co*-G) (**6** and **7**) and HA-SH.

5.2.3.2 FT-IR spectroscopy

Device: Nicolet iS10 spectrometer (Thermo Fisher Scientific, Waltham, MA, USA)
The FT-IR spectrometer is equipped with a diamant-ATR unit with which the samples were measured in the spectrum from 400 to 7500 cm^{-1}. Characteristic vibrations were referred to the respective functional groups.[160]

5.2.3.3 Raman spectroscopy

Device: DXR Raman Microscope (Thermo Fisher Scientific, Waltham, MA, USA)
The samples were measured with an excitation laser of 780 nm (laser power set to 15 mW) and an Olympus objective (20x). Characteristic peaks were referred to the respective functional groups.[160]

5.2.3.4 Size exclusion chromatography (SEC)

Approximately 5 mg sample was dissolved in 1 mL SEC eluent and filtered (cellulose or PTFE, pore size: 0.2 µm) before analysis.
Thiol-functionalized PGs **6** and **7**, were measured without and with quenching before measurement. By quenching with HEA the oxidation of the thiols and thus the potential blocking of the column could be prevented. For quenching reaction, thiols reacted in a thiol-ene reaction (30 min, UV: 365 nm) with HEA.

The elugrams of the intermediate stage polymers (**2** and **4**) are shown in the synthesis **chapter 5.3** with the respective analysis, whereas the elugrams of the product polymers **3** and **5** as well as of the functionalized PGs **6**-**8** are depicted and discussed in the results and discussion section (**chapter 3.1**).

Water SEC

Device: Viscotek GPCmax (Malvern, Herrenberg, Germany)

For water SEC measurements deionized water with additional 8.5 g/L $NaNO_3$ and 0.2 g/L NaN_3 was used as the solvent with a flow rate of 0.7 mL/min. The device consists of a column oven (35 °C), a multi angle light scattering (MALS) detector (Viscotek SEC-MALS 20), a refractive index (RI) detector (Viscotek VE3580), a viscosity detector (Viscotek 270) and Viscotek A-columns (length: 300 mm, width 8 mm, material: porous poly(hydroxy-methacrylate). Two different column sets were used for water SEC measurements: set1: A3000 (particle size: 6 µm) and A2000 (particle size: 8 µm) columns and set2: 2 x A6000 (particle size: 13 µm) columns. PEG (Malvern, Herrenberg, Germany) was used as calibration standard and measurements were evaluated with conventional calibration using the RI signal.

DMF SEC

Device: OmniSEC Resolve & Reveal (Malvern, Herrenberg, Germany)

For DMF SEC measurements DMF with additional 1 g/L LiBr was used as the solvent with an elution rate of 1.0 mL/min. The OmniSEC Resolve & Reveal consists of a column oven (45 °C), a right angle light scattering (RALS) detector, a low angle light scattering (LALS) detector, a RI detector, a viscosity detector, a precolumn (Dguard, Organic Column 10 x 4.6 mm) and two separation columns: D2000 and D3000 (length: 300 mm, width: 7.8 mm, material: styrene divinyl-benzene, particle size: 6 µm). PMMA standards (Malvern, Herrenberg, Germany) were used for calibration and measurements were evaluated with conventional calibration using the RI signal.

5.2.3.5 Dynamic viscosity measurements

Device (viscosity): LOVIS 2000 M (Anton Paar, Graz, Austria)
Device (density): DMA 4100 M (Anton Paar, Graz, Austria)
Dynamic viscosity of 0.5 wt.% aqueous polymeric solutions was measured at 23 °C with a falling ball viscometer with auto angle adjustment (20°–70°). The solutions were transferred into a capillary (LOVIS, capillary diameter: 1.8 respectively 1.59 mm) equipped with a steel ball. Prior to that, the density was measured and used for the viscosity calculations.

5.2.3.6 pH measurements

Device: inoLab pH Level 1 (WTW, Weilheim, Germany)
The pH value was measured for 5 wt.% HA-SH solutions (in PBS) prior to hydrogel preparation and for hydrogel precursor solutions to adjust the pH to 6.9 – 7.4.

5.2.4 Hydrogel preparation

P(AGE-*co*-G) (**5**) and P(SH-*co*-G) (**6** and **7**) respectively HA-SH were dissolved in PBS with an equimolar ratio of allyl and thiol groups. Subsequently the photoinitiator I2959 (0.05 wt.%) was added to the mixture. The precursor solution was transferred into cylindrical molds (h = 2 mm, Ø 6 mm) and cross-linked for 10 min with UV-light (365 nm, UV hand lamp).

5.2.4.1 Synthetic hydrogel system (P(AGE-*co*-G) + P(SH-*co*-G))

For pure PG hydrogels (**5** + **6** or **5** + **7**) a precursor solution with a total polymer amount of 15 wt.% was prepared.

5.2.4.2 Hybrid hydrogel system (P(AGE-*co*-G) + HA-SH)

Precursor solutions for hybrid hydrogels were produced with a total polymer concentration of 10 wt.%. The pH of the acidic solution was adjusted to 6.9 – 7.2 prior to cross-linking.

For several hydrogel characterization studies (see below) the polymer amount as well as the UV source and UV exposure time was modified for both systems.

5.2.4.3 Hydrogels with additives

HA

To achieve hydrogel solutions with higher viscosities additional HMW HA (1.36 MDa) was added to the precursor solution and mixed with a spatula before cross-linking. The amount of the supplementary HA was dependent on the application (see below: hydrogel characterization and printing).

Cells

Human mesenchymal stromal cells (hMSCs) were added to the hydrogel prior to cross-linking, to investigate the general material suitability of the hydrogel system for chondrogenic differentiation of encapsulated cells.

The preparation of the cell-laden hydrogels was conducted in cooperation with *Thomas Böck*[XIII]. Live/Dead assays to assess general cytocompatibility and biochemical analysis to analyse MSC chondrogenesis were performed by *Thomas Böck*.

5.2.4.4 Reinforced hydrogels

To increase the stability and stiffness of hydrogels, PCL plugs were 3D printed (h = 2 mm, Ø 6 mm; strand-to-strand distance: 1.00, 1.5 mm respectively), placed into the cylindrical molds, filled with hydrogel solution and cross-linked.

[XIII] Department of Trauma, Hand, Plastic and Reconstructive Surgery, University of Würzburg.

5.2.5 Hydrogel characterization

5.2.5.1 Swelling studies

Triplets of cylindrical hydrogels (h = 2 mm, Ø 6 mm) were prepared as described above, incubated at 37 °C in 2 mL PBS and weighed at specific time intervals (0 h, 0.5 h, 1 h, 4 h, 7 h, 24 h, 1 w, 2 w, 3 w, 4 w and 5 w). The supernatants were refreshed after each measurement and the obtained weights were set relative to the initial weight of the corresponding hydrogel.

Table 18: Hydrogel compositions and preparation conditions for swelling studies.

hydrogel composition	polymer amount [wt.%]	UV exposure time [min]
P(AGE-*co*-G) (**5**) + PG-SH_{ef} (**7**)	15	10
P(AGE-*co*-G) (**5**) + PG-SH_{ef} (**7**) + 3.5 wt.% HMW HA	15	10
P(AGE-*co*-G) (**5**) + PG-SH_{ec} (**6**)	15	10
P(AGE-*co*-G) (**5**) + HA-SH	10	10
P(AGE-*co*-G) (**5**) + HA-SH + 1 wt.% HMW HA	10	10

5.2.5.2 Mechanical testing and swelling ratio

Device: Bose ElectroForce 5500 (Bose Corporation, Eden Prairie, MN, USA)
Unconfined compression measurements were performed with a mechanical testing system equipped with a load cell of 200 N and 22 N, respectively. Cylindrical hydrogel samples (h = 2 mm, Ø 6 mm) were loaded and compressed with a constant cross head speed of 0.001 mm s^{-1}. The Young's modulus is given by the slope of the true stress-strain curve in the linear elastic range and was calculated from the raw data.
The mechanical testing was performed on hydrogels with different compositions, UV exposure times, UV sources, polymer amounts and swelling times (Table 19). Triplets of hydrogel samples were prepared for each condition and the samples were incubated at 37 °C in 2 mL PBS prior to testing. To investigate the influence of the

photoinitiator I2959 on the stiffness of the hydrogels, the hybrid system was additionaly tested with different I2959 concentrations (0.05, 0.1 and 0.25 wt.%).

Table 19: Overview of different conditions and compositions for mechanical testing. The varied condition is written in italic.

hydrogel composition	**polymer amount [wt.%]**	**UV exposure time [min]**	**swelling time in PBS**
P(AGE-*co*-G) (**5**) + PG-SH_{ef} (**7**)	15	*5, 10, 15*	4 h
		22 s (bluepoint 4)	
	5, 15, 25	10	4 h
	15	10	*0, 0.5, 4, 24 h, 1 w, 4 w*
+ 3.5 wt.% HMW HA	15	10	4 h
P(AGE-*co*-G) (**5**) + PG-SH_{ec} (**6**)	15	10	*0, 0.5, 4, 24 h, 1 w, 4 w*
P(AGE-*co*-G) (**5**) + HA-SH	10	*5, 10, 15*	24 h
	5, 10, 15, 25	5	24 h
	10	10	*0, 0.5, 4, 24 h, 1, 2, 3, 4, 5 w*
+ 1.0 wt.% HMW HA	10	10	24 h

To determine the swelling ratio (SR) the hydrogels were weighed before the mechanical testing (W_s) and freeze-dried and weighed again (W_d) after the mechanical testing. The swelling ratio (SR) was calculated by using the following equation: $SR = W_s / W_d$.

5.2.5.3 Diffusion tests

Device: Spark 20M (Tecan Group, Männerdorf, Switzerland)
Well plates for fluorescence measurements: Microplate Glass Bottom, 24 Well, Black (Porvair Sciences, Leatherhead, United Kingdom)

Diffusion of fluorescence dyes out of hydrogels

For time-dependent diffusion tests of fluurescence labeled polymers out of synthetic and hybrid hydrogels 4 kDa FITC-dextran and 800 kDa F-HA were used. Therefore the fluorescence polymers were mixed into the hydrogel solutions before cross-linking. F-HA was not completely solved in the PBS solution and thus the concentrations of the F-HA can not be assumed to be absolute values (Table 20, shown in italic). After preparation of the cylindrical hydrogels (see hydrogel preparation above) the gels were incubated in 2 mL PBS at 37 °C in 24 well plates and the fluorescence (λ_{ex}: 485 nm; λ_{em}: 535 nm) of the storage solution was measured at specific time intervals (0 h, 0.5 h, 1 h, 4 h, 7 h, 24 h, 1 w, 2 w, 3 w, 4 w and 5 w). The hydrogels were taken out of the PBS solution during the measurements. Triplets of hydrogels were produced for each condition.

Table 20: Diffusion tests of fluorescence dyes out of hydrogels.

hydrogel composition	**fluorescence labeled polymer**	**concentration of fluorescence dyes [µmol/l]**
P(AGE-*co*-G) (**5**) + PG-SH_{ef} (**7**)	F-HA	*0.34*
P(AGE-*co*-G) (**5**) + HA-SH	F-HA	*0.63*
	FITC-dextran	121
P(AGE-*co*-G) (**5**) + HA-SH + 1 wt.% HMW HA	F-HA	*0.63*
	FITC-dextran	121

Diffusion of fluorescence labelled polymers through hydrogels

The diffusion of FITC-dextrans with different molecular weights (4 kDa, 40 kDa, 500 kDa and 2 MDa) through hydrogels was examined with hybrid hydrogels with and without additional HA. The hydrogel solution was prepared as described above, 60 µL were filled into cell inserts (24 Well 8 µm pore size; Falcon®/Corning, Corning, USA) and cross-linked via UV light. The cell inserts with the hydrogels were placed into 24 well plates with each 700 µL PBS and incubated at 37 °C. After 24 h swelling in PBS, 60 µL fluorescence dye solution was pipetted on top of the hydrogels and the hydrogels were incubated again at 37 °C. The fluorescence (λ_{ex}: 485 nm; λ_{em}: 535 nm) of the storage solution was measured at specific time intervals (0 h, 0.5 h, 1 h, 4 h, 7 h, 24 h, 1 w, 2 w, 3 w, 4 w and 5 w). Therefore, the cell inserts with the hydrogels were removed. Cell inserts without hydrogel, with 60 µL dye solution were prepared and measured equally and taken as positive control. The fluorescence intensity of each flow-through solution was related to the positive control. Triplets were prepared for each hydrogel system and dye.

Table 21: Diffision tests of fluorescence dyes through hybrid hydrogels.

hydrogel composition	**molecular weight of FITC-dextran**	**concentration of fluorescence dyes**
P(AGE-*co*-G) (**5**) + HA-SH +/- 1 wt.% HMW HA	4 kDa	16.4 µmol/l
	40 kDa	440 nmol/l
	500 kDa	77.3 nmol/l
	2 MDa	1.31 nmol/l

5.2.5.4 Rheology

Device: Physica MCR301 rheometer (Anton Paar, Graz, Austria)
Rheological measurements were conducted at 24 °C (plate temperature) with a plate-plate geometry of 25 mm, a solvent trap and a measurement position of 0.5 mm.
Hydrogel precursor solutions for 3D printing (synthetic hydrogel: 15 wt.% polymer concentration + 3.5 wt.% HMW HA, hybrid hydrogel: 10 wt.% polymer concentration + 2.5 wt.% HMW HA) were examined with two different measurements: recovery test under rotation and rotational shear-viscosity measurement. For both hydrogel systems, shear-viscosity measurements were applied with a shear ramp ranging from 0.001 to 5 s^{-1}. The recovery tests were performed with a low shear rate of 0.01 s^{-1} for 100 s followed by a high shear rate of 5 s^{-1} for 100 s. The high-low shear rate shift was repeated nine times for each measurement.
HMW HA solutions (in PBS) with different amounts of HA (0.5, 1.0, 1.5, 2.0, 2.5, 3.0 and 3.5 wt.%) were also examined by recovery and shear-viscosity tests. The rotational shear-viscosity measurement was conducted with a shear ramp ranging from 0.01 s^{-1} to 1000 s^{-1}. The recovery test was applied with a low shear rate of 0.01 s^{-1} for 200 s^{-1} followed by a high shear rate of 100 s^{-1} for 100 s and a final low sear rate of 0.01 s^{-1} for 200 s. In addition, the precursor solutions for physically cross-linked hydrogels (2 wt.% HMW HA + 3 wt.% P(peptide-*co*-G) (**8c**) in H_2O; 1:1 ratio of positive/negative charge) were rheologically evaluated using the same settings as for HMW HA measurements.

5.2.6 3D Printing

Device: 3D Discovery bioprinter (RegenHU, Villaz-St-Pierre, Switzerland)
The printer is equipped with three different print-heads (PH): PH1 (electromagnetic valve dispenser, cell friendly printhead CF-300 N/H), PH2 (pneumatic driven print-head, DD135N) and PH3 (precision extrusion deposition print-head, screw based extruder, HM110EX).

All hydrogel precursor solutions were prepared as described above, transferred into 3 mL UV protected printing syringes (3cc, Nordson EFD, East Providence, Rhode Island, USA) and centrifuged (Mega Star 1.6R, Thermo Scientific, Waltham, MA, USA) (4500 rpm / 10 min) to produce homogenous solutions without air bubbles.

All constructs were printed in a laminar-flow hood and analysed with a stereo microscope (SteREO Discovery V20, Carl Zeiss Microscopy, Jena, Germany).

The used gcodes were generated by *Tomasz Jüngst*[XIV] and *Naomi Paxton*[XV], respectively.[161]

5.2.6.1 Hydrogel printing

Synthetic as well as hybrid hydrogel precursor solutions were printed with different amounts of additional HMW HA (1.36 MDa). Scaffolds with high resolution were obtained for synthetic hydrogel precursor solutions with additional 3.5 wt.% HA and for hybrid hydrogel precursor solutions with additional 2.5 wt.% HA. Both systems were extruded with PH1 with a valve opening time of 900 µs, a dosing distance of 0.075 mm, a layer height of 0.20 mm and a printing speed of 10 mm/s in a 12 mm x 12 mm building area. The inner needle diameters (0.45 mm and 0.30 mm), strand-to-strand distances (1.00 and 1.5 mm) and UV exposure time (2 s each layer or continuous exposure) was varied and the pressure was adjusted to the relative settings (0.2 – 3.2 bar, Table 22).

[XIV] Department for Functional Materials in Medicine and Dentistry, University of Würzburg.
[XV] Department for Functional Materials in Medicine and Dentistry, University of Würzburg.

Table 22: Printing settings for hydrogel precursor solution printing.

hydrogel composition	strand-to-strand distance [mm]	inner needle diameter [mm]	UV exposure time [s]	pressure [bar]
P(AGE-*co*-G) (**5**) + PG-SH_{ef} (**7**) + 1.5 wt.% HMW HA	1.5	0.45	2 (each layer)	0.2
+ 3.5 wt.% HMW HA	1.5	0.45	2 (each layer)	1.5
	1.5	0.30	2 (each layer)	3.2
	1.5	0.45	120 (continuous)	1.5
	1.0	0.45	40 (continuous)	1.3, 1.5
P(AGE-*co*-G) (**5**) + HA-SH + 2.5 wt.% HMW HA	1.5	0.45	90 (continuous)	2-3

5.2.6.2 Double printing with PCL

The hybrid hydrogel system with different amounts of additional HMW HA (1.36 MDa, 0.5 and 1.0 wt.%) was double printed with PCL. Therefore two different print-heads were used: PH3 with an inner needle diameter of 0.25 mm for PCL extrusion and PH2 with an inner needle diameter of 0.33 mm for hydrogel precursor printing. PCL was heated in the connected reservoir up to 85 °C and printed with a print-head temperature of 93 °C. The printing parameters for PCL deposition were set as follows: 1.0 mm strand-to-strand distance, 17.5 revs/min extrusion speed, 3 bar extrusion pressure and 5 mm/s collector plate speed. The hybrid hydrogel precursor solution was printed with a dosing distance of 0.13 mm and a pressure of 0.5-1.0 bar depending on the amount of additional HA. For double printing alternate layers of PCL and precursor solution were printed with a layer height of 0.2 mm in a 12 mm x 12 mm square. First, a PCL was extruded and second hydrogel precursor solution was printed in between the PCL strands. The following layers were printed in the same manner, in a right angle with respect to the previous layer. After four layers, the hydrogel solution was cross-linked via UV light (bluepoint 4) for 8 s.

5.2.6.3 Cell printing

For cell printing, MSCs (6.0×10^6 MSC/mL) were added to the hybrid hydrogel precursor solution with additional 1 wt.% HA. The polymeric precursors were sterilized before being mixed with cells. Therefore, PG based polymers were sterile filtrated and HA based polymers were irradiated with UV light (254 nm) for 10 min. Printing was conducted with PH2 with an inner needle diameter of 0.33 mm and a pressure of 1 bar. The solution was extruded into cylindrical molds with a diameter of 6 mm and a height of 1 mm and cross-linked for 8 s with UV light (bluepoint 4). Cell viability analysis (Live/Dead assay on day 2 and 21) of cell printed constructs were realized by *Thomas Böck*[XVI].

5.2.6.4 PCL plug printing

PCL plugs for reinforced molded hydrogels were printed with PH3 (settings for PCL extrusion see double printing). Plugs of different sizes (h = 0.8-2 mm, Ø 4 or 6 mm) and strand-to-strand distances (1.00, 1.50 mm respectively) were produced depending on the application. Reinforced molded gels were used for *in vitro* and *in vivo* experiments of several cooperation partners. [XVII]

5.2.7 Statistical analyses

Statistical analyses were performed using SigmaPlot 12.5 software. For the comparison of multiple groups a one-way analysis of variance (ANOVA) with a Tukey post hoc test was conducted. Two groups were compared using students t-test. The significant differences are generally marked with *($p<0.05$), **($p<0.01$) and ***($p<0.001$).

[XVI] Department of Trauma, Hand, Plastic and Reconstructive Surgery, University of Würzburg.

[XVII] Thomas Böck and Oliver Berberich Department of Trauma, Hand, Plastic and Reconstructive Surgery, University of Würzburg;
Irina Mancini, Regenerative Medicine Utrecht, Utrecht University;
Elisabeth Seebach, Eliane Hesse, Yvonne Renz and Frederike Bothe, Research Centre for Experimental Orthopaedics, University Hospital Heidelberg.

5.3 Synthesis

5.3.1 Monomer synthesis

Ethoxy ethyl glycidyl ether (EEGE) (1)

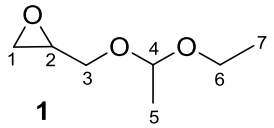

1

Synthesis adapted from literature.[141]

A mixture of glycidol (36.0 mL, 540 µmol) and ethyl vinyl ether (214 mL, 2.22 mol) was cooled down to 0°C in an ice bath. *p*TsOH (1.03 g, 5.40 mmol) was slowly added to the mixture without allowing temperature increase above 20 °C. The reaction mixture was stirred for 3 h at room temperature (RT) and afterwards washed with saturated $NaHCO_3$ solution (3 x 25 mL). The organic phase was dried with Na_2SO_4 and excess of ethyl vinyl ether was removed in vacuum. The raw product was purified via drying over CaH_2 for 3 d and distillation under reduced pressure (1 x 10^{-2} mbar, boiling point EEGE: 30 °C).

^{1}H-NMR (300 MHz, $CDCl_3$): δ = 4.78-4.70 (m, 1 H, *H*-4), 3.81-3.36 (m, 4 H, *H*-3,6), 3.13-3.12 (m, 1 H, *H*-2), 2.79-2.76 (m, 1 H, *H*-1), 2.63-2.57 (m, 1 H, *H*-1), 1.31-1.28 (m, 3 H, *H*-5), 1.20-1-15 (m, 3 H, *H*-7) ppm.

5.3.2 Polymer synthesis

5.3.2.1 Poly(ethoxy ethyl glycidyl ether) (P(EEGE)) (2)

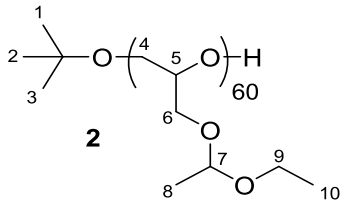

2

Synthesis adapted from literature.[26]

KO*t*Bu (1.00 mL, 1.00 mmol) and EEGE (**1**) (8.80 mL, 60.3 mmol) were mixed under argon atmosphere and heated up to 60 °C. The reaction mixture was stirred for 24 h at 60 °C and the polymerization was stopped by addition of EtOH (1.00 mL). The product (**2**) was dried under vacuum. The crude product **2** was used in the next step (**chapter 5.3.2.2**) without further purification.

^{1}H-NMR (300 MHz, $CDCl_3$): δ = 4.70-4.67 (m, 60 H, *H*-7), 3.73-3.41 (m, 420 H, *H*-4-6,9), 1.28-1.22 (m, 180 H, *H*-8), 1.20-1.16 (m, 197 H, *H*-10,1-3) ppm.

SEC (DMF): M_n: 1860 Da, M_w: 2030 Da, Đ: 1.09.

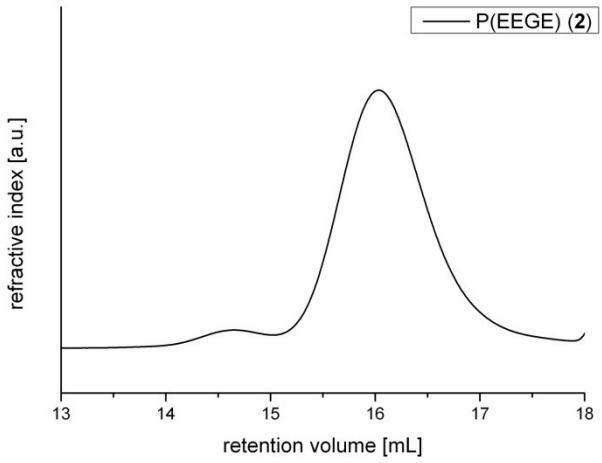

Figure 48: SEC elugram of P(EEGE) (**2**).

5.3.2.2 Poly(glycidol) (PG) (3)

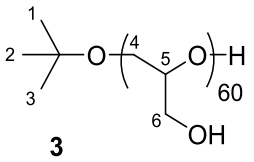

3

P(EEGE) (**2**) (4.27 g, 480 µmol) was dissolved in 250 mL THF and 9 mL HCl (32 %) was added dropwise. The mixture was stirred for 12 h at RT. After decantation of THF the remaining yellow oil was dissolved in water (Milli-Q) and dialysed (MW cut-off: 1000 g/mol) for 3 d. The product **3** was obtained as a light yellow oil after freeze-drying for 3 d.

^{1}H-NMR (300 MHz, D_2O): δ = 3.77-3.63 (m, 300 H, *H*-4-6), 1.22 (s, 5 H, *H*-1-3) ppm.

SEC (water, set1): M_n: 1870 Da, M_w: 3220 Da, Đ:1.73.

5.3.2.3 Poly(allyl glycidyl ether-*co*-ethoxy ethyl glycidyl ether) (P(AGE-*co*-EEGE)) (4)

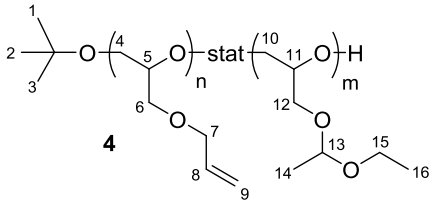

4

Synthesis was adapted from literature.[26]

General experimental procedure:

AGE and EEGE (**1**) were mixed with the initiator KO*t*Bu (1.00 mL, 1.00 mmol) under argon atmosphere. The mixture was heated up to 60 °C and stirred for 24 h. The anionic polymerization was stopped by addition of 1 mL EtOH. P(AGE-*co*-EEGE) (**4**) is dried under reduced pressure. Table 23 shows the used molar ratios of AGE and EEGE for **4a-c**. **4** was used in the next step (**chapter 5.3.2.4**) without further purification.

Table 23: Synthesis of P(AGE-*co*-EEGE) with different AGE-functionalities.

Number	AGE	EEGE	molar ratio AGE/EEGE
4a	500 µL, 4.21 mmol	11.1 mL, 75.9 mmol	1/18
4b	750 µL, 6.31 mmol	7.90 mL, 54.0 mmol	1/9
4c	1.50 mL, 12.6 mmol	7.90 mL, 54.0 mmol	1/4

Analysis **4a**

^{1}H-NMR (300 MHz, $CDCl_3$): δ = 5.94-5.81 (m, 4 H, *H*-8), 5.27-5.12 (m, 8 H, *H*-9), 4.71-4.66 (m, 57 H, *H*-13), 3.98-3.96 (m, 8 H, *H*-7), 3.66-3.42 (m, 424 H, *H*-4-6,10-12,15), 1.29-1.27 (m, 170 H, *H*-14), 1.20-1.16 (m, 185 H, *H*-16,1-3) ppm.

SEC (DMF): M_n: 2060 Da, M_w: 2260 Da, Đ: 1.10.

Analysis **4b**

^{1}H-NMR (300 MHz, $CDCl_3$): δ = 5.94-5.81 (m, 6 H, *H*-8), 5.28-5.13 (m, 12 H, *H*-9), 4.71 4.66 (m, 48 H, *H*-13), 3.98-3.97 (m, 12 H, *H*-7), 3.69-3.42 (m, 374 H, *H*-4-6,10-12,15), 1.29-1.27 (m, 145 H, *H*-14), 1.21-1.16 (m, 156 H, *H*-16,1-3) ppm.

SEC (DMF): M_n: 2420 Da, M_w: 2930 Da, Đ: 1.21.

Analysis **4c**

^{1}H-NMR (300 MHz, $CDCl_3$): δ = 5.94-5.84 (m, 12 H, *H*-8), 5.30-5.15 (m, 24 H, *H*-9), 4.74-4.69 (m, 48 H, *H*-13), 4.01-3.99 (m, 24 H, *H*-7), 3.77-3.45 (m, 450 H, *H*-4-6,10-12,15), 1.31-1.28 (m, 153 H, *H*-14), 1.20-1.16 (m, 162 H, *H*-16,1-3) ppm.

SEC (DMF): M_n: 2610 Da, M_w: 3150 Da, Đ: 1.21.

Table 24: Overview of allyl-functionality (^{1}H-NMR), M_n and Đ for P(AGE-*co*-EEGE) (**4**).

Number	AGE-functionality [%]	M_n [Da]	Đ
4a	7	2060	1.10
4b	11	2420	1.21
4c	20	2610	1.21

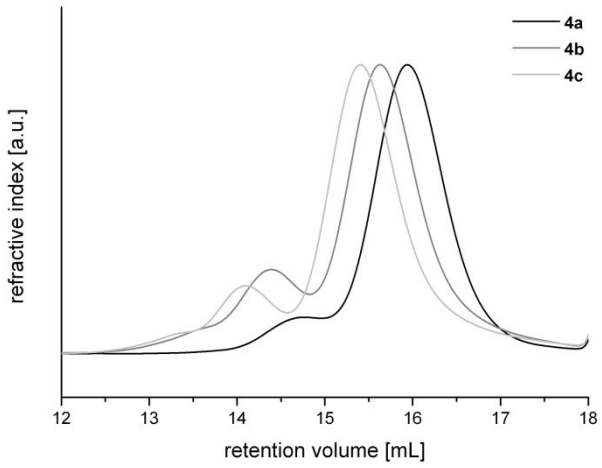

Figure 49: SEC elugrams of P(AGE-*co*-EEGE) (**4a-c**).

5.3.2.4 Poly(allyl glycidyl ether-*co*-glycidyl) (P(AGE-*co*-G)) (5)

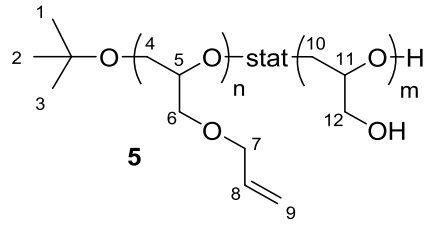

5

General experimental procedure:

The EEGE units of P(AGE-*co*-EEGE) (**4**) were deprotected to receive hydroxyl units. Therefore, P(AGE-*co*-EEGE) (**4**) was dissolved in THF (80 mL/g polymer) and HCl (2 mL/g polymer) was added dropwise to the solution. The reaction mixture was stirred for 4 h at RT and subsequently THF was decanted. The polymeric residue was dissolved in water (Milli-Q), dialyzed (MW cut-off: 1000 or 3500 g/mol) for 3 d and freeze-dried. P(AGE-*co*-G) (**5**) was received as a colourless oil.

FT-IR (ATR): = 3360 (-OH), 2920-2870 (-C-H, -CH_2), 1650 (-C=C-), 1040 (-C-O-C) cm^{-1}

Raman: = 2930-2880 (-CH_3, -CH_2), 1650 (-C=C-), 1460 (-CH_2-) cm^{-1}.

Analysis **5a**

^{1}H-NMR (300 MHz, D_2O): δ = 6.00-5.89 (m, 4 H, *H*-8), 5.37-5.26 (m, 8 H, *H*-9), 4.09-4.07 (m, 8 H, *H*-7), 3.77-3.66 (m, 281 H, *H*-4-6,10-12), 1.22 (s, 6 H, *H*-1-3) ppm.

SEC (water, setI): M_n: 2022 Da, M_w: 3451 Da, Đ: 1.71.

Analysis **5b**

^{1}H-NMR (300 MHz, D_2O): δ = 5.99-5.85 (m, 6 H, *H*-8), 5.34-5.22 (m, 12 H, *H*-9), 4.05-4.03 (m, 12 H, *H*-7), 3.77-3.60 (m, 280 H, *H*-4-6,10-12), 1.19 (s, 6 H, *H*-1-3) ppm.

SEC (water, setI): M_n: 2810 Da, M_w: 3450 Da, Đ: 1.23.

Analysis **5c**

^{1}H-NMR (300 MHz, D_2O):δ = 6.06-5.93 (m, 12 H, *H*-8), 5.41-5.29 (m, 24 H, *H*-9), 4.12-4.10 (m, 24 H, *H*-7), 3.80-3.66 (m, 296 H, *H*-4-6,10-12), 1.26 (s, 7 H, *H*-1-3) ppm.

SEC (water, setI): M_n: 1870 Da, M_w: 2580 Da, Đ: 1.38.

5.3.3 Thiol-functionalized PG (P(SH-*co*-G)) (6 and 7)

5.3.3.1 Ester-containing thiol-functionalized PG (PG-SH_{ec}) (6)

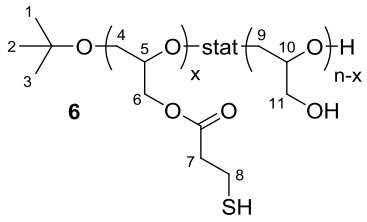

6

Reaction was adapted from literature.[147]

PG (**3**) (1.44 g, 320 µmol) was dissolved with DCC (123 mg, 600 µmol) and DMAP (68.0 mg, 0.56 mmol) in dry DMF (7 mL) and cooled down to 0 °C. Subsequently the disulfide cross-linker DTPA (53.0 mg, 250 µmol in 2 mL dry DMF) was added dropwise during ice bath cooling. The ice bath was removed and the reaction mixture stirred for 12 h at RT. The obtained gel-like oil was purified under reduced pressure. In a next step, the disulfide bonds were reduced with TCEP (108 mg, 380 µg; 1.5 eq with respect to disulfide units). The gel-like oil was then stirred with TCEP for 4 h at RT. The pH of the reaction mixture was adjusted with triethylamine to 6.5. Afterwards the raw product was purified via dialysis (1 d against water/HCl pH = 3.5, 1 d against water) and following freeze-drying. The ester-containing thiol-functionalized PG **6** was received as a yellow oil.

^{1}H-NMR (300 MHz, D_2O): δ = 4.46-4.28 (m, 20 H, *H*-6), 3.80-3.67 (m, 333 H, *H*-4-5,9-11), 2.82-2.81 (m, 42 H, *H*-7,8), 1.26 (m, 9 H, *H*-1-3) ppm.

SEC (water, setII, quenched): M_n: 1710 Da, M_w: 4221 Da, Đ: 2.47.

Raman: = 2940–2880 (-CH_2, -CH_3), 2570 (-SH), 1730 (-C=O), 1460 (-CH_2-) cm^{-1}.

5.3.3.2 Ester-free thiol-functionalized PG (PG-SH$_{ef}$) (7)

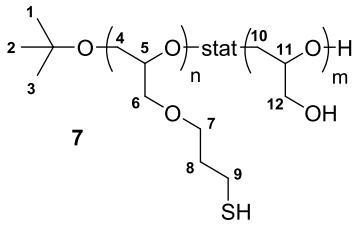

7

General experimental procedure:

P(AGE-*co*-G) (**5**) was dissolved in EtOH (140 mL/g polymer) and the solution was degassed with argon. Thioacetic acid (3.5 eq with respect to allyl groups) and DMPA (0.5 eq with respect to allyl groups) were added to the polymeric solution and stirred for 2 h at RT under UV irradiation (365 nm, UV LED cubes). Ethanol was removed under reduced pressure and the residual polymer was dissolved in water (Milli-Q) and precipitated in cold diethyl ether (1/10 polymer/diethyl ether). After removing the solvent, the polymer was dissolved in a 1 M sodium hydroxide solution. The reaction mixture was heated up to 100 °C and stirred for 2.5 h. Subsequently, the solution was cooled down to RT and neutralized with HCl. Next, TCEP (1.0-1.1 eq, with respect to allyl groups) was given to the mixture to reduce disulfides. After stirring for 12 h, the polymeric solution was dialyzed against water (3 d) and freeze-dried. Ester-free thiol-functionalized PG **7** was received as a light yellow oil.

Table 25: Synthesis of PG-SH$_{ef}$ (**7**) with different SH-functionalities.

Number	P(AGE-*co*-G)	Thioacetic acid	DMPA	TCEP
7a	1.16 g, 260 µmol	390 µL, 5.46 mmol	200 mg, 780 µmol	446 mg, 1.56 mmol
7b	1.45 g, 250 µmol	876 µL, 12.3 mmol	450 mg, 1.75 mmol	1.10 g, 3.83 mmol

Raman: = 2930–2880 (- CH_2, -CH_3), 2570 (SH-stretch), 1460 (-CH_2-) cm^{-1}.

Analysis **7a**

^{1}H-NMR (300 MHz, D_2O): δ = 3.78-3.61 (m, 324 H, *H*-4-7,10-12), 2.62-2.58 (m, 12 H, *H*-9), 1.89-1.84 (m, 12 H, *H*-8), 1.21 (s, 5 H, H-1-3) ppm.

SEC (water, setI): M_n: 1330 Da, M_w: 2740 Da, Đ: 2.06.

Analysis **7b**

^{1}H-NMR (300 MHz, D_2O): δ = 3.80-3.67 (m, 362 H, *H*-4-7,10-12), 2.68-2.64 (m, 24 H, *H*-9), 1.94-1.90 (m, 24 H, *H*-8), 1.26 (s, 8 H, H-1-3) ppm.

SEC (water, setI): M_n: 549 Da, M_w: 1260 Da, Đ: 2.92.

5.3.4 Peptide functionalized PG (P(peptide-*co*-G)) (8)

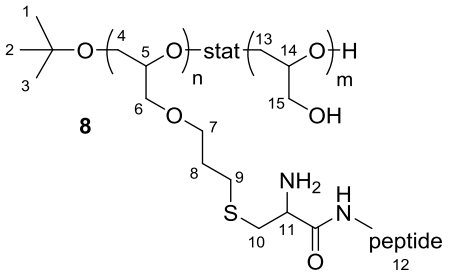

8

Table 26: Peptides used for peptide-functionalization of **5**.

Number	used peptide	peptide indication
8a	CGPRGQ-Orn-GVMGF-Orn	C-peptide1
8b	CGWYRGRL	C-peptide2
8c	RYPISRPRKRC	C-peptide3

General experimental procedure:

P(AGE-*co*-G) (**5b**) and C-peptide were dissolved in EtOH or H_2O/EtOH, respectively. The mixture was degassed with argon, the photoinitiator was added and the solution was stirred for 2 h at RT under UV irradiation (365 nm, UV LED cubes or UV hand lamp, respectively). Afterwards EtOH was removed under reduced pressure and the residual polymer was dissolved in H_2O, dialysed and freeze-dried.

Table 27: Synthesis of P(peptide-*co*-G) (**8**) with different peptides.

Number	P(AGE-*co*-G) **5b**	peptide	initiator	solvent
8a	18.0 mg, 3.78 µmol	*C-peptide1* 45.0 mg, 33.7 µmol	*DMPA* 4.00 mg, 15.6 µmol	*EtOH* 6 mL
8b	20.0 mg, 4.20 µmol	*C-peptide2* 38.0 mg, 37.8 µmol	*DMPA* 3.00 mg, 11.7 µmol	*EtOH* 6 mL
8c	150 mg 31.5 µmol	*C-peptide3* 405 mg, 284 µmol	*I2959* 21.0 mg, 94.5 µmol	*H_2O/EtOH* 90/30 mL

FT-IR (ATR): = 3500-3100 (-OH, -NH), 2900-2870 (-C-H, -CH_2), 1635 (-NH_2, -N-H), 1530 (-N-H), 1040 (-C-O-C-) cm^{-1}.

Analysis **8a**

^{1}H-NMR (300 MHz, D_2O): δ = 7.53-7.26 (m, *H*-12, aromatic peptide protons), 5.37-5.25 (m, 3 H, unreacted allyl protons of **5b**: *H*-9), 4.31-3.86 (m, *H*-12), 3.95-3.65 (m, 280 H, *H*-4-7, *H*-13-15), 3.26-0.80 (m, *H*-1-3, *H*-8-9, *H*-12) ppm.

Analysis **8b**

^{1}H-NMR (300 MHz, D_2O): δ = 7.59-6.75 (m, *H*-12, aromatic peptide protons), 5.39-5.25 (m, 3 H, unreacted allyl protons of **5b**: *H*-9), 4.31-3.91 (m, *H*-12), 3.71-3.65 (m, 280 H, *H*-4-7, *H*-13-15), 3.19-2.58 (m, *H*-9, *H*-12), 1.90-0.78 (m, *H*-1-3, *H*-8, *H*-12) ppm.

Analysis **8c**

^{1}H-NMR (300 MHz, D_2O): δ = 7.37-6.86 (m, *H*-12, aromatic peptide protons), 5.49-5.29 (m, 3 H, unreacted allyl protons of **5b**: *H*-9), 4.35-4.10 (m, *H*-12), 3.80-3.66 (m, 280 H, *H*-4-7, *H*-13-15), 3.24-2.96 (m, *H*-12), 2.07-1.50 (m, *H*-12), 1.26 (s, *H*-1-3), 0.98-0.90 (m, *H*-12) ppm.

References

1. Malda, J.; Visser, J.; Melchels, F. P.; Juengst, T.; Hennink, W. E.; Dhert, W. J. A.; Groll, J.; Hutmacher, D. W., 25th Anniversary Article: Engineering Hydrogels for Biofabrication. *Adv. Mater. (Weinheim, Ger.)* **2013**, *25*, 5011-5028.

2. Groll, J.; Boland, T.; Blunk, T.; Burdick, J. A.; Cho, D.-W.; Dalton, P. D.; Derby, B.; Forgacs, G.; Li, Q.; Mironov, V. A.; Moroni, L.; Nakamura, M.; Shu, W.; Takeuchi, S.; Vozzi, G.; Woodfield, T. B. F.; Xu, T.; Yoo, J. J.; Malda, J., Biofabrication: reappraising the definition of an evolving field. *Biofabrication* **2016**, *8*, 013001/1-013001/5.

3. Jungst, T.; Smolan, W.; Schacht, K.; Scheibel, T.; Groll, J., Strategies and Molecular Design Criteria for 3D Printable Hydrogels. *Chem. Rev. (Washington, DC, U. S.)* **2016**, *116*, 1496-1539.

4. Derby, B., Printing and Prototyping of Tissues and Scaffolds. *Science (Washington, DC, U. S.)* **2012**, *338*, 921-926.

5. Melchels, F. P. W.; Domingos, M. A. N.; Klein, T. J.; Malda, J.; Bartolo, P. J.; Hutmacher, D. W., Additive manufacturing of tissues and organs. *Prog. Polym. Sci.* **2012**, *37*, 1079-1104.

6. Murphy, S. V.; Atala, A., 3D bioprinting of tissues and organs. *Nat. Biotechnol.* **2014**, *32*, 773-785.

7. Chimene, D.; Lennox, K. K.; Kaunas, R. R.; Gaharwar, A. K.; Gaharwar, A. K.; Gaharwar, A. K., Advanced Bioinks for 3D Printing: A Materials Science Perspective. *Ann Biomed Eng* **2016**, *44*, 2090-102.

8. Hoelzl, K.; Lin, S.; Tytgat, L.; Van, V. S.; Gu, L.; Ovsianikov, A., Bioink properties before, during and after 3D bioprinting. *Biofabrication* **2016**, *8*, 032002/1-032002/19.

9. Billiet, T.; Vandenhaute, M.; Schelfhout, J.; Van Vlierberghe, S.; Dubruel, P., A review of trends and limitations in hydrogel-rapid prototyping for tissue engineering. *Biomaterials* **2012**, *33*, 6020-6041.

10. Klein, T. J.; Rizzi, S. C.; Reichert, J. C.; Georgi, N.; Malda, J.; Schuurman, W.; Crawford, R. W.; Hutmacher, D. W., Strategies for Zonal Cartilage Repair using Hydrogels. *Macromol. Biosci.* **2009**, *9*, 1049-1058.

11. Lee, K. Y.; Mooney, D. J., Hydrogels for Tissue Engineering. *Chem. Rev. (Washington, D. C.)* **2001**, *101*, 1869-1879.

12. Seliktar, D., Designing Cell-Compatible Hydrogels for Biomedical Applications. *Science (Washington, DC, U. S.)* **2012**, *336*, 1124-1128.

13. Zehnder, T.; Sarker, B.; Boccaccini, A. R.; Detsch, R., Evaluation of an alginate-gelatine crosslinked hydrogel for bioplotting. *Biofabrication* **2015**, *7*, 025001/1-025001/12.

14. Cohen, D. L.; Malone, E.; Lipson, H.; Bonassar, L. J., Direct Freeform Fabrication of Seeded Hydrogels in Arbitrary Geometries. *Tissue Eng.* **2006**, *12*, 1325-1335.

15. Melchels, F. P. W.; Dhert, W. J. A.; Hutmacher, D. W.; Malda, J., Development and characterisation of a new bioink for additive tissue manufacturing. *J. Mater. Chem. B* **2014**, *2*, 2282-2289.

16. Schuurman, W.; Levett, P. A.; Pot, M. W.; van Weeren, P. R.; Dhert, W. J. A.; Hutmacher, D. W.; Melchels, F. P. W.; Klein, T. J.; Malda, J., Gelatin-Methacrylamide Hydrogels as Potential Biomaterials for Fabrication of Tissue-Engineered Cartilage Constructs. *Macromol. Biosci.* **2013**, *13*, 551-561.

17. Billiet, T.; Gevaert, E.; De Schryver, T.; Cornelissen, M.; Dubruel, P., The 3D printing of gelatin methacrylamide cell-laden tissue-engineered constructs with high cell viability. *Biomaterials* **2014**, *35*, 49-62.

18. Burdick, J. A.; Prestwich, G. D., Hyaluronic Acid Hydrogels for Biomedical Applications. *Adv. Mater. (Weinheim, Ger.)* **2011**, *23*, H41-H56.

19. Owen, S. C.; Fisher, S. A.; Tam, R. Y.; Nimmo, C. M.; Shoichet, M. S., Hyaluronic Acid Click Hydrogels Emulate the Extracellular Matrix. *Langmuir* **2013**, *29*, 7393-7400.

20. Leach, J. B.; Bivens, K. A.; Patrick, C. W., Jr.; Schmidt, C. E., Photocrosslinked hyaluronic acid hydrogels: Natural, biodegradable tissue engineering scaffolds. *Biotechnol. Bioeng.* **2003**, *82*, 578-589.

21. Burdick, J. A.; Chung, C.; Jia, X.; Randolph, M. A.; Langer, R., Controlled Degradation and Mechanical Behavior of Photopolymerized Hyaluronic Acid Networks. *Biomacromolecules* **2005**, *6*, 386-391.

22. Aimetti, A. A.; Machen, A. J.; Anseth, K. S., Poly(ethylene glycol) hydrogels formed by thiol-ene photopolymerization for enzyme-responsive protein delivery. *Biomaterials* **2009**, *30*, 6048-6054.

23. Daly, A. C.; Critchley, S. E.; Rencsok, E. M.; Kelly, D. J., A comparison of different bioinks for 3D bioprinting of fibrocartilage and hyaline cartilage. *Biofabrication* **2016**, *8*, 045002.

24. Dworak, A.; Slomkowski, S.; Basinska, T.; Gosecka, M.; Walach, W.; Trzebicka, B., Polyglycidol - how is it synthesized and what is it used for? *Polimery (Warsaw, Pol.)* **2013**, *58*, 641-649.

25. Thomas, A.; Mueller, S. S.; Frey, H., Beyond Poly(ethylene glycol): Linear Polyglycerol as a Multifunctional Polyether for Biomedical and Pharmaceutical Applications. *Biomacromolecules* **2014**, *15,* 1935-1954.

26. Erberich, M.; Keul, H.; Moeller, M., Polyglycidols with Two Orthogonal Protective Groups: Preparation, Selective Deprotection, and Functionalization. *Macromolecules (Washington, DC, U. S.)* **2007**, *40*, 3070-3079.

27. Ulrich Meyer, T. M., Jörg Handschel, Hans Peter Wiesmann, Fundamentals of Tissue Engineering and Regenerative Medicine, Springer-Verlag Berlin Heidelberg, ISBN: 978-3-540-77754-0. 2009.

28. Zhu, J.; Marchant, R. E., Design properties of hydrogel tissue-engineering scaffolds. *Expert Rev. Med. Devices* **2011**, *8*, 607-626.

29. Pereira, R. F.; Bartolo, P. J., 3D bioprinting of photocrosslinkable hydrogel constructs. *J. Appl. Polym. Sci.* **2015**, *132*, n/a.

30. Nguyen, K. T.; West, J. L., Photopolymerizable hydrogels for tissue engineering applications. *Biomaterials* **2002**, *23*, 4307-4314.

31. Pescosolido, L.; Schuurman, W.; Malda, J.; Matricardi, P.; Alhaique, F.; Coviello, T.; van Weeren, P. R.; Dhert, W. J. A.; Hennink, W. E.; Vermonden, T., Hyaluronic Acid and Dextran-Based Semi-IPN Hydrogels as Biomaterials for Bioprinting. *Biomacromolecules* **2011**, *12*, 1831-1838.

32. Skardal, A.; Zhang, J.; McCoard, L.; Xu, X.; Oottamasathien, S.; Prestwich, G. D., Photocrosslinkable hyaluronan-gelatin hydrogels for two-step bioprinting. *Tissue Eng., Part A* **2010**, *16*, 2675-2685.

33. Klotz, B. J.; Gawlitta, D.; Rosenberg, A. J. W. P.; Malda, J.; Melchels, F. P. W., Gelatin-Methacryloyl Hydrogels: Towards Biofabrication-Based Tissue Repair. *Trends Biotechnol.* **2016**, *34*, 394-407.

34. Pereira, R. F.; Bártolo, P. J., 3D Photo-Fabrication for Tissue Engineering and Drug Delivery. *Engineering* **2015**, *1*, 090-112.

35. Dababneh, A. B.; Ozbolat, I. T., Bioprinting Technology: A Current State-of-the-Art Review. *Journal of Manufacturing Science and Engineering* **2014**, *136*, 061016-061016-11.

36. Calvert, P., Inkjet Printing for Materials and Devices. *Chem. Mater.* **2001**, *13*, 3299-3305.

37. Guillemot, F.; Souquet, A.; Catros, S.; Guillotin, B.; Lopez, J.; Faucon, M.; Pippenger, B.; Bareille, R.; Remy, M.; Bellance, S.; Chabassier, P.; Fricain, J. C.; Amedee, J., High-throughput laser printing of cells and biomaterials for tissue engineering. *Acta Biomater.* **2010**, *6*, 2494-2500.

38. Kim, J. D.; Choi, J. S.; Kim, B. S.; Choi, Y. C.; Cho, Y. W., Piezoelectric inkjet printing of polymers: Stem cell patterning on polymer substrates. *Polymer* **2010**, *51*, 2147-2154.

39. Chang, C. C.; Boland, E. D.; Williams, S. K.; Hoying, J. B., Direct-write bioprinting three-dimensional biohybrid systems for future regenerative therapies. *J. Biomed. Mater. Res., Part B* **2011**, *98B*, 160-170.

40. Guillotin, B.; Guillemot, F., Cell patterning technologies for organotypic tissue fabrication. *Trends Biotechnol.* **2011**, *29*, 183-190.

41. Wust, S.; Muller, R.; Hofmann, S., Controlled Positioning of Cells in Biomaterials-Approaches Towards 3D Tissue Printing. *J Funct Biomater* **2011**, *2*, 119-54.

42. Campbell, P. G.; Miller, E. D.; Fisher, G. W.; Walker, L. M.; Weiss, L. E., Engineered spatial patterns of FGF-2 immobilized on fibrin direct cell organization. *Biomaterials* **2005**, *26*, 6762-6770.

43. Khalil, S.; Nam J.; Sun W., Multi-nozzle deposition for construction of 3D biopolymer tissue scaffolds. *Rapid Prototyping Journal* **2005**, *11*, 9-17.

44. Smith, C. M.; Stone, A. L.; Parkhill, R. L.; Stewart, R. L.; Simpkins, M. W.; Kachurin, A. M.; Warren, W. L.; Williams, S. K., Three-Dimensional BioAssembly Tool for Generating Viable Tissue-Engineered Constructs. *Tissue Eng.* **2004**, *10,* 1566-1576.

45. Madou, M. J., *Fundamentals of Microfabrication: The Science of Miniaturization, Second Edition*. CRC Press: Boca Raton, FL: **2002**.

46. Sobral, J. M.; Caridade, S. G.; Sousa, R. A.; Mano, J. F.; Reis, R. L., Three-dimensional plotted scaffolds with controlled pore size gradients: Effect of scaffold geometry on mechanical performance and cell seeding efficiency. *Acta Biomater.* **2011**, *7,* 1009-1018.

47. Stichler, S.; Bertlein, S.; Tessmar, J.; Juengst, T.; Groll, J., Thiol-ene Cross-Linkable Hydrogels as Bioinks for Biofabrication. *Macromol. Symp.* **2017**, *372*, 102-107.

48. Aguado, B. A.; Mulyasasmita, W.; Su, J.; Lampe, K. J.; Heilshorn, S. C., Improving Viability of Stem Cells During Syringe Needle Flow Through the Design of Hydrogel Cell Carriers. *Tissue Eng., Part A* **2012**, *18*, 806-815.

49. Park, Y.; Lutolf, M. P.; Hubbell, J. A.; Hunziker, E. B.; Wong, M., Bovine Primary Chondrocyte Culture in Synthetic Matrix Metalloproteinase-Sensitive Poly(ethylene glycol)-Based Hydrogels as a Scaffold for Cartilage Repair. *Tissue Eng.* **2004**, *10*, 515-522.

50. Bryant, S. J.; Chowdhury, T. T.; Lee, D. A.; Bader, D. L.; Anseth, K. S., Crosslinking density influences chondrocyte metabolism in dynamically loaded photocrosslinked poly(ethylene glycol) hydrogels. *Ann Biomed Eng* **2004**, *32*, 407-17.

51. Guvendiren, M.; Lu, H. D.; Burdick, J. A., Shear-thinning hydrogels for biomedical applications. *Soft Matter* **2012**, *8*, 260-272.

52. Rezende, R. A.; Bartolo, P. J.; Mendes, A.; Maciel Filho, R., Rheological behavior of alginate solutions for biomanufacturing. *J. Appl. Polym. Sci.* **2009**, *113*, 3866-3871.

53. Mouser, V. H. M.; Melchels, F. P. W.; Visser, J.; Dhert, W. J. A.; Gawlitta, D.; Malda, J., Yield stress determines bioprintability of hydrogels based on gelatin-methacryloyl and gellan gum for cartilage bioprinting. *Biofabrication* **2016**, *8*, 035003/1-035003/13.

54. Paxton, N. C.; Smolan, W.; Bock, T.; Melchels, F. P. W.; Groll, J.; Juengst, T., Proposal to Assess Printability of Bioinks for Extrusion-Based Bioprinting and Evaluation of Rheological Properties Governing Bioprintability. *Biofabrication* **2017**, doi: 10.1088/1758-5090/aa8dd8.

55. Suri, S.; Schmidt, C. E., Photopatterned collagen-hyaluronic acid interpenetrating polymer network hydrogels. *Acta Biomater.* **2009**, *5*, 2385-2397.

56. Myung, D.; Koh, W.; Ko, J.; Hu, Y.; Carrasco, M.; Noolandi, J.; Ta, C. N.; Frank, C. W., Biomimetic strain hardening in interpenetrating polymer network hydrogels. *Polymer* **2007**, *48*, 5376-5387.

57. Hong, S.; Sycks, D.; Chan, H. F.; Lin, S.; Lopez, G. P.; Guilak, F.; Leong, K. W.; Zhao, X., 3D Printing of Highly Stretchable and Tough Hydrogels into Complex, Cellularized Structures. *Adv. Mater. (Weinheim, Ger.)* **2015**, *27*, 4035-4040.

58. Shin, H.; Olsen, B. D.; Khademhosseini, A., The mechanical properties and cytotoxicity of cell-laden double-network hydrogels based on photocrosslinkable gelatin and gellan gum biomacromolecules. *Biomaterials* **2012**, *33*, 3143-3152.

59. Chen, Q.; Chen, H.; Zhu, L.; Zheng, J., Fundamentals of double network hydrogels. *J. Mater. Chem. B* **2015**, *3*, 3654-3676.

60. Haque, M. A.; Kurokawa, T.; Gong, J. P., Super tough double network hydrogels and their application as biomaterials. *Polymer* **2012**, *53*, 1805-1822.

61. Schuurman, W.; Khristov, V.; Pot, M. W.; van Weeren, P. R.; Dhert, W. J. A.; Malda, J., Bioprinting of hybrid tissue constructs with tailorable mechanical properties. *Biofabrication* **2011**, *3*, 021001/1-021001/7.

62. Kundu, J.; Shim, J.-H.; Jang, J.; Kim, S.-W.; Cho, D.-W., An additive manufacturing-based PCL-alginate-chondrocyte bioprinted scaffold for cartilage tissue engineering. *J. Tissue Eng. Regener. Med.* **2015**, *9*, 1286-1297.

63. Visser, J.; Peters, B.; Burger, T. J.; Boomstra, J.; Dhert, W. J. A.; Melchels, F. P. W.; Malda, J., Biofabrication of multi-material anatomically shaped tissue constructs. *Biofabrication* **2013**, *5*, 035007/1-035007/9.

64. Thiele, J.; Ma, Y.; Bruekers, S. M. C.; Ma, S.; Huck, W. T. S., 25th Anniversary Article: Designer Hydrogels for Cell Cultures: A Materials Selection Guide. *Adv. Mater. (Weinheim, Ger.)* **2014**, *26*, 125-148.

65. Rice, J. J.; Martino, M. M.; De Laporte, L.; Tortelli, F.; Briquez, P. S.; Hubbell, J. A., Engineering the Regenerative Microenvironment with Biomaterials. *Adv. Healthcare Mater.* **2013**, *2*, 57-71.

66. Maia, F. R.; Fonseca, K. B.; Rodrigues, G.; Granja, P. L.; Barrias, C. C., Matrix-driven formation of mesenchymal stem cell-extracellular matrix microtissues on soft alginate hydrogels. *Acta Biomater.* **2014**, *10*, 3197-3208.

67. Fonseca, K. B.; Granja, P. L.; Barrias, C. C., Engineering proteolytically-degradable artificial extracellular matrices. *Prog. Polym. Sci.* **2014**, *39*, 2010-2029.

68. Lutolf, M. P.; Weber, F. E.; Schmoekel, H. G.; Schense, J. C.; Kohler, T.; Mueller, R.; Hubbell, J. A., Repair of bone defects using synthetic mimetics of collagenous extracellular matrices. *Nat. Biotechnol.* **2003**, *21*, 513-518.

69. Ehrbar, M.; Rizzi, S. C.; Hlushchuk, R.; Djonov, V.; Zisch, A. H.; Hubbell, J. A.; Weber, F. E.; Lutolf, M. P., Enzymatic formation of modular cell-instructive fibrin analogs for tissue engineering. *Biomaterials* **2007**, *28*, 3856-3866.

70. Zisch, A. H.; Lutolf, M. P.; Ehrbar, M.; Raeber, G. P.; Rizzi, S. C.; Davies, N.; Schmoekel, H.; Bezuidenhout, D.; Djonov, V.; Zilla, P.; Hubbell, J. A., Cell-demanded release of VEGF from synthetic, biointeractive cell-ingrowth matrices for vascularized tissue growth. *FASEB J.* **2003**, *17*, 2260-2262, 10.1096/fj.02-1041fje.

71. Liu, S. Q.; Tian, Q.; Wang, L.; Hedrick, J. L.; Hui, J. H. P.; Yang, Y. Y.; Ee, P. L. R., Injectable Biodegradable Poly(ethylene glycol)/RGD Peptide Hybrid Hydrogels for in vitro Chondrogenesis of Human Mesenchymal Stem Cells. *Macromol. Rapid Commun.* **2010**, *31*, 1148-1154.

72. Mauck, R. L.; Wang, C. C. B.; Oswald, E. S.; Ateshian, G. A.; Hung, C. T., The role of cell seeding density and nutrient supply for articular cartilage tissue engineering with deformational loading. *Osteoarthritis and Cartilage* **2003**, *11,* 879-890.

73. Buckley, C. T.; Thorpe, S. D.; O'Brien, F. J.; Robinson, A. J.; Kelly, D. J., The effect of concentration, thermal history and cell seeding density on the initial mechanical properties of agarose hydrogels. *Journal of the Mechanical Behavior of Biomedical Materials* **2009**, *2*, 512-521.

74. Chang, S. C. N.; Rowley, J. A.; Tobias, G.; Genes, N. G.; Roy, A. K.; Mooney, D. J.; Vacanti, C. A.; Bonassar, L. J., Injection molding of chondrocyte/alginate constructs in the shape of facial implants. *J. Biomed. Mater. Res.* **2001**, *55*, 503-511.

75. Guilak, F.; Mow, V. C., The mechanical environment of the chondrocyte: a biphasic finite element model of cell-matrix interactions in articular cartilage. *J Biomech* **2000**, *33,* 1663-73.

76. Yan, K. C.; Nair, K.; Sun, W., Three dimensional multi-scale modelling and analysis of cell damage in cell-encapsulated alginate constructs. *J Biomech* **2010**, *43*, 1031-8.

77. Blaeser, A.; Duarte Campos, D. F.; Puster, U.; Richtering, W.; Stevens, M. M.; Fischer, H., Controlling Shear Stress in 3D Bioprinting is a Key Factor to Balance Printing Resolution and Stem Cell Integrity. *Adv. Healthcare Mater.* **2016**, *5*, 326-333.

78. Buenger, D.; Topuz, F.; Groll, J., Hydrogels in sensing applications. *Prog. Polym. Sci.* **2012**, *37*, 1678-1719.

79. Oyen, M. L., Mechanical characterisation of hydrogel materials. *Int. Mater. Rev.* **2014**, *59*, 44-59.

80. Anseth, K. S.; Bowman, C. N.; Brannon-Peppas, L., Mechanical properties of hydrogels and their experimental determination. *Biomaterials* **1996**, *17*, 1647-1657.

81. Galli, M.; Comley, K. S. C.; Shean, T. A. V.; Oyen, M. L., Viscoelastic and poroelastic mechanical characterization of hydrated gels. *J. Mater. Res.* **2009**, *24*, 973-979.

82. Normand, V.; Lootens, D. L.; Amici, E.; Plucknett, K. P.; Aymard, P., New insight into agarose gel mechanical properties. *Biomacromolecules* **2000**, *1*, 730-738.

83. Flory, P. J., Statistical mechanics of swelling of network structures. *J. Chem. Phys.* **1950**, *18*, 108-11.

84. Flory, P. J.; Rehner, J., Jr., Statistical mechanics of cross-linked polymer networks. II. Swelling. *J. Chem. Phys.* **194**3, *11*, 521-6.

85. Schacht, K.; Juengst, T.; Schweinlin, M.; Ewald, A.; Groll, J.; Scheibel, T., Biofabrication of Cell-Loaded 3D Spider Silk Constructs. *Angew. Chem., Int. Ed.* **2015**, *54*, 2816-2820.

86. Cohen, D. L.; Lo, W.; Tsavaris, A.; Peng, D.; Lipson, H.; Bonassar, L. J., Increased Mixing Improves Hydrogel Homogeneity and Quality of Three-Dimensional Printed Constructs. *Tissue Eng., Part C* **2011**, *17*, 239-248.

87. Fedorovich, N. E.; De Wijn, J. R.; Verbout, A. J.; Alblas, J.; Dhert, W. J. A., Three-Dimensional Fiber Deposition of Cell-Laden, Viable, Patterned Constructs for Bone Tissue Printing. *Tissue Eng., Part A* **2008**, *14*, 127-133.

88. Tirella, A.; Orsini, A.; Vozzi, G.; Ahluwalia, A., A phase diagram for microfabrication of geometrically controlled hydrogel scaffolds. *Biofabrication* **2009**, *1*, 045002/1-045002/12.

89. Fedorovich, N. E.; Schuurman, W.; Wijnberg, H. M.; Prins, H.-J.; van Weeren, P. R.; Malda, J.; Alblas, J.; Dhert, W. J. A., Biofabrication of Osteochondral Tissue Equivalents by Printing Topologically Defined, Cell-Laden Hydrogel Scaffolds. *Tissue Eng., Part C* **2012**, *18*, 33-44.

90. Cohen, D. L.; Lipton, J. I.; Bonassar, L. J.; Lipson, H., Additive manufacturing for in situ repair of osteochondral defects. *Biofabrication* **2010**, *2*, 035004/1-035004/12.

91. Shim, J.-H.; Lee, J.-S.; Kim, J. Y.; Cho, D.-W., Bioprinting of a mechanically enhanced three-dimensional dual cell-laden construct for osteochondral tissue engineering using a multi-head tissue/organ building system. *J. Micromech. Microeng.* **2012**, *22*, 085014/1-085014/11.

92. Song, S.-J.; Choi, J.; Park, Y.-D.; Hong, S.; Lee, J. J.; Ahn, C. B.; Choi, H.; Sun, K., Sodium alginate hydrogel-based bioprinting using a novel multinozzle bioprinting system. *Artif Organs* **2011**, *35*, 1132-6.

93. Zhang, Y.; Yu, Y.; Chen, H.; Ozbolat, I. T., Characterization of printable cellular micro-fluidic channels for tissue engineering. *Biofabrication* **2013**, *5*, 025004/1-025004/11.

94. Arimura, H.; Ouchi, T.; Kishida, A.; Ohya, Y., Preparation of a hyaluronic acid hydrogel through polyion complex formation using cationic polylactide-based microspheres as a biodegradable cross-linking agent. *J. Biomater. Sci., Polym. Ed.* **2005**, *16*, 1347-1358.

95. Cross, D.; Jiang, X.; Ji, W.; Han, W.; Wang, C., Injectable Hybrid Hydrogels of Hyaluronic Acid Crosslinked by Well-Defined Synthetic Polycations: Preparation and Characterization In Vitro and In Vivo. *Macromol. Biosci.* **2015**, *15*, 668-681.

96. Kuehbeck, D.; Mayr, J.; Haering, M.; Hofmann, M.; Quignard, F.; Diaz Diaz, D., Evaluation of the nitroaldol reaction in the presence of metal ion-crosslinked alginates. *New J. Chem.* **2015**, *39*, 2306-2315.

97. Lutolf, M. P.; Hubbell, J. A., Synthesis and Physicochemical Characterization of End-Linked Poly(ethylene glycol)-co-peptide Hydrogels Formed by Michael-Type Addition. *Biomacromolecules* **2003**, *4*, 713-722.

98. Jin, R.; Teixeira, L. S. M.; Krouwels, A.; Dijkstra, P. J.; van Blitterswijk, C. A.; Karperien, M.; Feijen, J., Synthesis and characterization of hyaluronic acid-poly(ethylene glycol) hydrogels via Michael addition: an injectable biomaterial for cartilage repair. *Acta Biomater.* **2010**, *6*, 1968-1977.

99. Boere, K. W. M.; Soliman, B. G.; Rijkers, D. T. S.; Hennink, W. E.; Vermonden, T., Thermoresponsive Injectable Hydrogels Cross-Linked by Native Chemical Ligation. *Macromolecules (Washington, DC, U. S.)* **2014**, *47*, 2430-2438.

100. Hu, B.-H.; Su, J.; Messersmith, P. B., Hydrogels Cross-Linked by Native Chemical Ligation. *Biomacromolecules* **2009**, *10*, 2194-2200.

101. Takahashi, A.; Suzuki, Y.; Suhara, T.; Omichi, K.; Shimizu, A.; Hasegawa, K.; Kokudo, N.; Ohta, S.; Ito, T., In Situ Cross-Linkable Hydrogel of Hyaluronan Produced via Copper-Free Click Chemistry. *Biomacromolecules* **2013**, *14*, 3581-3588.

102. Crescenzi, V.; Cornelio, L.; Di Meo, C.; Nardecchia, S.; Lamanna, R., Novel Hydrogels via Click Chemistry: Synthesis and Potential Biomedical Applications. *Biomacromolecules* **2007**, *8*, 1844-1850.

103. Tibbitt, M. W.; Kloxin, A. M.; Sawicki, L. A.; Anseth, K. S., Mechanical Properties and Degradation of Chain and Step-Polymerized Photodegradable Hydrogels. *Macromolecules (Washington, DC, U. S.)* **2013**, *46*, 2785-2792.

104. Toepke, M. W.; Impellitteri, N. A.; Theisen, J. M.; Murphy, W. L., Characterization of Thiol-Ene Crosslinked PEG Hydrogels. *Macromol. Mater. Eng.* **2013**, *298*, 699-703.

105. Gramlich, W. M.; Kim, I. L.; Burdick, J. A., Synthesis and orthogonal photopatterning of hyaluronic acid hydrogels with thiol-norbornene chemistry. *Biomaterials* **2013**, *34*, 9803-9811.

106. Hoyle, C. E.; Bowman, C. N., Thiol-Ene Click Chemistry. *Angew. Chem., Int. Ed.* **2010**, *49*, 1540-1573.

107. Roberts, J. J.; Bryant, S. J., Comparison of photopolymerizable thiol-ene PEG and acrylate-based PEG hydrogels for cartilage development. *Biomaterials* **2013**, *34*, 9969-9979.

108. Williams, C. G.; Malik, A. N.; Kim, T. K.; Manson, P. N.; Elisseeff, J. H., Variable cytocompatibility of six cell lines with photoinitiators used for polymerizing hydrogels and cell encapsulation. *Biomaterials* **2005**, *26*, 1211-8.

109. Mironi-Harpaz, I.; Wang, D. Y.; Venkatraman, S.; Seliktar, D., Photopolymerization of cell-encapsulating hydrogels: Crosslinking efficiency versus cytotoxicity. *Acta Biomater.* **2012**, *8*, 1838-1848.

110. Fedorovich, N. E.; Oudshoorn, M. H.; van Geemen, D.; Hennink, W. E.; Alblas, J.; Dhert, W. J. A., The effect of photopolymerization on stem cells embedded in hydrogels. *Biomaterials* **2008**, *30*, 344-353.

111. Wong, D. Y.; Ranganath, T.; Kasko, A. M., Low-Dose, Long-Wave UV Light Does Not Affect Gene Expression of Human Mesenchymal Stem Cells. *PLOS ONE* **2015**, *10*, e0139307.

112. Rouillard, A. D.; Berglund, C. M.; Lee, J. Y.; Polacheck, W. J.; Tsui, Y.; Bonassar, L. J.; Kirby, B. J., Methods for Photocrosslinking Alginate Hydrogel Scaffolds with High Cell Viability. *Tissue Eng., Part C* 2011, 17, 173-179.

113. Fairbanks, B. D.; Schwartz, M. P.; Bowman, C. N.; Anseth, K. S., Photoinitiated polymerization of PEG-diacrylate with lithium phenyl-2,4,6-trimethylbenzoylphosphinate: polymerization rate and cytocompatibility. *Biomaterials* **2009**, *30*, 6702-6707.

114. Hu, J.; Hou, Y.; Park, H.; Choi, B.; Hou, S.; Chung, A.; Lee, M., Visible light crosslinkable chitosan hydrogels for tissue engineering. *Acta Biomater.* **2012**, *8*, 1730-1738.

115. Jeon, O.; Powell, C.; Solorio, L. D.; Krebs, M. D.; Alsberg, E., Affinity-based growth factor delivery using biodegradable, photocrosslinked heparin-alginate hydrogels. *J. Controlled Release* **2011**, *154*, 258-266.

116. Sahoo, S.; Chung, C.; Khetan, S.; Burdick, J. A., Hydrolytically Degradable Hyaluronic Acid Hydrogels with Controlled Temporal Structures. *Biomacromolecules* **2008**, *9,* 1088-1092.

117. Fairbanks, B. D.; Schwartz, M. P.; Halevi, A. E.; Nuttelman, C. R.; Bowman, C. N.; Anseth, K. S., A Versatile Synthetic Extracellular Matrix Mimic via Thiol-Norbornene Photopolymerization. *Adv. Mater. (Weinheim, Ger.)* **2009**, *21*, 5005-5010.

118. Munoz, Z.; Shih, H.; Lin, C.-C., Gelatin hydrogels formed by orthogonal thiol-norbornene photochemistry for cell encapsulation. *Biomater. Sci.* **2014**, *2*, 1063-1072.

119. Bertassoni, L. E.; Cardoso, J. C.; Manoharan, V.; Cristino, A. L.; Bhise, N. S.; Araujo, W. A.; Zorlutuna, P.; Vrana, N. E.; Ghaemmaghami, A. M.; Dokmeci, M. R.; Khademhosseini, A., Direct-write bioprinting of cell-laden methacrylated gelatin hydrogels. *Biofabrication* **2014**, *6*, 24105/1-24105/11, 11.

120. Yan, Y.; Wang, X.; Pan, Y.; Liu, H.; Cheng, J.; Xiong, Z.; Lin, F.; Wu, R.; Zhang, R.; Lu, Q., Fabrication of viable tissue-engineered constructs with 3D cell-assembly technique. *Biomaterials* **2005**, *26*, 5864-5871.

121. Collins, M. N.; Birkinshaw, C., Hyaluronic acid based scaffolds for tissue engineering—A review. *Carbohydrate Polymers* **2013**, *92*, 1262-1279.

122. Shu, X. Z.; Liu, Y.; Luo, Y.; Roberts, M. C.; Prestwich, G. D., Disulfide Cross-Linked Hyaluronan Hydrogels. *Biomacromolecules* **2002**, *3*, 1304-1311.

123. Dahlmann, J.; Krause, A.; Möller, L.; Kensah, G.; Möwes, M.; Diekmann, A.; Martin, U.; Kirschning, A.; Gruh, I.; Dräger, G., Fully defined in situ cross-linkable alginate and hyaluronic acid hydrogels for myocardial tissue engineering. *Biomaterials* **2013**, *34*, 940-951.

124. Dhanasingh, A.; Salber, J.; Moeller, M.; Groll, J., Tailored hyaluronic acid hydrogels through hydrophilic prepolymer cross-linkers. *Soft Matter* **2010**, *6*, 618-629.

125. Duan, B.; Kapetanovic, E.; Hockaday, L. A.; Butcher, J. T., Three-dimensional printed trileaflet valve conduits using biological hydrogels and human valve interstitial cells. *Acta Biomaterialia* **2014**, *10*, 1836-1846.

126. Zhu, J., Bioactive modification of poly(ethylene glycol) hydrogels for tissue engineering. *Biomaterials* **2010**, *31*, 4639-4656.

127. Lutolf, M. P.; Hubbell, J. A., Synthetic biomaterials as instructive extracellular microenvironments for morphogenesis in tissue engineering. *Nat. Biotechnol.* **2005**, *23*, 47-55.

128. Abbadessa, A.; Mouser, V. H. M.; Blokzijl, M. M.; Gawlitta, D.; Dhert, W. J. A.; Hennink, W. E.; Malda, J.; Vermonden, T., A Synthetic Thermosensitive Hydrogel for Cartilage Bioprinting and Its Biofunctionalization with Polysaccharides. *Biomacromolecules* **2016**, *17*, 2137-2147.

129. Alcantar, N. A.; Aydil, E. S.; Israelachvili, J. N., Polyethylene glycol-coated biocompatible surfaces. *J. Biomed. Mater. Res.* **2000**, *51*, 343-351.

130. Beamish, J. A.; Zhu, J.; Kottke-Marchant, K.; Marchant, R. E., The effects of monoacrylated poly(ethylene glycol) on the properties of poly(ethylene glycol) diacrylate hydrogels used for tissue engineering. *J. Biomed. Mater. Res., Part A* **2010**, *92A*, 441-450.

131. Yom-Tov, O.; Seliktar, D.; Bianco-Peled, H., PEG-Thiol based hydrogels with controllable properties. *Eur. Polym. J.* **2016**, *74*, 1-12.

132. Ju, H.; McCloskey, B. D.; Sagle, A. C.; Kusuma, V. A.; Freeman, B. D., Preparation and characterization of crosslinked poly(ethylene glycol) diacrylate hydrogels as fouling-resistant membrane coating materials. *Journal of Membrane Science* **2009**, *330*, 180-188.

133. DeForest, C. A.; Polizzotti, B. D.; Anseth, K. S., Sequential click reactions for synthesizing and patterning three-dimensional cell microenvironments. *Nat Mater* **2009**, *8*, 659-64.

134. P.S., M.; R.P., K.; K., D.; R.E., M.; J.Z., P., Construction of 3D biological matrices using rapid prototyping technology. *Rapid Prototyping Journal* **2009**, *15*, 204-210.

135. Hockaday, L. A.; Kang, K. H.; Colangelo, N. W.; Cheung, P. Y. C.; Duan, B.; Malone, E.; Wu, J.; Girardi, L. N.; Bonassar, L. J.; Lipson, H.; Chu, C. C.; Butcher, J. T., Rapid 3D printing of anatomically accurate and mechanically heterogeneous aortic valve hydrogel scaffolds. *Biofabrication* **2012**, *4*, 035005/1-035005/12.

136. Gao, G.; Yonezawa, T.; Hubbell, K.; Dai, G.; Cui, X., Inkjet-bioprinted acrylated peptides and PEG hydrogel with human mesenchymal stem cells promote robust bone and cartilage formation with minimal printhead clogging. *Biotechnol. J.* **2015**, *10*, 1568-1577.

137. Cui, X.; Breitenkamp, K.; Finn, M. G.; Lotz, M.; D'Lima, D. D., Direct Human Cartilage Repair Using Three-Dimensional Bioprinting Technology. *Tissue Eng., Part A* **2012**, *18*, 1304-1312.

138. Imran ul-haq, M.; Lai, B. F. L.; Chapanian, R.; Kizhakkedathu, J. N., Influence of architecture of high molecular weight linear and branched polyglycerols on their biocompatibility and biodistribution. *Biomaterials* **2012**, *33*, 9135-9147.

139. Kainthan, R. K.; Janzen, J.; Levin, E.; Devine, D. V.; Brooks, D. E., Biocompatibility Testing of Branched and Linear Polyglycidol. *Biomacromolecules* **2006**, *7*, 703-709.

140. Singh, S.; Topuz, F.; Hahn, K.; Albrecht, K.; Groll, J., Embedding of Active Proteins and Living Cells in Redox-Sensitive Hydrogels and Nanogels through Enzymatic Cross-Linking. *Angew. Chem., Int. Ed.* **2013**, *52*, 3000-3003.

141. Fitton, A. O.; Hill, J.; Jane, D. E.; Millar, R., Synthesis of simple oxetanes carrying reactive 2-substituents. *Synthesis* **1987**, 1140-2.

142. Hans, M.; Keul, H.; Moeller, M., Chain transfer reactions limit the molecular weight of polyglycidol prepared via alkali metal based initiating systems. *Polymer* **2009**, *50*, 1103-1108.

143. Kuhlmann, M.; Groll, J., Dispersity control of linear poly(glycidyl ether)s by slow monomer addition. *RSC Adv.* **2015**, *5*, 67323-67326.

144. Singh, S.; Zilkowski, I.; Ewald, A.; Maurell-Lopez, T.; Albrecht, K.; Moeller, M.; Groll, J., Mild Oxidation of Thiofunctional Polymers to Cytocompatible and Stimuli-Sensitive Hydrogels and Nanogels. *Macromol. Biosci.* **2013**, *13,* 470-482.

145. Schulte, B.; Walther, A.; Keul, H.; Moeller, M., Polyglycidol-Based Prepolymers to Tune the Nanostructure of Microgels. *Macromolecules (Washington, DC, U. S.)* **2014**, *47*, 1633-1645.

146. Lutz, J. Synthese und Charakterisierung Azid/Alkin-klickbarer Polyglycidole. Master Thesis, University of Würzburg,, **2016**.

147. Groll, J.; Singh, S.; Albrecht, K.; Moeller, M., Biocompatible and degradable nanogels via oxidation reactions of synthetic thiomers in inverse miniemulsion. *J. Polym. Sci., Part A: Polym. Chem.* **2009**, *47*, 5543-5549.

148. Rothenfluh, D. A.; Bermudez, H.; O'Neil, C. P.; Hubbell, J. A., Biofunctional polymer nanoparticles for intra-articular targeting and retention in cartilage. *Nat. Mater.* **2008**, *7*, 248-254.

149. Roberts, J. J.; Elder, R. M.; Neumann, A. J.; Jayaraman, A.; Bryant, S. J., Interaction of Hyaluronan Binding Peptides with Glycosaminoglycans in Poly(ethylene glycol) Hydrogels. *Biomacromolecules* **2014**, *15*, 1132-1141.

150. Schmitz, M.; Kuhlmann, M.; Reimann, O.; Hackenberger, C. P. R.; Groll, J., Side-Chain Cysteine-Functionalized Poly(2-oxazoline)s for Multiple Peptide Conjugation by Native Chemical Ligation. *Biomacromolecules* **2015**, *16*, 1088-1094.

151. Nichol, J. W.; Koshy, S. T.; Bae, H.; Hwang, C. M.; Yamanlar, S.; Khademhosseini, A., Cell-laden microengineered gelatin methacrylate hydrogels. *Biomaterials* **2010**, *31*, 5536-5544.

152. Lim, K. S.; Schon, B. S.; Mekhileri, N. V.; Brown, G. C. J.; Chia, C. M.; Prabakar, S.; Hooper, G. J.; Woodfield, T. B. F., New Visible-Light Photoinitiating System for Improved Print Fidelity in Gelatin-Based Bioinks. *ACS Biomater. Sci. Eng.* **2016**, *2*, 1752-1762.

153. Chung, C.; Burdick, J. A., Influence of Three-Dimensional Hyaluronic Acid Microenvironments on Mesenchymal Stem Cell Chondrogenesis. *Tissue Eng., Part A* **2009**, *15*, 243-254.

154. Nettles, D. L.; Vail, T. P.; Morgan, M. T.; Grinstaff, M. W.; Setton, L. A., Photocrosslinkable hyaluronan as a scaffold for articular cartilage repair. *Ann Biomed Eng* **2004**, *32*, 391-7.

155. Wu, S.-C.; Chang, J.-K.; Wang, C.-K.; Wang, G.-J.; Ho, M.-L., Enhancement of chondrogenesis of human adipose derived stem cells in a hyaluronan-enriched microenvironment. *Biomaterials* **2009**, *31*, 631-640.

156. Boere, K. W. M.; Blokzijl, M. M.; Visser, J.; Linssen, J. E. A.; Malda, J.; Hennink, W. E.; Vermonden, T., Biofabrication of reinforced 3D-scaffolds using two-component hydrogels. *J. Mater. Chem. B* **2015**, *3*, 9067-9078.

157. Woodfield, T. B. F.; Malda, J.; de Wijn, J.; Peters, F.; Riesle, J.; van Blitterswijk, C. A., Design of porous scaffolds for cartilage tissue engineering using a three-dimensional fiber-deposition technique. *Biomaterials* **2004**, *25*, 4149-4161.

158. Stichler, S.; Bertlein, S.; Schill, V.; Smolan, W.; Tessmar, J.; Bock, T.; Paxton, N. C.; Levato, R.; Malda, J.; Blunk, T.; Groll, J., Double printing of hyaluronic acid /

poly(glycidol) hybrid hydrogels with poly(ε-caprolactone) for MSC chondrogenesis. *Biofabrication* **2017,** doi: 10.1088/1758-5090/aa8cb7.

159. Mancini, I. A. D.; Brommer, H.; van, L. J. P. A. M.; Malda, J.; van, W. R.; Vindas, B. R. A.; Castilho, M.; Ribeiro, A.; Mensinga, A.; van, R. M. H. P.; Malda, J.; Castilho, M., Fixation of Hydrogel Constructs for Cartilage Repair in the Equine Model: A Challenging Issue. *Tissue Eng Part C Methods* **2017**, *23*, 804-814.

160. Lemanski, G., Organikum. (20. Aufl.) Von H. G. O. Becker et al. J. A. Barth Verlag, Heidelberg, **1996**. ISBN 3-335-00492-2.

161. Paxton, N. Processing and characterisation of inks for biofabrication. Master Thesis, University of Würzburg, **2016**.

162. Stichler, S.; Jungst, T.; Schamel, M.; Zilkowski, I.; Kuhlmann, M.; Tessmar, J.; Groll, J.; Bock, T.; Blunk, T., Thiol-ene Clickable Poly(glycidol) Hydrogels for Biofabrication. *Ann Biomed Eng* **2017**, *45*, 273-285.

163. Bian, L.; Guvendiren, M.; Mauck, R. L.; Burdick, J. A., Hydrogels that mimic developmentally relevant matrix and N-cadherin interactions enhance MSC chondrogenesis. *Proc. Natl. Acad. Sci. U. S. A.* **2013**, *110*, 10117-10122, S10117/1-S10117/6.

164. Böck, T. Multifunctional Hyaluronic Acid / Poly(glycidol) Hydrogels for Cartilage Regeneration Using Mesenchymal Stromal Cells. Doctoral Thesis, University of Würzburg, Würzburg, **2017**.

Appendix

Biological evaluation

The overall aim of this thesis was to develop a bioink for 3D bioprinting, therefore the hydrogels had to be examined concerning their suitability for cell applications. In particular, since the gels were used for the EU project HydroZONES[XVIII], which deals with the development of hydrogels for cartilage regeneration, it had to be proven if the established hydrogels support chondrogenesis of embedded cells.

Within the project a variety of different *in vitro* as well as *in vivo* experiments were carried out by collaboration partners of the consortium. For the *in vivo* evaluation hydrogels were implanted subcutaneously in rodent and equine models and at orthotopic locations in equine and porcine models. The experiments revealed biocompatibility of the developed hybrid hydrogels. Nevertheless, there are some ongoing experiments and the final assessment of the *in vivo* studies is still pending. The detailed discussion of this examinations, are part of the work of the corresponding partners[XIX] and thus not further discussed throughout this thesis.

The fundamental *in vitro* results are, however, briefly summarized herein to give an insight into the suitability of the developed gels for cartilage regeneration and thus on the suitability of the gels as bio-inks. Furthermore, the hydrogel formulation for 3D printing has been finally optimized for biological applications on the basis of the obtained *in vitro* results. Therefore, the *in vitro* results have to be considered to understand the altered hydrogel composition. The here presented *in vitro* experiments focused on the performance of human mesenchymal stromal cells (hMSCs) in hybrid and non-degradable synthetic hydrogels and the associated differences of the two systems concerning cytocompatibility and chondrogenic differentiation.
The biological analysis presented herein were carried out by Thomas Böck[XX] and parts of the results were already published in literature [158, 162].

[XVIII] Seventh Framework Programme FP7/2007-2013 under grant agreement n°309962.
[XIX] Emma Muiños López, Department of Orthopaedics and Traumatology, Universidad de Navarra;
Elisabeth Seebach, Anne-Kathrin Knauf, Yvonne Renz, Eliane Hesse and Friederike Bothe, Research Centre for Experimental Orthopaedics, University Hospital Heidelberg;
Irina Mancini, Regenerative Medicine Utrecht , Utrecht University.
[XX] Department of Trauma, Hand, Plastic and Reconstructive Surgery, University of Würzburg.

The live/dead assay, showing viable cells in green and dead cells in red, of hMSCs embedded in hybrid and synthetic gels revealed good cell viability after 21 d (hybrid gel) and 28 d (synthetic gel), respectively (**Figure A1**).

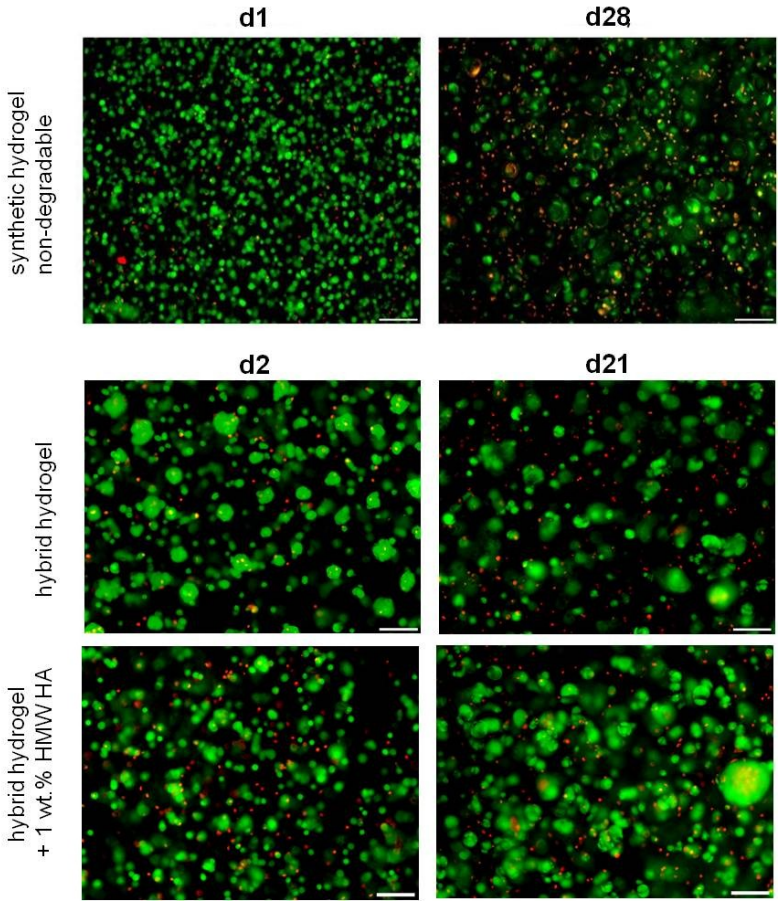

Figure A1: Live/dead assay of hMSCs embedded in synthetic hydrogels (top) and hybrid hydrogels with (bottom) and without (middle) 1 wt.% HMW HA. Viable cells are shown in green (labelled with calcein acetoxymethyl ester) and dead cells are shown in red (labelled with ethidium homodimer III). Scale bars represent 100 µm. Live/dead assay was carried out and analysed by *Thomas Böck*.[158, 162]

However, the chondrogenesis of hMSCs differed depending on the hydrogel system. hMSCs embedded in hybrid hydrogels showed a robust chondrogenic differentiation (day 21) in contrast to hMSCs embedded in the synthetic hydrogel (**Figure A2**). The condrogenic differentiation can be seen by a prominent glycosaminoglycan (GAG) staining with safranin O, and strong signals for aggrecan and Col-II. The superior differentiation of hMSCs in hybrid hydrogels can be directly attributed to the used cross-linking polymers. The synthetic hydrogel includes only bioinert PG as cross-

linking agents, whereas the hybrid hydrogel includes the thiol-functionalized biopolymer HA-SH. HA is present in the extracellular matrix (ECM) of native cartilage and is known to have beneficial effects on MSC chondrogenesis.[153] For othe hydrogel systems described in this thesis this positive influence could also been demonstrated.

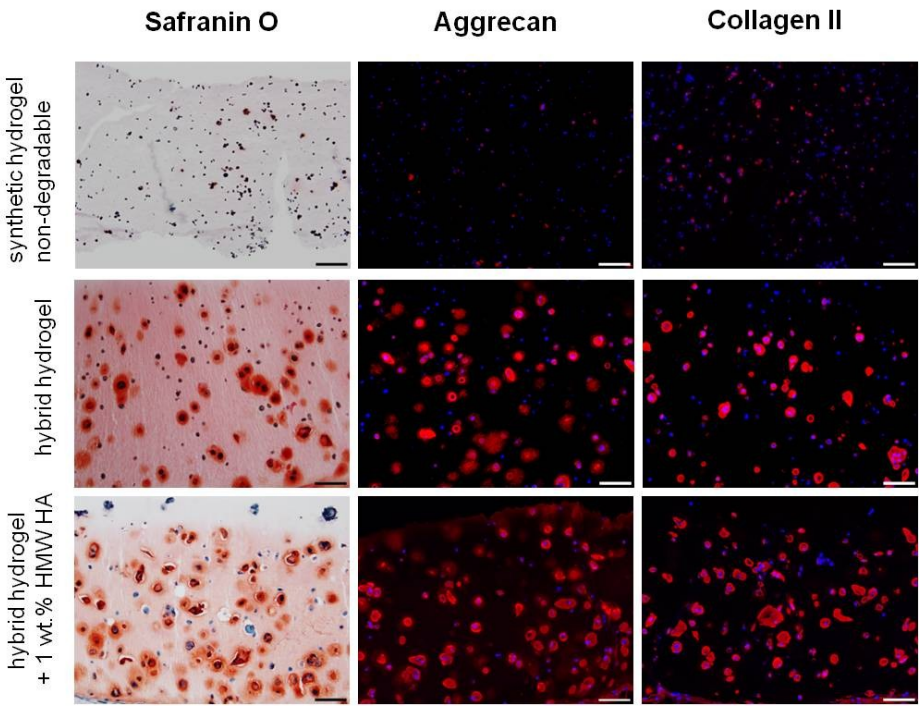

Figure A2: Histology and immunohistochemistry of hMSCs embedded in synthetic hydrogels (top) and hybrid hydrogels with (bottom) and without (middle) 1 wt.% HMW HA after 21 d of chondrogenic differentiation. For the visualization of ECM production, cryosections were stained for the deposition of GAG with safranin O (left), aggrecan (red, middle) or Coll-II (red, right). The nuclei (blue) were stained with DAPI. Scale bars represent 100 µm. The analysis was carried out by *Thomas Böck*.[158]

Although it was shown that by introducing the naturally-based polymer HA-SH, the chondrogenic differentiation of hMSCs could be significantly improved, the addition of supplemented HMW HA led to a slightly less robust chondrogenesis of embedded MSCs. Concerning the improvement of the hydrogel composition for bio-inks, the addition of HMW HA should thus minimized when using cells.

In addition to the presented results, the synthetic hydrogel system was further examined. Thomas Böck[XXI] bio-functionalized these hydrogel with the peptide sequence histidine-alanine-valine (HAV) and investigated the influence of this sequence on the chondrogenic differentiation of the gels. It was previously shown that HAV enhances the chondrogenic differentiation of MSCs.[163] This positive influence was also demonstrated for the herein presented synthetic hydrogel system. All details are discussed in the thesis of Thomas Böck[164].

[XXI] Department of Trauma, Hand, Plastic and Reconstructive Surgery, University of Würzburg.